National Library of Canada
Bibliothèque nationale du Canada

Canadian Theses Service
Service des thèses canadiennes

Ottawa, Canada
K1A 0N4

NOTICE

The quality of this microform is heavily dependent upon the quality of the original thesis submitted for microfilming. Every effort has been made to ensure the highest quality of reproduction possible.

If pages are missing, contact the university which granted the degree.

Some pages may have indistinct print especially if the original pages were typed with a poor typewriter ribbon or if the university sent us an inferior photocopy.

Reproduction in full or in part of this microform is governed by the Canadian Copyright Act, R.S.C. 1970, c. C-30, and subsequent amendments.

AVIS

La qualité de cette microforme dépend grandement de la qualité de la thèse soumise au microfilmage. Nous avons tout fait pour assurer une qualité supérieure de reproduction.

S'il manque des pages, veuillez communiquer avec l'université qui a conféré le grade.

La qualité d'impression de certaines pages peut laisser à désirer, surtout si les pages originales ont été dactylographiées à l'aide d'un ruban usé ou si l'université nous a fait parvenir une photocopie de qualité inférieure.

La reproduction, même partielle, de cette microforme est soumise à la Loi canadienne sur le droit d'auteur, SRC 1970, c. C-30, et ses amendements subséquents.

NL-339 (r. 88/04) c

Canada

Intra- and Inter-zone Airflow with Heat and Mass Transfer in Multi-zone Buildings

Zheng Jiang

A Thesis
in
The Faculty
of
Engineering and Computer Science

Presented in Partial Fulfillment of the Requirements
for the Degree of Doctor of Philosophy at
Concordia University
Montreal, Quebec, Canada

September 1990

© Z. Jiang, 1990

National Library of Canada
Bibliothèque nationale du Canada

Canadian Theses Service
Service des thèses canadiennes

Ottawa, Canada
K1A 0N4

The author has granted an irrevocable non-exclusive licence allowing the National Library of Canada to reproduce, loan, distribute or sell copies of his/her thesis by any means and in any form or format, making this thesis available to interested persons.

L'auteur a accordé une licence irrévocable et non exclusive permettant à la Bibliothèque nationale du Canada de reproduire, prêter, distribuer ou vendre des copies de sa thèse de quelque manière et sous quelque forme que ce soit pour mettre des exemplaires de cette thèse à la disposition des personnes intéressées.

The author retains ownership of the copyright in his/her thesis. Neither the thesis nor substantial extracts from it may be printed or otherwise reproduced without his/her permission.

L'auteur conserve la propriété du droit d'auteur qui protège sa thèse. Ni la thèse ni des extraits substantiels de celle-ci ne doivent être imprimés ou autrement reproduits sans son autorisation.

ISBN 0-315-64714-0

Canada

ABSTRACT

Intra- and Inter-zone Airflow with Heat and Mass Transfer in Multi-zone Buildings

Zheng Jiang, Ph.D.
Concordia University, 1990

The design of ventilation systems and development of control strategies require detailed knowledge of airflow, contaminant dispersion and the distributions of temperature and moisture. Moreover, as technology advances, modern ventilation systems tend toward a more compact and highly efficient design. Existing empirical approach and simplified analysis are inadequate for assessing newly developed systems and resolving problems related to "sick building syndrome". Advanced analysis is therefore required.

This thesis describes the development both of a numerical model which has aimed at enhancing the knowledge of airflow and contaminant removal in two-zone enclosures, and of control strategies for improving indoor environments. The model allows the simulation of intra- and inter-zone heat and mass transfer in three-dimensional turbulent flows in natural, forced, and mixed convection circumstances.

The model has been applied to predict the airflow, temperature distribution, and contaminant dispersion in a two-zone enclosure under various operating conditions,

emphasizing the effects of door size and location. The ventilation effectiveness and thermal comfort in two-zone enclosures with various door locations have also been investigated. A number of correlations of heat and mass transfer with main parameters have been obtained.

This numerical model has been verified against available experimental results. The model can provide useful information for designers in choosing proper locations for doors, ventilation supply and exhaust openings, and in assessing the indoor air quality and thermal comfort in two-zone enclosures.

ACKNOWLEDGEMENTS

The author wishes to express her appreciation to her supervisors Dr. J. C. Y. Wang and Dr. F. Haghighat, for their guidance, continued support and encouragement during the course of this study. Acknowledgement is also due to Dr. Q. Chen for his helpful suggestions.

TABLE OF CONTENTS

LIST OF FIGURES

LIST OF TABLES

NOMENCLATURE

A = general cell surface area

A = Van driest's constant

A_x, A_y, A_z = cell surface areas in the x, y and z direction respectively

Ar = Archimedes number, $\beta g h(T_I - T_E)/U_I^2$

a = neighbor coefficient of finite difference form

b = source term in discretization equation

b' = source term without pressure difference

C = contaminant concentration

C_1, C_2, C_3 = coefficients in k-ε model

C'_μ, C_μ, C_D = coefficients in turbulence model

C_p = specific heat at constant pressure

D = diffusion coefficient

D = diffusion transportation at interfaces of control volumes, $\Gamma A_x/\delta x$

d = coefficient in pressure correction equation

E = wall roughness coefficient in Wall Function

e = source emission rate

F = convection transportation at the interfaces of control volumes, $\rho u A_x$

g = acceleration due to gravity

G_B = generation of turbulent kinetic energy related to buoyancy

G_K = stress production of turbulent kinetic energy

Gr = Grashof number, $\beta g \Delta T H^3/\nu^2$

H = height of room

H = enthalpy

h = specific enthalpy

h = height of openings

h_x = convective heat transfer coefficient

I = turbulence intensity

k = kinetic energy of turbulence

L = room length

l = length scale in turbulence model

l_I = hydraulic diameter of inlet, $2w_I h_I/(w_I+h_I)$

l_m = mixing length

Nu, Nu_H = Nusselt number based on room height, $qH/(T_H-T_C)\lambda$

Nu_L = Nusselt number based on room length, $qL/(T_H-T_C)\lambda$

p = pressure

PD = percentage dissatisfied people

Pe = cell Peclet number, F/D

Pr = Prandtl number ν/α

q = heat flux per unit area

R_a = dimension ratio, h_D/H

Ra = Rayleigh number based on room height, $g\beta H^3(T_H-T_C)/\nu\alpha$

Ra_L = Rayleigh number based on room length, $g\beta L^3(T_H-T_C)/\nu\alpha$

Ra^* = flux Rayleigh number, $g\beta qH^4/k\nu\alpha$

Re = Reynolds number, $U_I l_I/\nu$

R_f = flux Richardson number, $-G_B/G_K$

S_ϕ = source term for variable ϕ

T = temperature

T_C = cold wall temperature

T_H = hot wall temperature

t = time

$u_i(u,v,w)$ = velocity in x, y, z direction respectively

U_I = air velocity at ventilation inlet

U_{IF} = air infiltration velocity

V_t = turbulent random velocity

x,y,z = Cartesian coordinate system

x_D = distance from western wall (x=0) to partition

y_D = distance from southern wall (y=0) to door axis

w = width of opening

W = width of room

Greek Symbols

α = thermal diffusivity

α = under-relaxation factor

β = expansion coefficient of air

Γ_ϕ = exchange coefficient of ϕ

δx = distance between nodes

δ_{ij} = Kronecker delta function

Δ = difference

$\Delta x, \Delta y, \Delta z$ = dimensions of control volume

ε = dissipation rate of turbulence energy

κ = von Karman's constant

λ = thermal conductivity

μ = dynamic viscosity

ν = kinematic viscosity

ρ = density

σ = exchange coefficient

σ_t = turbulent Schmidt number or Prandtl number

τ = time related to air age

τ = shear stress

θ = relative temperature

ϕ = dependent variables in conservation equation

Subscripts

c = contaminant

D = door

E = exhaust opening

E,W,N,S,T,B = grid node at east, west, north, south, top and bottom respectively

e,w,n,s,t,b = interface at east, west, north, south, top and bottom respectively

eff = effective

f = turbulent fluctuation

h = door height

h = enthalpy

I = supply inlet

IF = infiltration

l = laminar

p = currently considered node

p	= grid node adjacent to solid surface
s	= source
s	= solid surface
t	= turbulent
ϕ	= dependent variables

CHAPTER 1

INTRODUCTION

The knowledge of intra- and inter-zone convective heat and mass transfer is a fundamental requirement in study of indoor air quality, thermal comfort and energy saving in buildings. Comprehension of the mechanism of convective heat and mass transfer is the key to the solution of problems related to ventilation effectiveness and the thermal performance of buildings. In residential buildings, for example, kitchen and living areas are usually made in one or connected through a doorway. Naturally, occupants are concerned about how much contamination and heat from a combustion source in the kitchen are brought into the living room, and how the infiltration air from windows affects the distributions of temperature and contaminants. In the case of the partitioning of a large office room, it would be of interest to know how to arrange partitions and locations of supply and exhaust properly to make the removal of contaminants released by occupants and computers more efficient. Again, consider a passive solar heated building where the southern zone is warmer than the northern zone due to the solar energy transmitted through south-facing windows; a more uniform temperature distribution for southern and northern zones would rely on the inter-zone transportation of solar heat gains by natural convection. The convective heat transfer rate from the south-zone to the north-zone depends on the location and the size of the door, and this dependence needs to be fully understood. The problems in all of these examples are

related to intra- and inter-zone convective heat and mass transfer.

The mechanism of the intra- and inter-zone heat and mass transfer is quite complex. Convection, diffusion, and radiation are all involved. Since air serves not only as a diluter but also as a carrier of energy and of gaseous and particle contaminants (such as smoke, dust, odors and so on), the convective transportation of heat and mass is directly dependent on the flow pattern of the air movement within and between zones. Air movement in buildings can be due to the temperature differences of room air, called natural convection; due to infiltration or mechanical ventilation, called forced convection; or due to the combination of these two, namely mixed convection. Diffusion of heat and mass is the result of, respectively, differences in temperature and the non-uniformity of the mass component field. Radiation takes place whenever there is a temperature difference between object surfaces. In general, the radiation heat transfer between walls can be well predicted, and the radiation between room objects may even be neglected when the temperature difference within an enclosure is small.

The three-dimensional heat and mass transfer in buildings can be described by a set of conservation equations: the continuity, momentum, and energy equations with appropriate boundary conditions. Since these non-linear, second order partial differential equations are coupled with each other, an exact solution has not yet been obtained. Therefore, analytical study has to be based either on very rough and simplified models in which the distributions of properties are considered to be uniform, or on numerical method. In most cases, experimental measurement and numerical simulation are used to investigate the intra- and inter-zone heat and mass transfer. In experimental studies, using either

full-sized or scale models, the temperature and velocity of the air and contaminant concentration are measured at chosen points. These measurements are then used to obtain some sort of correlation between the rate of heat or mass transfer and other involved parameters, such as the temperature difference between walls, the dimensions of the enclosure, the location of the air supply and exhaust openings etc. Numerical simulation, on the other hand, is based on discrete equations. The designated region is divided into a number of subvolumes in which all variables are considered to be uniform. The differential conservative equations are then integrated in each subvolume to obtain a set of linear algebraic equations, one for each grid node, which can be solved by some available techniques. Because of the non-linearities in the fundamental differential equations, the process requires an iteration approach. Subsequently, each equation is linearized and solved sequentially until a convergent solution is obtained. In this technique, in order to make the integrated equations solvable, properly assigned boundary conditions are required; for example, air velocity and temperature at solid surfaces should be specified. Furthermore, assumptions are usually adopted to simplify the problems physically.

A review of research works concerning intra- and inter-zone convective heat and mass transfer in buildings is presented in the following section.

1.1 Review of the Literature

1.1.1 Experimental studies on inter-zone heat and mass transfer

Brown and Solvason (1962) carried out their experimental work on inter-zone natural convection heat transfer in a full-sized air filled enclosure which was divided into hot and cold zones by a partition with a centrally located rectangular opening. The inter-zone heat convection was expressed via dimensionless numbers Nu, Gr, and Pr as follows:

$$Nu_h = C\, Gr_h^{0.5}\, Pr \qquad (1.2.1)$$

where C was suggested to be in the range of 0.2-0.33. The Nu_h and Gr_h are both based on the height of the opening. The temperature difference used in the calculation of Nu_h and Gr_h is the average of those of the two zones. In their experiment, the effects of the opening size and of the ratio of the partition thickness over opening height on inter-zone convective heat transfer were examined for the air temperature differences from 8.3 to 47.2 K.

Shaw (1972) studied the heat transfer through doorways caused by both natural and mixed convections, and presented the results in the following expression,

$$Nu_h = C'\, Sw\, Pr \qquad (1.2.2)$$

where Sw is a coefficient equal to $Re^3 h_D^{\ 3}/GrD_h^{\ 3}$. The Grashof number and the Reynolds number are based on the door width and the hydraulic diameter of the door opening, $D_h = 2w_D h_D/(w_D+h_D)$, respectively. The coefficient C' was found to be a product of the coefficient for the

natural convection case and a forced velocity coefficient C_v.

Wray and Weber (1979) performed experiments on a small scale laboratory model to develop an empirical law relating inter-zone natural convection heat transfer rates to the geometric properties of the enclosure and the temperature fields in the separate zones. The following functional relationship was determined from experimental data.

$$Nu_H = K (R_a) Gr_H^b \qquad (1.2.3)$$

where R_a is the dimension ratio, h_D/H, and b is approximately equal to 0.46. K is in the range of 0.19-0.29. The characteristic length in the Nusselt and Grashof numbers is the room height.

Nansteel and Greif (1981, 1984) experimentally investigated the effects of the size and location of the aperture on the natural convective heat transfer between two zones in a two-dimensional scaled model (1981) and a three-dimensional scaled model (1984). In the three-dimensional investigation, the scaled model had dimensions of H=15.2cm, L=30.5cm and W=83.8cm. Tests were carried out over the Ra_L range from 2.4×10^{10} to 1.1×10^{11}. The opening width ratio was fixed at $w_D/W=0.093$, while the height ratio, h_D/H, was varied at 1/4, 1/2, 3/4 and 1. The end-walls were maintained at constant temperatures T_H and T_C respectively. The heat transfer rate through the door opening for the three-dimensional case was expressed as

$$Nu_L = 1.19(h_D/H)^{0.401} Ra_L^{0.207} \qquad \begin{cases} 1/4 < h_D/H < 1 \\ w_D/W = 0.093 \end{cases} \qquad (1.2.4)$$

where h_D and w_D are, respectively, the door height and width. Ra_L is the

Rayleigh number defined as $\beta g L^3 (T_H - T_c)/\upsilon\alpha$.

Hill and Mahajan (1986) modified the airflow model based on the Bernoulli equation with isothermal zone temperature to account for the vertical non-linear temperature distribution. The area between the floor and the top of the door opening was divided into n horizontal isothermal temperature sections. They calculated the total heat and mass transfer rate by adding those calculated in each isothermal section. Experiments were performed to verify the model, in which the height of the doorway was divided into eight isothermal zones. The inter-zone heat transfer rates were obtained by summing up the product of the density, velocity, temperature, specific heat and respective area of the eight measurement locations in the doorway. They concluded that the modified model correlated very well with the experimental data.

Mahajan (1987) measured the velocity and temperature profiles of the airflow through door openings at the NBS Passive Solar Test Facility to calculate the inter-zone heat and mass transfer rates. The results were compared with the values predicted by a simple algorithm based on the Bernoulli equation. He found that the air temperature across the width of the opening was fairly uniform, but that the air velocity was not. This non-uniformity of the velocity across the width of the opening was due to the three-dimensional nature of the flow. The results indicated that the existing algorithms for estimating inter-zone heat and mass transfer did not account for these lateral variations of the flow velocity, and therefore that they need to be improved.

Kirkpatrick and Hill (1988) examined natural and forced convection in a two-zone and a three-zone full-scale building to determine the effects of the zone temperature difference, temperature stratification

and forced convection on the inter-zone heat and mass transfer. The temperature stratification in each zone was assumed to be linear for the two-zone model, and to be isothermal for the three-zone model. The forced convection was simulated by adding an additional mass flow rate to the mass flow rate calculated in the natural convection case. A model based on the experimental temperature profiles in each zone was developed to determine the inter-zone mass flow and heat transfer for mixed convection cases.

Scott et al. (1988) reported the results of their experimental study, which examined the transition between two flow regimes as a function of the aperture size. The two primary mechanisms driving natural convection flow through apertures in multi-zone enclosures are: (1) the bulk density difference between hot and cold zones and (2) the motion pressure differences generated by the natural convection boundary layer. Results showed that when the width of the aperture was reduced, the bulk fluid temperature difference between the hot and cold zones rapidly approached the temperature difference between the hot and cold walls, and the boundary layer flow was blocked. The critical aperture area in which the boundary layer driving mode was changed to a density driving one was about 2% of the total cross-sectional area of the chamber.

Neymark et al. (1988) conducted experiments in partially divided enclosures with high flux Rayleigh number to examine the conditions in which an enclosure would become horizontally stratified and determine the resulting effect on the inter-zone heat transfer. A small-scale water model and a full-size air enclosure were tested. The opening area ratio A_P, defined as $A_P=h_D w_D/HW$, was varied by changing the opening

width, while the height was kept constant. The results were presented via diagrams of Nu_H against Ra_H^*, which indicated that the critical values of A_p, at which the flow changed from a boundary layer driving mode to density driving mode, were 0.04 for air and 0.02 for water.

Boardman et al. (1989) investigated the influence of aperture height and width on the inter-zone high-Rayleigh number natural convection in a full-size, air-filled enclosure. The aperture height relative to the test cell height varied from 1/8 to 1 and the aperture width relative to the test cell width ranged from 0.009 to 1. They concluded that a 10 percent doorway area relative to glazing area would be sufficient for good inter-zone heat transfer, and that the Nusselt number Nu_H ranged between 15-165 with a strong dependence on the aperture height for the flux Rayleigh number, Ra_H^* between 5×10^{11} and 5×10^{12}.

Extensive studies concerning the inter-zone heat and mass transfer conducted before 1987 can be found in a review paper by Barakat (1987).

1.1.2 Numerical simulations

Numerical simulation is another technique for studying the convective heat and mass transfer within and between zones. A large number of works have been done on this subject. The majority considered cases with single enclosures.

Nielsen (1974) studied the air movement and moisture distribution in an air conditioned room by numerical simulation. The stream function - vorticity formulation and the k-ε two-equation turbulent model* were

---

* k-ε turbulent model in this paper refers to the high-Reynolds-number k-ε model

used in his two-dimensional analysis. The buoyancy effect was not considered.

In a later study, Nielsen et al. (1979) extended the previous work to take the buoyancy force into account. The equations in the finite-difference form were solved by using the TEACH computer code (Gosman et al. 1974). To examine the effect of increasing temperature difference on the airflow, four different values of the Archimedes number, defined as the ratio of buoyancy force over inertial force

$$Ar = \frac{\beta g h (T_I - T_E)}{U_I^2},$$

for the case of a uniformly heated floor at the fixed Reynolds number were computed. Experimental measurements were conducted to verify the computation results.

Nielsen (1981) also studied the contaminant distribution in a forced ventilated enclosure with two-dimensional consideration and the k-ε turbulent model. The two cases considered were: (1) contaminant emitted along the whole floor surface and (2) the contaminant source emitted along a line. An experimental comparison was also made.

Natural convection in an enclosed cavity has been investigated by many researchers (for example, Catton, 1978; Ostrach, 1982; Van de Davis, 1983; Markatos et al., 1984; Lin and Nansteel, 1987; and Hadjisophocleous et al, 1988). Markatos and Pericleous (1984) studied natural convection in an enclosure with both laminar and turbulent flows. With the two-dimensional approximation, the classical boundary conditions for natural convection were used: the two side walls were at constant but different isothermal temperatures, while the floor and

ceiling were insulated. The SIMPLEST algorithm was adopted to solve the finite-difference equations. Solutions were computed for Ra from 10^3 to 10^{16}. The criterion for switching laminar flow to turbulent flow was the Rayleigh number at 10^6. The computed results were compared with the benchmark solution, which was considered to be accurate for the laminar case.

Gadgil (1979) developed a three-dimensional model to study the laminar, natural convection, heat transfer in an enclosure. The SIMPLE algorithm (Patankar, 1980) was used for solving the coupled difference equations. This model is applicable for steady flow with Rayleigh number up to 10^{10}.

Lemaire (1987) applied the CHAMPION computer code (Pun and Spalding, 1976) coupled with a radiation model to compute the air movement and heat transfer in a room heated by a radiator. CHAMPION is a general computer code which can be applied to two-dimensional steady laminar and turbulent flow cases. The k-ε turbulent model and SIMPLE algorithm were used in this code.

The PHOENICS code has been used for three-dimensional analysis on convective heat and mass transfer in enclosures by a number of researchers (for example, Holmes, 1982; Markatos, 1983; Jones and Sullivan, 1985; and Chen and Van der Kooi, 1988). It is a general computer code which can deal with parabolic, hyperbolic and elliptic flows. In order to achieve a more accurate prediction of heat transfer through walls, Chen and Van der Kooi (1988) combined the PHOENICS code with an extensive program ACCURACY, which can provide the coupled boundary conditions in the simulation.

Markatos and Cox (1984) applied the modified PHOENICS to predict the

development of a fire and the contaminant concentration distribution within a shopping mall. The fire was simulated by heat and contaminant sources. Both steady and transient cases were predicted, either for a fixed heat release rate or for a linearly growing fire reaching the fixed rate at 3 min from ignition. The results obtained from the three-dimensional program were not verified by experimental data because of the difficulty in measuring hot gas velocity. The airflow pattern and contaminant distributions in single enclosures were also studied by Gosman et al. (1980) and Markatos and Malin (1982).

November and Nansteel (1987) considered steady natural convection in a square water-filled enclosure with more complex boundary conditions. They numerically solved the two-dimensional laminar momentum and energy equations by the vorticity-stream function method. The boundary conditions in their study were as follows: the lower boundary was partially heated and partially insulated; one vertical boundary was at a constant cold temperature, while the other and the top boundary were insulated. The results indicated that the case studied was quite distinct from that of cooling from below and heating on a vertical wall.

Berne and Villand (1987) described the three-dimensional thermohydraulic code TRIO-VF which can handle laminar or turbulent flows of incompressible fluids with the Boussinesq approximation. The eddy viscosity was simulated using the k-ε model. This code was applied to model ventilated single enclosures with a complex environment. The airflow patterns in the ventilated enclosures under different boundary conditions were demonstrated.

Murakami et al. (1988) reported their study on contaminant transport in a turbulent diffusion field. They examined the cases with supplies

located on the ceiling and the exhausts mounted near the floor on the one pair of opposite side-walls. Four types of single, clean room models were used for analysis: the number of supplies on the ceiling was varied at one, four, six and nine. The concentration distributions for cases with different contaminant source locations were examined.

Horstman (1988) developed a numerical model to predict the two-dimensional velocity distribution, circulation pattern, and airborne contaminant distribution within a ventilated volume for a steady state condition. The two-dimensional laminar flow field was solved in the form of finite-difference stream functioning equations and modified Taylor series approximations of the vorticity equations. The model was applied to predict the airflow pattern and contaminant build-up in the passenger cabins of commercial aircraft. The central difference scheme was used for the momentum equation, while the upwind difference scheme was adopted for the contaminant conservation equation to ensure the transport in the proper direction.

Kuehn (1988) conducted a review of the two-phase flow simulation method and described some recent applications to airflow and contaminant transport in clean rooms. The coupling between particles and airflow can be modeled either by the Eulerian approach or by the Lagrangian approach. In the Eulerian approach, the particles are divided into several groups according to their diameters. Each group is considered as a "phase". These phases are dispersed in the airflow with different diffusivities. It is most important in the Eulerian approach to determine the particle diffusivities. However, particle diffusivity in turbulent flow is not completely understood. In the Lagrangian approach, the particles act as a drag force on the airflow, and this drag force,

in turn, accelerates the particles' movement in the airflow.

Chen et al. (1990a) applied a low-Reynolds-number k-ε turbulence model to predict the velocity and temperature distributions in an enclosure with natural convection flow. They concluded that for computation of indoor air movement, the low-Reynolds-number k-ε model provides a better velocity profile in the region near the walls and more accurate simulations of the convective heat transfer from walls to room air than the k-ε model.

In a later work, Chen et al. (1990b) numerically investigated indoor air quality and thermal comfort in a ventilated enclosure in six cases using different kinds of air diffusers. The blockage due to furniture and contaminants emitted from the furniture were simulated. Again, the low-Reynolds-number k-ε model was employed.

The above-mentioned numerical studies are limited to cases of a single zone. Chang et al. (1982) undertook a finite-difference study of natural convection in a two-dimensional square enclosure with a partition mounted either on the ceiling or on the floor . One wall parallel to the partition was kept at cold while the opposite was kept hot; the ceiling and the floor were well insulated. The two-dimensional laminar flow cases for the Grashof number region from 10^3 to 10^8 were computed with different combinations of the partition geometry and location. It was found that when the partition was set close to the cold wall, the total heat transfer rate was reduced. The maximum heat transfer rate occurred when the partition was set slightly off the center of the enclosure, towards the hot wall. The average Nusselt number, $\overline{Nu}$, was plotted against the height ratio, the thickness ratio and the location of the partition. This study was not validated.

Kelkar and Patankar (1985) predicted natural convection in partitioned enclosures by numerical simulation. The partitions in their studies were two-dimensional. The opening on the partition ran the whole width of the rooms; the flow conditions were laminar.

1.2 Objective and Methodology of the Present Study

From the preceding review of the literature, it can be seen that experimental works on two-zone enclosures have focused only on the rate of heat and mass transfer across door openings, without providing the airflow pattern and the distributions of temperature and contaminant concentration in each zone. However, this information could be vitally important. For instance, when the performance of an HVAC system is being evaluated, not only is information about inter-zone heat and mass transfer important, but also information about the short-circuiting, stratification, mixing, and stagnation of contaminated air, since temperature stratification, maximum air velocity and contaminant concentration should be kept within certain limits to ensure occupants' comfort and health. All these parameters are closely related to air movement.

The air movement in a complex enclosure is affected by many parameters, such as the dimension of the enclosure, the size and the location of the door opening, the locations of the ventilation inlet and outlet, the infiltration from walls, and so on. One of the main limitations of experimental studies is their lack of generalities

because of their reliance on fixed boundary conditions. There are many different configurations and layouts of ventilation systems. It is difficult to deal with the variations in parameters in an experimental study. The extent to which the existing correlations could be extrapolated to cases with boundary conditions other than what the experiments based on is unknown. Besides, experimental investigation requires a large amount of time, money and equipment. In this respect, numerical simulation has a distinct advantage over experiments. A validated numerical model would not only allow a research effort carried on over a short period of time and at less expense to cover a wider range of boundary conditions encountered in buildings, but also provide an overall view on the field distributions of all important factors. The capability of a numerical model to simulate heat and contaminant sources enables one to estimate the necessary heating or cooling load which would maintain air temperature and contaminant concentration in occupied zones at designated levels. As mentioned in the last section, this method has been used successfully in various problems related to airflow and convective heat and mass transfer in buildings.

However, there are still some uncertainties involved in obtaining numerical solutions to the Navier-Stokes equations in three-dimensional flows with source terms dominating and complex boundary conditions. For example, the uncertainty of stability still exists, and the convergence of numerical procedures is not guaranteed. In the prediction of turbulent flows, the success of turbulence models, which are still semi-empirically based, in various boundary conditions is unsure. Moreover, the degree of accuracy in applying turbulence models cannot be estimated very well. Thus, an experimental validation is needed.

The majority of previous numerical simulation studies on indoor air movement considers only single-zone enclosures. For multi-zone enclosures, in fact, there are still many problems remaining unsolved. When two rooms are to be connected by a doorway, or a large room needs to be partitioned, a number of choices exist for arranging the locations of the partition, the door opening, and the ventilation supply and exhaust. The effects of these parameters on airflow pattern and distributions of temperature and contaminant concentration need to be assessed. In partitioned two-zone enclosures, door size and location can be important factors influencing the heat and mass transfer, and thus receive special attention in this study.

There are a number of existing universal computer codes which can be applied for prediction of heat and mass transfer in partitioned enclosures with three-dimensional turbulent flow, such as PHOENICS code. However, these codes are usually provided as a "black box". When applying, users can only create a file containing all input information according to the problems to be solved, without knowing what happens inside the black boxes. The users can do nothing if they are not satisfied with the solver, or if there is a numerical instability observed. For a special problem, sometimes a small change in numerical procedure could make a great improvement of the convergence.

The objective of this study is to establish a numerical model and to apply it to:

(1) predict the convective heat and mass transfer in two-zone enclosures;

(2) determine the effects of the location of the door opening on air movement, temperature distribution, contaminant dispersion, ventilation

effectiveness, and thermal comfort in two-zone enclosures;

(3) establish correlations between contaminant migration and the main parameters, such as air change rate and the locations of door opening, ventilation supplies and exhausts for specific cases.

The methodology adopted is numerical simulation. As explained earlier, for this type of problem, numerical simulation is the preferred technique. In this study, the conservation equations of fluid mechanics will be solved through finite-difference approximation.

According to the characteristics of the problems being dealt with, it will first be decided what sort of numerical model is more appropriate. It is known that the airflow in ventilated enclosures is mainly turbulent. As for natural convection flow, the transition from laminar flow to turbulent flow may take place when the Rayleigh number increases over 10^9 (Cheesewright, 1968). In a partitioned enclosure, a door opening in the partition would introduce a disturbance into the passing airflow and enhance its turbulence. The mechanism of a turbulent transportation is completely different from that of laminar transportation. Thus, turbulence modeling needs to be included in the numerical model.

For two-zone airflow simulation, two-dimensional approximation can no longer be accepted because the velocity component in the third direction is not negligible. Moreover, investigations of the effects of the locations of door opening, ventilation supply and exhaust, and contaminant sources on the heat and mass transfer require a three-dimensional system.

This study, then, will develop and present a three-dimensional numerical model which can be applied in turbulent flows. The model is

expected to be able to predict the airflow pattern, the heat and mass transfer within and between rooms, and the distributions of temperature and contaminant in turbulent flows with variable boundary conditions. It is hoped as well that the model will be found useful in estimating thermal comfort and the ventilation effectiveness in partitioned enclosures.

1.3 Contributions and Summary

The main contributions of this thesis are as follows:

(1) A numerical model has been developed which is able to handle three-dimensional convective heat and mass transfer in the turbulent flows of two-zone enclosures in buildings.

(2) Based on the model developed, numerical investigation on the indoor airflow, air quality, and thermal comfort is extended into two-zone enclosures. Parameter studies have been carried out under natural convection, forced convection and mixed convection conditions. The correlations of heat and mass transfer with main parameters are obtained, clarifying the effects of door location on air movement and contaminant dispersion.

(3) The numerical model here presented can provide designers with information essential to the proper arrangement of doors, ventilation supplies and exhausts with special needs. The model can also be applied to solve other engineering problems related to heat and mass convection in three-dimensional rectangular enclosures.

The physical foundations of the model and the turbulence simulation approaches are described in Chapters 2 and 3, respectively. In Chapter 4, the structure of the mesh system adopted in the model and the derivation of the finite-difference equations is demonstrated. The numerical procedure and the techniques used for solving the finite-difference equations are explained in this chapter as well. In Chapter 5, the results of five case studies in which the computational model was applied are presented. The first case study investigated natural convection in a two-zone enclosure. Its purpose was to obtain correlations between inter-zone convective heat transfer and door location while other parameters remained unchanged. The second case studied air movement and contaminant dispersion caused by either mechanical ventilation or natural ventilation (air infiltration) in a partitioned enclosure. The third case study focused on the effects of air infiltration on ventilation airflow in a partitioned room with various door locations. Infiltration and mechanical ventilation were thus both assumed to be taking place in this case. The fourth study investigated the ability of a ventilation system to remove contaminants; the influence of door location on ventilation effectiveness was included. The fifth case study assessed thermal comfort and indoor air quality in a two-zone enclosure with mixed convection. Three different temperatures of supply air were considered, while the door was located in three different positions.

The geometrical configuration of the enclosure for the five case studies was the same, but with different arrangements of the ventilation openings. In all cases, the effects of door location on flow properties were emphasized. These case studies may be considered as the first step

towards the application of numerical simulation to multi-zone airflow and heat and mass transfer.

CHAPTER 2

GOVERNING EQUATIONS

2.1 Governing Equations

Air movement in rooms can be considered as an incompressible viscous flow, where the Boussinesq approximation is applicable. With this assumption, air density could be considered constant except for the buoyancy influence. The governing equations describing three-dimensional convective heat and mass transfer in incompressible viscous flow fields are the continuity equation, the momentum equation, the energy equation and the component conservation equation. They can be written as follows:

Continuity equation

$$\frac{\partial \rho}{\partial t} + \frac{\partial}{\partial x_j}(\rho u_j) = 0 \qquad (2.1.1)$$

Momentum equation in three directions

$$\frac{\partial u_i}{\partial t} + \frac{\partial u_i u_j}{\partial x_j} = -\frac{1}{\rho}\frac{\partial p}{\partial x_i} + \frac{\partial}{\partial x_j}\left[\frac{\mu}{\rho}\left(\frac{\partial u_i}{\partial x_j} + \frac{\partial u_j}{\partial x_i}\right)\right] + \beta(T_0 - T)g_i \qquad (2.1.2)$$

where the subscripts i and j denote the x, y or z, and μ is the dynamic viscosity of air. The second term and the last term of the right-hand side in Equation (2.1.2) represent, respectively, the viscous force and the buoyancy force, which acts as a body force.

Energy equation

$$\frac{\partial \rho h}{\partial t} + \frac{\partial}{\partial x_j}(\rho u_j h) = \frac{\partial}{\partial x_j}\left(\frac{\lambda}{c_p}\frac{\partial h}{\partial x_j}\right) + S_h \qquad (2.1.3)$$

where λ and c_p are the thermal conductivity and the specific heat at constant air pressure, respectively. The first term on the right-hand side of Equation (2.1.3) is the conduction term. S_h denotes the heat produced by sources such as chemical reaction. Generally speaking, the heat generated by dissipation of mechanical energy has negligible effects on the airflow in rooms.

Component conservation equation

$$\frac{\partial \rho c}{\partial t} + \frac{\partial}{\partial x_j}(\rho u_j c) = \frac{\partial}{\partial x_j}\left(\rho D \frac{\partial c}{\partial x_j}\right) + S_c \qquad (2.1.4)$$

where D is the diffusion coefficient of contaminant in air. S_c denotes the source of the component.

For laminar flows, μ, λ and D in the above equations are all material properties, called molecular transportation coefficients. They indicate the ability of transportations of momentum, energy and mass, respectively.

These differential equations are coupled with each other and must be solved simultaneously. So far, there is no general analytical solution available. Attempts are concentrated on numerical methods.

In order to make the set of differential equations closed, proper initial and boundary conditions are required.

2.2 Boundary Conditions

The initial conditions consist of the given velocity, pressure, temperature and concentration distributions over the entire flow field. For steady state problems, initial conditions are not needed.

Because boundary conditions are differently assigned in each case, it will be better to give detailed discussion individually for each case study. The physically general boundary conditions for an impermeable and smooth solid surface may be described as follows:

$$u = v = w = 0 \tag{2.2.1}$$

$$h/c_p = T = \text{constant} \quad \text{for isothermal surface} \tag{2.2.2}$$

$$dh/dn = 0 \quad \text{for insulated surface} \tag{2.2.3}$$

$$c = 0 \tag{2.2.4}$$

$$\frac{\partial \phi}{\partial n} = 0 \quad \text{for exit} \tag{2.2.5}$$

where ϕ stands for flow properties (velocity, temperature, turbulence energy etc), and n denotes the outward direction perpendicular to the solid surface. The velocity boundary condition is based on the assumption that viscous fluids adhere to solid surfaces.

CHAPTER 3

TURBULENCE SIMULATION

3.1 Mathematical Model of Turbulence

Air movement in enclosures can be driven by temperature differences, by infiltration, by ventilation, or by any combination thereof. In the case of natural convection, airflow may begin a transition from laminar to turbulent flow when the Rayleigh number is over 10^9 (Cheesewright 1968). In ventilated enclosures, the airflow is mainly turbulent. It is difficult to give a precise definition of turbulence. However, the nature of turbulence can be described by its characteristics, such as irregularity, diffusivity, high Reynolds number, three-dimensional vorticity fluctuation, and dissipation (Tennekes and Lumley, 1972). It makes a deterministic approach to turbulence problems impossible; instead, one relies on statistical method. The methods which are applied to predict turbulent flows are called turbulent models.

For turbulent flow, the variables in the momentum equation (Equation 2.1.2) are their instantaneous values. These values change rapidly with random turbulent fluctuation. Reynolds (1894) proposed that, in turbulent flow, the instantaneous variables be decomposed into two terms, a local value averaged over time and a fluctuating value. Taking the velocity component in the x direction as an example, one would have

$$u_t = \bar{u} + u' \qquad (3.1.1)$$

where u_t is the instantaneous value in the turbulence flow. $\bar{u}$ and u' represent the value averaged over time (called mean value for simplicity) and the turbulent fluctuating component, respectively. The symbol $\bar{}$ means averaging over time, the definition of which is

$$\bar{u} = \frac{1}{t_2-t_1} \int_{t_1}^{t_2} u \, dt \qquad (3.1.2)$$

The averaging time (t_2-t_1) should be long enough when compared with the time scale of the turbulence. The relation between the mean value and fluctuation is what a turbulence theory focuses on.

Substituting Equation (3.1.1) into Equation (2.1.2) and averaging the resultant equation over time lead to the averaged equation of turbulent motion, namely, the Reynolds equation

$$\frac{\partial \bar{u}_i}{\partial t} + \frac{\partial \bar{u}_i \bar{u}_j}{\partial x_j} = -\frac{1}{\rho}\frac{\partial \bar{p}}{\partial x_i} + \frac{\partial}{\partial x_j}\left[\frac{\mu}{\rho}\left(\frac{\partial \bar{u}_i}{\partial x_j} + \frac{\partial \bar{u}_j}{\partial x_i}\right) - \overline{u_i' u_j'}\right] + \beta\,(\bar{T}_o - \bar{T})g_i \qquad (3.1.3)$$

The following relations are applied for any fluctuating quantity q or f in the averaging process:

$$(1)\ \bar{\bar{q}} = \bar{q} \qquad (3.1.4)$$

$$(2)\ \bar{q}' = 0 \qquad (3.1.5)$$

$$(3)\ \overline{\bar{q} f'} = 0 \qquad (3.1.6)$$

$$(4)\ \overline{\frac{\partial^m q}{\partial x^m}} = \frac{\partial^m \bar{q}}{\partial x^m} \qquad (3.1.7)$$

$$(5)\ \overline{\frac{\partial q}{\partial t}} = \frac{\partial \bar{q}}{\partial t} \qquad (3.1.8)$$

$$(6)\ \overline{\frac{\partial^{m+n} q}{\partial t^m \partial x^n}} = \frac{\partial^{m+n} \bar{q}}{\partial t^m \partial x^n} \qquad (3.1.9)$$

Derivations of these relations are based on Reynolds averaging rules (Pan, 1982).

The new term $\overline{u_i' u_j'}$ appearing in Equation (3.1.3) is a second-order tensor. Physically, it indicates the momentum transfer by turbulent fluctuation, or turbulent diffusion of momentum. This term plays the similar role as the simple Newtonian shear stress in a laminar flow. Therefore the grouping $(-\rho\ \overline{u_i' u_j'})$ is termed turbulent stress, or the Reynolds stress tensor, denoted by $\bar{\tau}_t$. Since this term is unknown, the Reynolds equation is not solvable unless it can be somehow determined. The problem in solving turbulent flow turns out to be how to predict the turbulent stress.

There are a number of approaches predicting the turbulent stress. They can be placed in two categories: first-order and second-order models. In the first-order model, the turbulent shear stress is directly related to the mean velocity field by the Boussinesq suggestion (1877); in the second-order model, the turbulent shear stress is determined by solving the conservation equation together with mean flow equations.

The method of prediction adopted in this study belongs to the first-order model, which is more suitable for engineering application. In these approaches, the eddy viscosity concept introduced by Boussinesq (1877) is employed. Following Newton's law of molecular viscosity, Boussinesq suggested that the effective turbulent shear stress could be

replaced by the products of the mean velocity gradient and a quality termed the "turbulent viscosity". Thus, the turbulent transportation of momentum is attributed to the turbulent (or eddy) viscosity. With this in mind, the Reynolds stress can be written in the following form:

$$- \overline{u_i' u_j'} = \nu_t \left(\frac{\partial u_i}{\partial x_j} + \frac{\partial u_j}{\partial x_i} \right) - \frac{2}{3} \delta_{ij} k \qquad (3.1.10)$$

where ν_t is named turbulent viscosity. It should be understood that the mechanism of turbulent transportation is completely different from that of molecular transportation. Molecular momentum transfer in a gas is characterized by a large number of identifiable and small particles exchanging momentum through discontinuous interactions. Turbulent momentum transport, on the other hand, is characterized by a much smaller number of large and poorly defined fluid eddies exchanging momentum through continuous interactions. Unlike molecular viscosity, which is a property of fluid, the turbulent viscosity is not a property of a fluid, but a characteristic of flows. Its value varies from point to point and is determined by models of turbulence. Using the Boussinesq suggestion, the problem of turbulent flows becomes how to determine the turbulent viscosity, ν_t.

Prandtl (1926) proposed the mixing-length hypothesis. He supposed that this turbulent viscosity might be determined by the product of a length (called mixing length) and a random velocity (turbulence velocity) as

$$\nu_t = l_m V_t \qquad (3.1.11)$$

where l_m is the mixing length, which is similar to the mean free path

between molecules, but here between eddies. The turbulence velocity, V_t, was assumed to be

$$V_t = l_m \left|\frac{\partial u}{\partial y}\right| \qquad (3.1.12)$$

Thus, the turbulent stress can be written as

$$-\rho \overline{u'v'} = \rho l_m^2 \left|\frac{\partial u}{\partial y}\right| \frac{\partial u}{\partial y} \qquad (3.1.13)$$

Combining Equation (3.1.11) with (3.1.12), the turbulent viscosity, ν_t, is in the form of

$$\nu_t = \mu_t/\rho = l_m^2 \left|\frac{\partial u}{\partial y}\right| \qquad (3.1.14)$$

This model has been applied to relatively simple flows, in which l_m can be specified by simple empirical formulae, such as free layers, wall boundary layers, developed duct flows and so on. The shortcomings of this model, however, are evident. Equation (3.1.14) indicates that the turbulent viscosity vanishes wherever the mean velocity gradient is zero. It is not physically reasonable.

In order to sidestep the shortcomings of the mixing-length hypothesis, Prandtl (1945) and Kolmogorov (1942) independently suggested that the turbulence velocity be expressed in terms of a time-averaged turbulence kinetic energy. As turbulent diffusion is caused by turbulent fluctuation, the kinetic energy of turbulence, k, is a direct measure of the turbulent fluctuation, and, therefore, could be a meaningful scale for the turbulent viscosity. Thus, the following expression was introduced to relate the turbulent viscosity to k:

$$\nu_t = c'_\mu \, l \, (k)^{1/2} \qquad (3.1.15)$$

where c'_μ is an empirical constant, and l is the length scale of turbulence. The kinetic energy of turbulence, k, is defined as

$$k = 1/2 \, u_i'^2 \qquad (3.1.16)$$

and is determined by another differential conservation equation. This model is classified as a one-equation model. There are other one-equation models, such as that proposed by Bradshaw (1967). However, in the one-equation models, the distribution of the length scale, l, still needs to be prescribed. In other words, the application of the one-equation models, just as with the mixing-length hypothesis, is based on a well predicted distribution of l. Thus, because of the difficulty in specifying l, this model is not applicable to complex flows. Besides, this model does not account for the transportation of turbulence, i.e., the convection and diffusion of turbulent fluctuation.

The above-mentioned limitations can be overcome by some higher level models, i.e., two-equation models. The idea behind two-equation models is to determine the distribution of the length scale of turbulence by solving an additional differential conservation equation. Harlow and Nakayama (1968) proposed a quantity ($k^{3/2}/l$) as a dependent variable to be solved in the second differential equation. Since the quantity ($k^{3/2}/l$) indicates another turbulence property, the dissipation rate of the turbulent energy ε, this model, after modification by Launder and Spalding (1974), has been called the k-ε two-equation model. In this model, the length scale in Equation (3.1.15) is determined from k and ε in the following expression:

$$l = C_D k^{3/2}/\varepsilon \qquad (3.1.17)$$

where C_D is another empirical constant, and ε is defined as

$$\varepsilon = \frac{\mu}{\rho} \frac{\overline{\partial u_i' \partial u_i'}}{\partial x_j \partial x_j} \qquad (3.1.18)$$

Combining Equations (3.1.15) and (3.1.17) gives the expression of ν_t in k-ε model

$$\nu_t = C_\mu' . C_D k^2/\varepsilon \qquad (3.1.19)$$

Replacing the product of $C_\mu' . C_D$ by C_μ, the above expression becomes

$$\nu_t = c_\mu \, k^2/\varepsilon \qquad (3.1.20)$$

The turbulence properties, k and ε, are functions of position. Their distributions in a flow field are determined by their own conservation equations (Rodi, 1984) as

$$\frac{\partial \rho k}{\partial t} + \frac{\partial (u_i \rho k)}{\partial x_i} = \frac{\partial}{\partial x_i} \left(\frac{\mu_{eff}}{\sigma_{k,eff}} \frac{\partial k}{\partial x_i} \right) + G_K + G_B - \rho\varepsilon \qquad (3.1.21)$$

$$\frac{\partial \rho \varepsilon}{\partial t} + \frac{\partial (u_i \rho \varepsilon)}{\partial x_i} = \frac{\partial}{\partial x_i} \left(\frac{\mu_{eff}}{\sigma_{\varepsilon,eff}} \frac{\partial \varepsilon}{\partial x_i} \right) + C_1 \frac{\varepsilon}{k} (G_K + G_B)(1 + C_3 R_f) - C_2 \rho \frac{\varepsilon^2}{k} \qquad (3.1.22)$$

where G_K is the stress production term, denoting the transfer of kinetic energy from the mean flow to the turbulent motion. G_B is the generation term related to buoyancy, representing the exchange between the kinetic

energy of the turbulence and the potential energy of the flow. They are expressed by

$$G_K = \mu_{eff}\left(\frac{\partial u_i}{\partial x_j} + \frac{\partial u_j}{\partial x_i}\right)\frac{\partial u_i}{\partial x_j} \qquad (3.1.23)$$

$$G_B = -\beta\,\rho\,g\,\frac{\nu_t}{\sigma_t}\,\frac{\partial \theta}{\partial z} \qquad (3.1.24)$$

R_f is the flux Richardson number, which is in the form

$$R_f = -G_B/G_K \qquad (3.1.25)$$

In stable stratification, G_B becomes a sink term, so that the turbulent mixing is reduced while the potential energy is increased. In unstable stratification, turbulent energy is produced at the expense of potential energy. The numerical values of the coefficients appearing in the conservation equations for k and ε are all determined from experiments. At high Reynolds numbers, they are approximately constant.

In this study, the following values, recommended by Launder and Spalding (1974), are assigned to the constants:

$C_1 = 1.44$	$C_2 = 1.92$	$C_\mu = 0.09$	$C_D = 1.0$
$\sigma_k = 1.0$	$\sigma_\varepsilon = 1.3$	$\sigma_t = 1.0$	

Coefficient C_3, the multiplier of the flux Richardson number R_f, is an additional buoyancy constant. Its value should be close to zero for vertical buoyancy shear layers and close to unity for horizontal layers. The k-ε model is so far the simplest means available for computing

Reynolds stress in complex flow fields. It has been widely applied to investigate air movement and other phenomena dealing with recirculation and separated flow.

Equations (2.1.1) through (2.1.4), together with Equations (3.1.21) and (3.1.22), the conservation equations for k and ε, compose the governing equations for three-dimensional turbulent heat and mass transfer problems in incompressible turbulent flow fields. For the sake of simplification in numerical simulation, these equations can be written in a common form, as follows:

$$\frac{\partial \rho\phi}{\partial t} + \frac{\partial}{\partial x_i}(\rho u_i \phi) = \frac{\partial}{\partial x_i}\left(\Gamma_{\phi,eff}\frac{\partial \phi}{\partial x_i}\right) + S_\phi \qquad (3.1.26)$$

where ϕ denotes the variables u_i, h, c, k, or ε. S_ϕ represents the source term for each of the variables, listed in Table (3.1.1). $\Gamma_{\phi,eff}$ is the effective exchange coefficient. For the momentum equation, it is the sum of eddy viscosity and molecular viscosity

$$\Gamma_{u,eff} = \mu_{u,eff} = \mu_t + \mu \qquad (3.1.27)$$

For other scalars, the effective exchange coefficients can be expressed in terms of the effective viscosity coefficient as

$$\Gamma_{\phi,eff} = \mu/\sigma_\phi + \mu_t/\sigma_{\phi,t} \qquad (3.1.28)$$

where σ_ϕ and $\sigma_{\phi,t}$ are the laminar and turbulent exchange-coefficient ratios respectively. They are referred to the laminar and the turbulent Prandtl number or Schmidt number. Their values are usually obtained from experimental data.

The first and second terms on the left-hand side of Equation

(3.1.26) are the transient and convection terms, respectively. The first and second terms on the right-hand side are the diffusion and source terms, respectively. The physical meaning of the conservation equations is thus easily to be understood, i.e., for each variable, the variation due to the transition together with the variation caused by convection is equal to the variation due to diffusion plus the increase/decrease from the source/sink.

It should be mentioned that the k-ε two-equation model of turbulence is valid only for the high-Reynolds-number flow. At the region near a solid surface, where the viscosity effects become important, the high-Reynolds-number model is not applicable. Special treatments for the region near the wall are required. The wall function method is widely adopted in engineering applications to reflect the character of a flow in the region near a solid surface. The rationale of the wall functions will be explained in the next section.

The high-Reynolds-number k-ε model can be extended to low-Reynolds-number models by employing additional empirical information. With the low-Reynolds-number k-ε model, no special treatment for the region near the solid surface is needed. However, the boundary conditions for k and ε must be specified. There are a number of low-Reynolds-number k-ε models, reviewed by Patel et al. (1985). The one developed by Lam and Bremhorst (1981) and later modified by Chen et al. (1990A) for buoyant flow seems to present more reasonable results for airflow in buildings

The turbulence models which do not adopt the Boussinesq suggestion but employ differential equations for solving the Reynolds stress are regarded as second-order models or Reynolds stress models (Hanjalic and

Launder, 1972; Daly and Harlow, 1970; and Donaldson, 1972). These models have been used mainly to study turbulence rather than to solve engineering problems because of their complexity.

Large eddy simulation (Deardorff, 1970) is a more elaborate approach to simulate turbulent flow. Although this approach has been applied in room airflow simulation, and its accuracy has been confirmed (Sakamoto et al. 1980; Murakami et al. 1985), it is too time-consuming to be useful in engineering.

3.2 Wall Function

A narrow region exists near solid surfaces where the turbulent fluctuations must be strongly dampened since right at the surface, $u'=v'=w'=0$. In this region, the turbulent viscosity is no longer dominant. Thus, the k-ε model, which is applicable only for high-Reynolds number turbulent flows, is not valid in this region, and a special treatment is required to describe the flow properties. The wall function method is the most widely used to deal with this problem.

The wall functions are based on the one-dimensional steady-state boundary layer equations and the mixing-length hypothesis. The principle of the wall function method is using the momentum flux due to shear stress and the heat flux at solid surfaces to modify the source terms in the conservation equations for the grid nodes near the solid surfaces. Thus, the boundary information of solid surfaces can be transferred into the flow field. The shear stress reduces the velocity component parallel

to the walls. The turbulent energy in the region near the wall is diminished as well. Therefore, the shear stress contributes to the sink term of their conservation equations. The derivation of the wall functions employed in this study is presented in the following paragraph.

The actual turbulent flow is always three-dimensional regardless of how simple the flow boundary is. However, according to the characteristics of the boundary layer flow, the momentum equation and energy equation in this region can be simplified, with some assumptions, into the two-dimensional boundary layer equations

$$\rho u\frac{\partial u}{\partial x} + \rho v\frac{\partial u}{\partial y} = -\frac{dp}{dx} + \frac{\partial}{\partial y}\left(\mu_{eff}\frac{\partial u}{\partial y}\right) \qquad (3.2.1)$$

$$\rho u\frac{\partial h}{\partial x} + \rho v\frac{\partial h}{\partial y} = -\frac{\partial}{\partial y}\left(\frac{\mu_{eff}}{\sigma_{h,eff}}\frac{\partial h}{\partial y} - u\tau\right) \qquad (3.2.2)$$

where v is the velocity component perpendicular to the wall. τ and $\sigma_{h,eff}$ represent shear stress and the effective Prandtl number, respectively. $u\tau$ denotes the work produced by viscous shear stress which belongs to the source term in Equation (2.1.3).

If the gradient of variables in the x direction (parallel to the solid surface) is negligible, the boundary layer equations become equations for Couette flow, a one-dimensional flow. Integrating the resultant equations yields:

$$\tau = \tau_s + m_s u + y\frac{dp}{dx} \qquad (3.2.3)$$

$$-q = -q_s + m_s(h - h_s) - u\tau \qquad (3.2.4)$$

where m_s represents the product $\rho_s v_c$, the mass flux across the layer. q_s stands for the heat conduction at the solid surface, which is determined by $q_s = \left(\frac{\lambda}{C_p}\frac{\partial h}{\partial y}\right)_s$. The subscript s stands for the wall surface.

In order to simplify Equations (3.2.3) and (3.2.4), the following set of dimensionless parameters and variables is defined.

$$\tau^+ = \tau / \tau_s \qquad (3.2.5)$$

$$y^+ = y\, u_\tau/\nu = \frac{y}{\mu}(\tau_s\rho)^{1/2} \qquad (3.2.6)$$

$$u_\tau = (\tau_s/\rho)^{1/2} \qquad (3.2.7)$$

$$u^+ = u/u_\tau = u/(\tau_s/\rho)^{1/2} \qquad (3.2.8)$$

$$p^+ = \mu\,(dp/dx)(\tau_s^3\rho)^{-1/2} \qquad (3.2.9)$$

$$m^+ = m_s/(\tau_s\rho)^{1/2} \qquad (3.2.10)$$

$$q^+ = q/q_s \qquad (3.2.11)$$

$$T^+ = (h-h_s)(\tau_s\rho)^{1/2}/(-q_s) \qquad (3.2.12)$$

$$\mu^+ = \mu_{eff}/\mu \qquad (3.2.13)$$

$$W = (\tau_s^3/\rho)^{1/2}/(-q_s) \qquad (3.2.14)$$

Then, Equations (3.2.3) and (3.2.4) can be rewritten as

$$\tau^+ = 1 + p^+y^+ + m^+u^+ \qquad (3.2.15)$$

$$q^+ = 1 + m^+T^+ - W\, u^+\tau^+ \qquad (3.2.16)$$

Combining the transport laws, Newton's for momentum, Fourier's for energy, with above two equations yields

$$\frac{du^+}{dy^+} = \frac{1+m^+u^+ + p^+y^+}{\mu^+} \qquad (3.2.17)$$

$$\frac{dT^+}{dy^+} = \frac{1+ m^+T^+}{\mu^+/\sigma_{h,eff}} + \left(\frac{1-\sigma_{h,eff}}{2} \right) W \frac{d(u^+)^2}{dy^+} \qquad (3.2.18)$$

The mixing-length hypothesis is applicable for the Couette flow in the fully turbulent region. Assuming the distribution of the mixing length to be in the form

$$l_m = \kappa y \qquad (3.2.19)$$

and that the molecular viscosity is negligible in comparison with the turbulent viscosity ($\mu_{eff} \cong \mu_t$), the mixing-length hypothesis gives the dimensionless viscosity μ^+ in the Couette flow as follows:

$$\mu^+ = \kappa^2 (y^+)^2 \frac{du^+}{dy^+} \qquad (3.2.20)$$

For the case where $m^+=0$ and $p^+=0$, substituting Equation (3.2.20) into Equation (3.2.17) and integrating the resultant equation yields the dimensionless velocity distribution

$$u^+ = \ln(Ey^+)/\kappa \qquad (3.2.21)$$

where κ is von Karman's constant (κ=0.435). E is a coefficient reflecting the roughness of the wall. For rough walls, the only way to

determine E is through experiments. For smooth walls, supposing that the mixing-length hypothesis applies for the fully turbulent region, E may be determined by employing the Van Driest hypothesis (1956):

$$\mu^+ = 1 + \kappa^2 y^{+2} \left[1-\exp\left(-\frac{y^+\tau^{+1/2}}{A}\right)\right]^2 \frac{du^+}{dy^+} \qquad (3.2.22)$$

where A is Van Driest's constant, equal to 26.0 for smooth walls. The second term in the brackets on the right-hand side of Equation (3.2.22) represents the turbulent viscosity which diminishes in an exponential fashion with the increase in distance from a solid wall. Substituting this equation into Equation (3.2.17) and integrating the resultant equation, the E-value can be determined as 9.0.

Equation (3.2.18) has an analytical solution when the mixing-length hypothesis prevails in the outer part of the Couette flow, and when there is no pressure gradient. Also, kinetic heating should be negligibly small. Equations (3.2.17) and (3.2.18) can then be combined, with the result

$$\frac{d\bar{T}^+}{du^+} = \sigma_{h,eff} \frac{1+m^+T^+}{1+m^+u^+} \qquad (3.2.23)$$

In the fully turbulent part of the boundary layer, The molecular viscosity is negligible, and $\sigma_{h,eff}$ takes on the constant value $\sigma_{h,t}$. Integrating Equation (3.2.23) yields

$$\ln(1+m^+T^+) = \sigma_{h,t}\left[\ln(1+m^+u^+) + m^+P\right] \qquad (3.2.24)$$

where P is independent of u^+, but may be expected to depend on both $\sigma_{h,t}$ and m^+. When the mass transfer rate is zero, this equation reduces to

$$T^+ = \sigma_t \, (u^+ + P) \tag{3.2.25}$$

The value of P depends on the way in which $\sigma_{h,eff}$ varies in the region where laminar viscosity is not negligible. P can be either deduced directly from experimental data or evaluated theoretically based on the Van Driest hypothesis, which results (Patankar and Spalding, 1970) in

$$P = \frac{\pi}{4 \sin(\pi/4)} \left(\frac{A}{\kappa}\right)^{1/2} (\sigma_h/\sigma_{h,t} - 1)(\sigma_{h,t}/\sigma_h)^{1/4} \tag{3.2.26}$$

The fluxes of momentum and heat to solid surfaces are determined by Equations (3.2.21) and (3.2.25). They can also be written (Launder and Spalding, 1974) as

$$\frac{u_p}{\tau_s/\rho} C_\mu^{1/4} k_p^{1/2} = \frac{1}{\kappa} \ln \left[E \, y_p \frac{(C_\mu^{1/2} k_p)^{1/2}}{\nu} \right] \tag{3.2.27}$$

$$\frac{(T_p - T_s) C_p \rho \, C_\mu^{1/4} k_p^{1/2}}{q_s} = \frac{\sigma_{h,t}}{\kappa} \ln \left[E \, y_p \frac{(C_\mu^{1/2} k_p)^{1/2}}{\nu} \right] + \sigma_{h,t} \frac{\pi}{4 \sin(\pi/4)} \left(\frac{A}{\kappa}\right)^{1/2} (\sigma_h/\sigma_{h,t} - 1)(\sigma_{h,t}/\sigma_h)^{1/4} \tag{3.2.28}$$

At the grids near a wall, the source term in kinetic energy of turbulence needs to be modified by the shear stress, τ_s. Thus, the shear stress determined from Equation (3.2.21) is rearranged in the form

$$\tau_s = \frac{\mu \kappa y^+}{\ln(E y^+)} \frac{U_w}{y} \tag{3.2.29}$$

where U_w is the total velocity parallel to the wall. If the wall is perpendicular to the z direction, U_w is calculated from the latest value of u and v as

$$U_w = (u^2 + v^2)^{1/2} \qquad (3.2.30)$$

Note that the molecular viscosity is neglected in the derivation of this equation.

In the laminar sublayer, the dimensionless velocity is a linear function of y^+, as

$$u^+ = y^+ \qquad (3.2.31)$$

A value of y^+ less than 11.5 is suggested for the region of the laminar sublayer. The shear stress in the viscous sublayer can be written as

$$\tau_s = \mu\, u/y \qquad (3.2.32)$$

In numerical computation, the effects of solid walls on flow properties are taken into account by modification of the source in the conservation equations through τ_s or q_s. When calculating k at the grid nodes near walls, the normal generation term G_k is replaced by the volume averaged rate of generation across the control volume for k, i.e.

$$\bar{G} = \frac{1}{V} \int_V \tau \frac{\partial U_w}{\partial y}\, dv \cong \tau_s \frac{(U_w)}{\Delta y} \qquad (3.2.33)$$

The source terms of variables at the grids near a wall are corrected by shear stress and heat fluxes as follows:

$$(s_u)_p = s_u - \tau_s A \qquad \text{for the velocity component parallel to the wall} \qquad (3.2.34)$$

$$(s_h)_p = s_h - q_s A \qquad \text{for enthalpy} \qquad (3.2.35)$$

$$(s_k)_p = s_k + \tau_s \frac{(U_w)}{\Delta y} - G_k \qquad \text{for turbulent energy} \qquad (3.2.36)$$

where subscript p stands for the grid point near the wall. A is the area of the control volume surface parallel to the wall. In the three expressions above, s stands for the source term integrated over the control volume, u represents the velocity component parallel to the wall.

It is known that the laminar sublayer is very thin. In this region, one can suppose that the shear stress, τ, is constant and equal to the shear stress at the wall τ_s. Furthermore, the convection and diffusion terms in Equation (3.1.21) could be negligible, which would indicate a balance between the production term and dissipation term

$$\frac{\tau_s}{\rho} \frac{\partial U_w}{\partial y} = \varepsilon \qquad (3.2.37)$$

This equation, together with Equation (3.2.21) and (3.2.7), leads to

$$\varepsilon_p = C_\mu^{0.75} k^{1.5}/(\kappa y_p) \qquad (3.2.38)$$

from which the dissipation rate at the grids near a wall could be computed directly.

With the wall function, the high-Reynolds-number k-ε model can predict the turbulence properties for the entire flow region. The wall function has some merits. It economizes computing time and storage and allows the introduction of additional empirical information in special cases, such as for rough walls.

However, when the wall function method is applied, the grid nodes near walls must be sufficiently remote from them to ensure that the turbulent Reynolds number, $(k^{1/2}l/\nu)_p$, is much greater than unity, and that the viscous effects are entirely overwhelmed by those of turbulent viscosity.

CHAPTER 4

NUMERICAL PROCEDURE

4.1 The Concept of Discretization

In general, exact solutions for the system of second-order partial differential equations described in Chapter 2 are not available, except for some very special cases. Thus, the only way to solve the governing equations described in Chapter 2 is through numerical method. There are two main approaches used in the numerical solution of the conservation equations: the finite-difference method and the finite-element method. In this study, the finite-difference method is employed. This method is preferable when the boundary of the flow field is relatively simple.

In order to solve the governing equations by the finite-difference method, discretization of the differential equations is necessary; i.e., the continuous problem domain must be replaced by a finite-difference mesh or grid. This can be done in many ways, such as Taylor-series formulation, variational formulation, control volume formulation, etc. In the control-volume method, which is employed in this study, the continuous calculation domain is discretized into a number of subdomains, namely control volumes. The differential equation is integrated over each control volume. Piecewise profiles expressing the variation of dependent variables, ϕ, between the grid points are used to evaluate the required integrals. It is this systematic discretization of space and of the dependent variables that make it possible to replace

the governing differential equations with simple algebraic equations, which can be solved with relative ease. The discretization equation obtained in this manner expresses the conservation principle for ϕ in the finite-control volume, just as the differential equation expresses it for an infinitesimal control volume. Thus, the solution of the discretization equations implies that the integral conservation of all dependent variables is exactly satisfied over any group of control volumes and the whole calculation domain. In other words, even the coarse-grid solution achieves exact integral balance.

4.2 Grid Structure

A three-dimensional mesh system in Cartesian coordinates is employed in this study. However, for the sake of simplicity, a two-dimensional structure of the mesh system is illustrated in Figure 4.2.1. The boundaries of the control volume for h, c, k and ε (solid line) are identical with the physical boundaries. For the velocity components u, v and w, the staggered control volumes are employed; i.e., the grid nodes of u, v and w lie on the centers of the interfaces of the control volumes for the scalar variables. For example, the velocity component in the x direction, u, is calculated at the interfaces that are normal to the x direction as shown by small horizontal arrows. Note that with respect to the main grid points, the u locations are staggered only in the x-direction. As a result, the number of u grid nodes to be computed in this direction is one node less than the other dependent

variables. For velocities v and w, the control volumes are staggered in the y and z directions, respectively. The advantages of the staggered grid are as follows.

(1) The mass flow rate across the control volume interfaces of the main grid points can be calculated without any interpolation for the relevant velocity component.

(2) The pressure difference between two adjacent grid points becomes a natural driving force for the velocity component located between them. Consequently, a zigzag pressure field would no longer be felt as a uniform pressure field (Patankar, 1980).

4.3 Derivation of the Finite-Domain Equations

In each of the control volumes, the variables are assumed to have a uniform value. Consequently, integrations can be performed over each control volume to yield the discretization equations of finite-difference form.

The differential conservation equation (3.1.26) can be written as

$$\frac{\partial}{\partial t}(\rho\phi) + \frac{\partial}{\partial x} J_x + \frac{\partial}{\partial y} J_y + \frac{\partial}{\partial z} J_z = S_\phi \qquad (4.3.1)$$

where

$$J_x = \rho u\phi - \Gamma_{\phi,eff} \frac{\partial \phi}{\partial x} \qquad (4.3.2)$$

$$J_y = \rho v\phi - \Gamma_{\phi,eff} \frac{\partial \phi}{\partial y} \qquad (4.3.3)$$

$$J_z = \rho w \phi - \Gamma_{\phi,eff} \frac{\partial \phi}{\partial z} \qquad (4.3.4)$$

Integration of Equation (4.3.1) in the x, y and z directions respectively, yields

$$\frac{\rho_p \phi_p - \rho_p^\circ \phi_p^\circ}{\Delta t} \Delta x \Delta y \Delta z + (J_e - J_w) + (J_n - J_s) + (J_t - J_b) = S_\phi \Delta x \Delta y \Delta z \qquad (4.3.5)$$

where J_e, J_w, J_n, J_s, J_t and J_b stand for the integrated total flux; for example, J_e stands for $\int J_x dydz$ over the interface e. Subscripts e, w, n, s, t and b represent the six interfaces of the control volumes, as illustrated in Figure 4.2.2 (interfaces t and b are not included), while subscript p indicates the currently computed node. Superscript o stands for the values at the previous time step.

The continuity equation (2.1.1) can be integrated over control volumes to obtain

$$\frac{\rho_p - \rho_p^\circ}{\Delta t} \Delta x \Delta y \Delta z + (F_e - F_w) + (F_n - F_s) + (F_t - F_b) = 0 \qquad (4.3.6)$$

where

$$F_e = (\rho u)_e \Delta y \Delta z \qquad (4.3.7)$$

$$F_w = (\rho u)_w \Delta y \Delta z \qquad (4.3.8)$$

$$F_n = (\rho v)_n \Delta x \Delta z \qquad (4.3.9)$$

$$F_s = (\rho v)_s \Delta x \Delta z \qquad (4.3.10)$$

$$F_t = (\rho w)_t \Delta x \Delta y \qquad (4.3.11)$$

$$F_b = (\rho w)_b \, \Delta x \Delta y \qquad (4.3.12)$$

Multiplying Equation (4.3.6) by ϕ_p and subtracting it from (4.3.5), one obtains

$$(\phi_p - \phi_p^\circ) \frac{\rho_p^\circ \Delta x \Delta y \Delta z}{\Delta t} + (J_e - F_e \phi_p) - (J_w - F_w \phi_p) + (J_n - F_n \phi_p) - (J_s - F_s \phi_p) + (J_t - F_t \phi_p) - (J_b - F_b \phi_p) = S_\phi \, \Delta x \Delta y \Delta z \qquad (4.3.13)$$

The term $(J - F\phi_p)$ denotes physically the net flux of variable ϕ at interfaces caused by diffusion and convection. It can be expressed as

$$J_e - F_e \phi_p = a_E (\phi_p - \phi_E) \qquad (4.3.14a)$$

$$J_w - F_w \phi_p = a_W (\phi_W - \phi_P) \qquad (4.3.14b)$$

Similar equations can be written for the interfaces n, s, t, and b. a is named neighbor coefficient, which is dependent on the scheme employed in the numerical computation. The Hybrid scheme developed by Spalding (1972) is adopted here, which is a combination of the central-difference scheme and the upwind scheme with neglecting the diffusion term in upwind scheme. This scheme has been widely applied in the computation of fluid mechanics since it is easy to use and presents a reasonable approximation to the real situation. In the Hybrid scheme, the determination of the neighbor coefficient is dependent on the cell Peclet number, which denotes the strength ratio of convection to diffusion, defined as

$$Pe = \frac{F}{D} = \frac{\rho u(\Delta x)}{\Gamma} \qquad (4.3.15)$$

where F has the same content as that in Equation (4.3.7), and D stands for the diffusion transport at control volume interfaces. For interface e, it can be expressed as

$$D_e = \frac{\Gamma_e \Delta y \Delta z}{(\delta x)_e} \qquad (4.3.16)$$

At interface w, a_W could be one of three values, depending on the Peclet number. They are

$$a_W = 0 \qquad \text{when} \quad Pe < -2 \qquad (4.3.17)$$

$$a_W = D_w\,(1 + Pe/2) = D_w + F_w/2 \qquad \text{when} \quad -2 < Pe < 2 \qquad (4.3.18)$$

$$a_W = D_w Pe = F_W \qquad \text{when} \quad Pe > 2 \qquad (4.3.19)$$

At interface e, the neighbor coefficient is expressed as:

$$a_E = D_e\,(-Pe) = -F_e \qquad \text{when} \quad Pe < -2 \qquad (4.3.20)$$

$$a_E = D_e\,(1 - Pe/2) = D_e - F_e/2 \qquad \text{when} \quad -2 < Pe < 2 \qquad (4.3.21)$$

$$a_E = 0 \qquad \text{when} \quad Pe > 2 \qquad (4.3.22)$$

Similar relations can be written for a_S, a_N, a_B, and a_T. For simplicity, all the neighbor coefficients can be written as

$$a_E = \| \, |0.5F_e|, D_e \, \| - 0.5F_e \qquad (4.3.23)$$

$$a_W = \| \, |0.5F_w|, D_w \, \| + 0.5F_w \qquad (4.3.24)$$

$$a_N = \| \, |0.5F_n|, D_n \, \| - 0.5F_n \qquad (4.3.25)$$

$$a_S = \| |0.5F_s|, D_s \| + 0.5F_s \tag{4.3.26}$$

$$a_T = \| |0.5F_t|, D_t \| - 0.5F_t \tag{4.3.27}$$

$$a_B = \| |0.5F_b|, D_b \| + 0.5F_b \tag{4.3.28}$$

where the symbol $\| \quad \|$ stands for the larger value of the quantities contained within it.

The upwind scheme is also included in the numerical model as an option. In the upwind scheme, the convected property at the interface is always equal to the one on the upwind side of the interface. Thus, the neighbor coefficients can be written in the following form

$$a_E = \| -F_e, 0 \| + D_e \tag{4.3.29}$$

$$a_W = \| F_w, 0 \| + D_w \tag{4.3.30}$$

$$a_N = \| -F_n, 0 \| + D_n \tag{4.3.31}$$

$$a_S = \| F_s, 0 \| + D_s \tag{4.3.32}$$

$$a_T = \| -F_t, 0 \| + D_t \tag{4.3.33}$$

$$a_B = \| F_b, 0 \| + D_b \tag{4.3.34}$$

The three-dimensional discretization equation can finally be expressed as

$$\phi_p = \frac{a_W\phi_W + a_E\phi_E + a_N\phi_N + a_S\phi_S + a_T\phi_T + a_B\phi_B + b}{a_p} \tag{4.3.35}$$

with

$$b = S_c \Delta x \Delta y \Delta z + a_p^\circ \phi_p^\circ \tag{4.3.36}$$

$$a_p = a_W + a_E + a_N + a_S + a_T + a_B + a_p^\circ - S_p \Delta x \Delta y \Delta z \tag{4.3.37}$$

$$a_p^\circ = \rho_p^\circ \Delta x \Delta y \Delta z / \Delta t \tag{4.3.38}$$

It should be mentioned that in Equation (4.3.35), the source term, S_ϕ in Equation (4.3.13), appears in a linearized form as

$$S_\phi = S_c + S_p \phi_p \tag{4.3.39}$$

where the coefficient, S_p must have a value equal to or less than zero to ensure the convergence. The reason for this is that the discretization equations will be solved by the techniques for linear algebraic equations. Thus, the source terms should be considered to be either a linear dependence on the variable ϕ or a constant. The source terms are often the cause of divergence of iteration, and the proper linearization of the source term could be the key to achieve a converged solution. The source term linearization is by no means unique. However, the negative value of S_p must be guaranteed (Patankar, 1980). The coefficients S_c and S_p themselves may depend on ϕ, and need to be renewed during each iteration cycle. Furthermore, the under-relaxation of the source term may be required when it is relatively large.

For each variable, there is an algebraic equation like equation (4.3.35) in each of the control volumes. The solution for these algebraic equations can be obtained by solving a triangle matrix.

4.4 Cell Continuity Correction and Overall Continuity Correction

It is noticed that in Table 3.1.1, the pressure gradient appears in the source term of the momentum equation. However, there is no obvious equation for obtaining pressure field. The pressure field is related with the continuity equation in such a way that if the correct pressure field is used to solve the momentum equation, the resultant velocity field would satisfy the continuity equation automatically. At the beginning of the iteration, a guessed pressure field is needed to make the momentum equation solvable. It would result in a velocity field with which the continuity equation may not be satisfied, and a pressure correction may be required to improve the previous pressure field. That is

$$p = p^* + p' \qquad (4.4.1)$$

where p^* and p' are the guessed pressure field and pressure correction, respectively. The velocity field is to be corrected correspondingly as,

$$u = u^* + u'; \quad v = v^* + v'; \quad w = w^* + w' \qquad (4.4.2)$$

The relationship between the pressure correction and the correspondent velocity correction is derived below.

For u_e, the velocity component in the x direction at node e (see Figure 4.2.2), Equation (4.3.34) can be written as

$$a_e u_e = \sum_i a_i u_i + b' + (p_P - p_E) A_x \qquad (4.4.3)$$

Where b' is the source term of momentum equation in the x direction

without pressure term. Subscript, i, indicates the six neighbor grid nodes. A_x is the control volume interface perpendicular to the x direction. When the guessed pressure field is employed, the momentum equation becomes

$$a_e u_e^* = \sum a_i u_i^* + b' + (p_P^* - p_E^*) A_x \qquad (4.4.4)$$

Subtracting Equation (4.4.4) from (4.4.3), the result is

$$a_e u_e' = \sum a_i u_i' + (p_P' - p_E') A_x \qquad (4.4.5)$$

With the assumption that the first term in the right-hand side in above equation is negligible, the dependence of the velocity correction on the pressure correction then becomes

$$u_e' = d_e (p_P' - p_E') \qquad (4.4.6)$$

where $d_e = A_x / a_e$. Equation (4.4.2) can then be written as

$$u_e = u_e^* + d_e (p_P' - p_E'), \quad \text{and so on} \qquad (4.4.7)$$

Integrating the steady state continuity equation over a control-volume results in

$$[(\rho u)_e - (\rho u)_w] A_x + [(\rho v)_n - (\rho v)_s] A_y + [(\rho w)_t - (\rho w)_b] A_z = 0 \qquad (4.4.8)$$

Substituting Equation (4.4.7) into Equation (4.4.8) and rearranging the resultant equation give the discretization equation for the pressure correction p' at any grid node p:

$$p'_p = \frac{a_E p'_E + a_W p'_W + a_N p'_N + a_S p'_S + a_T p'_T + a_B p'_B + b}{a_p} \qquad (4.4.9)$$

where

$$a_E = \rho\, d_e A_x \qquad (4.4.10)$$

$$a_W = \rho\, d_w A_x \qquad (4.4.11)$$

$$a_N = \rho\, d_n A_y \qquad (4.4.12)$$

$$a_S = \rho\, d_s A_y \qquad (4.4.13)$$

$$a_T = \rho\, d_t A_z \qquad (4.4.14)$$

$$a_B = \rho\, d_b A_z \qquad (4.4.15)$$

$$a_p = a_E + a_W + a_N + a_S + a_T + a_B \qquad (4.4.16)$$

and

$$b = [(\rho u^*)_w - (\rho u^*)_e]A_x + [(\rho v^*)_s - (\rho v^*)_n]A_y + [(\rho w^*)_b - (\rho w^*)_t]A_z \qquad (4.4.17)$$

The pressure correction equation is solved together with the other dependent variables in iteration cycles, while the velocities are corrected through Equation (4.4.7). The corrected velocity field is then employed in the computation of other scalars, and the up-dated pressure field is used for momentum equation in the next iteration.

In order to ensure the mass continuity at the door opening where the flow properties may change rapidly, an overall correction on the velocity component in the direction perpendicular to the partition (the x direction) is added. The necessity of the overall continuity correction is caused by the accumulated error in each iteration process.

The overall correction term is derived from the mass continuity over the sections parallel to the partition. If the upstream volume flow rate is Q_{up}, the volume flow rate at downstream section may become either larger or smaller because of the accumulated error in this section. The discrepancy is evenly distributed to each control volume as an overall velocity correction. The overall velocity correction ensures the same amount of air flowing through each section of downstream. It can be expressed as

$$\sum_j (u_j + \Delta u)\, A_{x,j} = Q_{up} \qquad (4.4.18)$$

where Δu is the overall velocity correction term which is constant for each control volume in the same section. The summation is carried out over the whole section perpendicular to the x direction.

From Equation (4.4.18), the overall velocity correction can be calculated. It is

$$\Delta u = \frac{Q_{up} - Q}{\sum_j A_{x,j}} \qquad (4.4.19)$$

where Q represents the air volume flow rate across the section before velocity is overall-corrected.

The overall velocity correction leads to the requirement of an overall pressure correction. The overall pressure correction can be determined through Bernoulli Equation,

$$\frac{p}{\rho g} + \frac{u^2}{2g} = \text{constant} \qquad (4.4.20)$$

Differentiating the above equation with respect to x and replacing dp and du by Δp and Δu, respectively, yield

$$\Delta p = -\rho u \Delta u = -\rho u(\sum_j A_{x,j})\Delta u/(\sum_j A_{x,j})$$
$$\cong -\Delta u \rho Q_{up}/(\sum_j A_{x,j}) \qquad (4.4.21)$$

The approximation in the above equation is a result of taking u at its average value in this section. The overall pressure correction is added to all pressure grid nodes in the downstream flow field.

4.5 Numerical Procedure

4.5.1 The computation process

The SIMPLE algorithm (Patankar and Spalding, 1972) is employed to solve the finite-difference equations. SIMPLE stands for Semi-Implicit Method for Pressure Linked Equations. The sequence of operations is:

(1) Guess the initial values of the pressure field p^*.

(2) With the estimated pressure field, p^*, solve the momentum equations to obtain u^*, v^* and w^*.

(3) Since u^*, v^* and w^* are based on an estimated pressure field, they may not satisfy the continuity equation. A pressure correction term, p', and velocity correction terms u', v' and w' are needed to improve the pressure and velocity fields. Compute the pressure correction, p', from the continuity equation, and add it to the p^*

field.

(4) Compute the velocity correction terms u', v' and w' from the p' field, and add them to starred velocities.

(5) Add the overall velocity correction term Δu to the velocity component in the x direction. This term is computed from the overall continuity equation in the x direction.

(6) Compute the other scale variables, such as temperature, turbulent energy, dissipation rate of turbulent energy and contaminant concentration.

(7) Take the corrected pressure field as a new estimated pressure p^* field, and repeat the operations from the second step until convergence is achieved.

4.5.2 Numerical technique

Under-Relaxation

The under-relaxation technique is necessary to ensure convergence. It promotes stability during iterations. With the under-relaxation technique, the newly computed results from Equation (4.3.35) and the results obtained at last iteration are combined by weighing average as

$$\phi = \alpha \phi_{new} + (1-\alpha) \phi_{old} \qquad (4.5.1)$$

where α is the under-relaxation factor (URF). It has a value from 0 to 1. The only available method for choosing the most satisfactory URF is that of trial and error. In practice, the values of the URF are usually no larger than 0.5 for the momentum and pressure correction equations. Different under-relaxation factors are adopted for different boundary

conditions. A higher value for the URF may be adopted for pressure correction in natural convection cases than in forced convection cases. However, the reverse is true for the URF for velocity: a higher value could be used in forced convection cases. This makes sense physically. Since the pressure difference is the driving force in forced convection cases, the flow field would be very sensitive to the variation of the pressure field. In order to ensure convergence, the URF for pressure should be relatively low.

The under-relaxation factors used in this study are listed in Table 4.4.1.

False-Time Step and ADI Procedure

The false-time step and the Alternative Direction Implicit (ADI) iterative procedure are employed in this numerical model. The false-time step is based on the idea that the steady-state solution can be obtained from its transient equation by marching in time. Since only the final steady-state solutions are of interest, it is not necessary to obtain convergent results for the transient difference equations at each time step. Thus, the coefficients are computed only once at each time step. The ADI method involves the division of a time step, Δt, into three equals, $\Delta t/3$. For the first $\Delta t/3$, the computation sweep goes in the x direction. For the second and third $\Delta t/3$, sweeps go in the y and z directions, respectively. Actually, the false-time step works as a kind of under-relaxation too. The smaller the time step, Δt, the stronger the under-relaxation. When Δt is taken to be infinity, the false-time step does not function any longer.

The sweep goes in the three directions respective to the line iteration in each direction, i.e. the lines parallel to the x direction

are considered first. The variables along the computing line are solved simultaneously. The sweep starts from the lowest horizontal plane, z=0, to the topmost, z=H. In each horizontal plane, the sweep is carried out from y=O to y=W, as illustrated in Figure 4.4.1. After all grid nodes are swept in lines parallel to the x direction, sweeps in lines parallel to the y direction start. Finally, the z direction is considered.

Convergence Criterion

Incompleteness of the iteration process is indicated by the existence of unreasonable residual sources, i.e., the imbalance of the finite-difference equation when using the currently computed variables. Divergency may occur when the variables with large residual sources are used for computing other variables. More sweeps may be required within each iteration.

Convergence of the iteration process is pronounced when the total absolute value of residual sources in the continuity equation with starred velocity field is small enough (less than 1% relative error) and when the variation in value of variables between two iterations is small enough (less than 0.01% relative error). The reason for choosing the residual source in continuity equation as a monitor is that the convergence of continuity equation in this study is slower than other variables.

The Source of Error

The accuracy of a numerical model indicates the degree to which a well-converged solution from finite-difference equations would satisfy the differential conservation equations. It is dependent on a number of factors. The source of error associated with the grid resolution comes

from the interpolation procedures. This type of error can be reduced by increasing the number of grid nodes where the gradient of variables is large. A grid refinement test would be helpful in choosing a proper mesh system.

Another source of error is false diffusion. At low Peclet numbers, because the real diffusion is relatively large, false diffusion has less effect. It becomes serious when a high Peclet number is encountered. In fact, false diffusion is a result of the numerical nature of the differencing equations, because in multi-dimensional flows, the velocity at each control volume is considered to be locally one-dimensional at each control-volume interface. The remedy for false diffusion is to reduce the sizes of the control volumes where the flow is oblique to the grid line.

Inappropriate specification of boundary conditions could result in errors as well. This can be checked by changing the boundary conditions and then examining the sensitivity of the solution to the change.

The turbulence model could also cause some error. Thus, the comparison of the numerical solution with experimental data would be useful in assessing the turbulence model. However, when a discrepancy between the numerical prediction and experimental data exists, it may not all be attributed to the turbulence model employed in the numerical simulation; all factors affecting the accuracy of the numerical model need to be examined.

Grid Dependence Tests (sensitivity analysis)

The accuracy of computation results is affected by the number of grid nodes to a certain extent. However, computation cost requires that the grid number be minimized. The aim of grid dependence test is to

select a mesh system with smallest possible grid number and satisfactory accuracy. In grid dependence test, computations are carried out with increasing number of grid node until the further increment shows negligible change in solution. The compromise between economy and accuracy should be based on the characteristics of problem to be solved.

In grid dependence test, the velocity components in three directions at the center of the enclosure are computed, with the following five mesh systems. They are: 8x8x14, 10x10x16, 12x12x18, 14x14x20, and 24x24x36 (Further refinement is beyond the limit of central memory allowed). The magnitudes of the velocity component in the x-direction obtained from the five mesh systems, and the relative variations are:

mesh system	8x8x14	10x10x16	12x12x18	14x14x20	24x24x36
u	1.55E-2	1.62E-2	1.66E-2	1.69E-2	1.72E-2
difference		4.5%	2.5%	1.8%	1.7%

The grid dependence test indicates that, for the sake of economy, the accuracy with a 10x10x16 system would be acceptable. However, in forced and mixed convection studies, a finer mesh system is required to simulate ventilation supply, exhaust, and contaminant source.

CHAPTER 5

APPLICATIONS OF THE NUMERICAL MODEL

The numerical model has been applied to investigate airflow patterns and field distributions of contaminant concentration, temperature, and comfort parameters in a two-zone enclosure under various boundary conditions. The effects of door location on air movement have been emphasized in the case studies because door openings make two-zone enclosures different from single-zone ones. Validation of the model has been conducted by comparing the predicted results with available experimental measurements.

Since air movement in buildings can be caused by natural convection, forced convection, or mixed convection, applications of the numerical model in the study of room airflow should cover each of these three modes. The following five case studies are presented in this Chapter:

(1) "Natural Convection and Air Flow Pattern in a Partitioned Room with Turbulent Flow" (Haghighat et al. 1989)

(2) "Three-dimensional Analysis of Airflow Pattern and Contaminant Dispersion in a Ventilated Two-zone Enclosure" (Haghighat et al. 1990a)

(3) "Influence of Air Infiltration on Isothermal Airflow and Contaminant Field in a Partitioned Enclosure" (Wang et al. 1990)

(4) "Development of a Three-Dimensional Numerical Model to Investigate the Airflow and Age Distribution in a Multi-Zone Enclosure" (Haghighat et al. 1990b)

(5) "Thermal Comfort and Indoor Air Quality in a Partitioned

Enclosure with Mixed Convection"

5.1 Natural Convection and AirFlow Pattern in a Partitioned Enclosure with Turbulent Flow

Outline

This section discusses airflow patterns and inter-zone convective heat transfer in a partitioned enclosure with natural convection for different locations and sizes of the door opening. Results indicate that the airflow is quite sensitive to the variations of the door height and location, while the inter-zone convective heat transfer rate is only sensitive to the variation of the door height.

5.1.1 Problem statement

The physical problem concerns a three-dimensional rectangular enclosure of LxWxH = 10x4x3 m^3 with a partition in it. A door opening is located on the partition as shown in Figure 5.1.1. The two opposite end walls parallel to the partition are at different constant temperatures, T_H and T_C respectively, while the ceiling, the floor and the other walls are assumed to be well insulated. The temperature difference between the warm and cold walls causes a natural convective heat flow across the door in the partition. This inter-zone convective heat transfer and air flow pattern are investigated for variable temperature differences between the warm and cold walls, for variable door dimensions

represented by h_D/H, and for different door locations represented by x_D/L and y_D/W, respectively. In the present study the door width w_D/W=0.25 is kept constant.

A mesh system of 16x10x10 is employed in this case study.

5.1.2 Physical foundation

For the natural heat transfer process of the fore-mentioned problem, the governing equations consist of the continuity equation, the momentum equations in three directions, the energy equation, and the conservation equations for the turbulent properties, k and ε.

The non-slip condition at the solid surfaces is applied for velocities. Zero temperature gradient is used for the surfaces of the partition, the insulated walls, the floor and the ceiling. Zero kinetic energy of turbulence, and a constant gradient of dissipation rate of k are adopted for k and ε at solid surfaces. The turbulent wall functions are applied to describe the properties at the grid nodes near the solid surfaces. It is found that the wall function gives a lower value of the heat flux between a constant temperature wall and the adjacent air than that obtained from experiments (Chen, 1988). Therefore, the heat flux from constant temperature wall is computed by using a semi-empirical convective heat transfer coefficient obtained by Alameda and Hammond (1983):

$$\alpha_c = \{ [b_1(\Delta T/L)^{b_3}]^{b_5} + [b_2(\Delta T)^{b_4}]^{b_5} \}^{1/b_5} \qquad (5.1.1)$$

where ΔT is the temperature difference between the wall and the adjacent

air, and L is the length of the room. The values of the coefficients are as follows:

$$b_1=1.5, \quad b_2=1.23, \quad b_3=1/4, \quad b_4=1/3 \quad \text{and} \quad b_5=6.$$

The Nusselt number is usually employed to describe the natural convective heat transfer which is defined as

$$Nu = h_x x/\lambda \tag{5.1.2}$$

It is the ratio of convection strength to conduction strength. The choice of the length scale in the Nusselt number is based on the characteristics of the problem being solved. For natural convection through vertical planes, the length scale is the height of the plane. For natural convective heat transfer in enclosed spaces, the distance between two walls which are in different temperatures can be taken as a length scale (Holman, 1990). With a known heat flux from a wall, the Nusselt number can be expressed by either

$$Nu = qL/(T_H-T_C)/\lambda \tag{5.1.3}$$

or

$$Nu = qH/(T_H-T_C)/\lambda \tag{5.1.4}$$

5.1.3 Validation of the numerical model

In order to verify the computational model, a comparison of the computed Nusselt number, as a function of Rayleigh number, with

experimental results reported by Nansteel and Greif (1984) are shown in Figure 5.1.2. The thermal boundary conditions used in the computation are the same as those in the experiment. Since the cell size is restricted by the number of grids, the parameter w_D/W, which is 0.25 in numerical calculation, does not match the value 0.093 adopted in the experiment performed by Nansteel and Greif (1984). However, it was found in their experiment that the door width has little influence on the inter-zone heat convection rate. For example, the inter-zone convective heat transfer rate for the case with $w_D=W$ was only 5% higher than that with $w_D/W = 0.093$ when the door height is 3/4 of room height.

Figure 5.1.2 shows that in the relatively high Rayleigh number region ($Ra_L>3\times10^{11}$), the computed Nusselt number is slightly higher than the projection of the correlation line obtained by Nansteel and Greif, and slightly lower than the experimental data obtained by Weber. In the region of $Ra_L<3\times10^{11}$, the predicted Nusselt number is slightly lower than experimental data obtained by Nansteel and Greif. The k-ε model combined with the wall function method, although applicable in the region that the experiment covers, may not give good predictions of heat flux from walls when the Rayleigh number is relatively low. The low-Reynolds-number k-ε model of turbulence would be more suitable to predict the natural convection phenomena in buildings. However, with low-Reynolds-number k-ε model, a much finer mesh system near walls is required; such a mesh calculation would require excessive central memory.

In general, the agreement is satisfactory between computed values of Nu and the experimental data obtained by Nansteel and Greif, and by Weber.

For a further validation of the numerical model with natural convection study, the predicted velocity distribution at the center of the door opening is compared with the experimental measurements conducted by Lieman (1990). The experiment was carried out in a full-scale air-filled enclosure under a natural convection condition. The two-zone enclosure used in the experimental study has a dimension of LxWxH=6.3mx3.1mx2.5m. A partition is placed at the middle of the room length with a centrally located door opening (1.85m height and 0.77m width). There is a step of 0.08m height on the floor of the door opening. The thickness of the partition is 0.07m. The isothermal boundary conditions for walls, ceiling and floor are:

T_W= 11.7°C T_E= 17.93°C

T_N= 17.32°C T_S= 17.20°C

T_T= 17.10°C T_B= 16.71°C

Figure 5.1.3 shows the velocity distributions at the center of the door opening obtained by experimental measurement and numerical computation. Discrepancy is observed in the low region of the door opening. This is probably due to the 0.08m step on the floor of the door opening which is neglected in the computation since it is too small to be considered in the mesh system adopted. In the remaining part of the door opening, the predicted velocity distribution is in good agreement with the experimental data.

5.1.4 Results

Figure 5.1.4 illustrates the flow patterns in a room divided by a partition having a centrally located door opening with $h_D/H=0.75$ and $w_D/W=0.25$. The air near the floor at z/H=0.0625 moves from the cold zone into the hot zone. At the height z=0.3125H, the air in the hot zone starts changing the flow direction from the hot wall towards the cold wall, while the air in the cold zone still moves towards the hot zone. The horizontal counterflows interact in the hot zone. A similar phenomenon occurs in the cold zone at the height about z=0.5625H. Figure 5.1.4e shows that the neutral levels in the hot and cold zones are not at the same height. In the hot zone the neutral level (for the section of y=0.5625W) is at about z=0.3125H while the neutral level in the cold zone for the same section is at about z=0.625H. This phenomenon may be explained as follows: in the hot zone, the velocities in the x direction near floor are higher than those in the upper part of the hot zone (see Figure 5.1.4e). The acceleration of the horizontal flow near the floor as it passes through the aperture from the cold zone into the hot zone is attributed to the three-dimensional characteristic of the air flow and the boundary-layer type of the flow. In order to satisfy the mass continuity equation, the flow area for the reverse velocities in the upper part of the hot zone must be larger. Thus, the neutral line is pushed downwards. In the cold zone, the velocities in the x direction near ceiling are higher than those in the lower part of the cold zone. Thus, the neutral level in the cold zone rises. At the height z=0.8125H (Figure 5.1.4d) the flow is completely divided by the door soffit. The air in the hot zone has a slow vortex motion, while the warm air, after

entering the cold zone, flows quickly along the ceiling. There is a region of recirculation in each of the partition corner in the cold zone.

Figure 5.1.5 demonstrates the flow patterns, in x-z plane at y=0.5625W, for centrally located door opening with five door heights (i.e h=0.5H, 0.625H, 0.75H, 0.875H and 1.0H). For the cases of h/H lower than 0.875, there exists a weak clockwise recirculation region near the ceiling of the hot zone which was also observed by Nansteel and Greif (1984) and Neymark et al (1988). This recirculation flow does not make significant contribution to the convective heat transfer across the door. Thus, the active area for convective heat transfer from hot wall is decreased when the door height is decreased. It results in a lower Nusselt number, Nu_H, as shown in Figure 5.1.6.

To examine the effect of moving aperture in the y direction on the Nusselt number, the door size is kept unchanged at h/H=0.75 and W_D/W=0.25 with the partition located at the middle of the room. The computed results, shown in Figure 5.1.7, indicate that the heat transfer rate increases slightly with the door moving along the y direction from the center towards the side-wall. This result could be understood by examining Figures 5.1.8 through 5.1.10. Moving the door location from the central position at y_D/W=0.5 towards the side-wall at y_D/W=0.875 produces a counter-clockwise vortex flow in the hot zone and a clockwise vortex flow in the cold zone. The vortex flow patterns are different at various elevations, as shown in Figures 5.1.8 through 5.1.10. For example, consider the case of the door located at y_D/W=0.875: at the plane of z/H=0.0625 (Figure 5.1.8d), a vortex flow is seen in the hot zone at the front corner of the partition. This vortex moves along the

partition towards the opening when the horizontal plane moves up to z/H=0.3125 (Figure 5.1.9d). At the plane z/H=0.8125 (Figure 5.1.10d), where two zones are completely separated by the door soffit, two separate recirculation flows exist in both regions: a large one in the hot zone and a small one in the cold zone. It can be seen that due to the vortex flow, the velocity component, v, increases near both hot and cold walls, which leads to a favorable convective heat transfer rate.

To examine the effect of the partition location on the convective heat transfer, the door size (h_D/H=0.75 and w_D/W=0.25) and its position in partition (y_D/W=0.5) remain unchanged. Figure 5.1.11 shows the air velocity vectors in the x-z vertical planes for three locations of the partition at x_D/L=0.2857, 0.5 and 0.7143. It can be seen that when the partition moves apart from the central position of the room, there is a redistribution of the two vortex flows in the hot and cold zones. Figures 5.1.12 through 5.1.14 present the air velocity vectors in the x-y horizontal planes at z/H=0.0625, 0.3125, and 0.8125, respectively, for the same three locations of the partition. The flow patterns are symmetric to the door opening. It seems that the change of the flow patterns at different partition locations does not significantly affect the computed convective heat transfer rates across the doorway.

The computed convective heat transfer rates across the doorway represented by the ratio of Nu_H/ Nu_H^*, where Nu_H^* refers to the Nusselt number for the centrally located partition, as a function of x_D/L are plotted in Figure 5.1.15. It shows that the heat transfer rate is not sensitive to the change in the partition location.

The vertical temperature distributions in the x-z plane at different locations along the x-axis for the case of y_D/W=0.5 and h_D/H=0.75 are

plotted in Figure 5.1.16. The vertical temperature variation adjacent the hot wall (curve 1) is larger than that adjacent the cold wall (curve 4). The temperature in the upper part ($z/H > 0.75$) near the hot wall increases rapidly because of the clockwise recirculation in this region, which is separated from the cold zone by the door soffit. The heat in this region is less likely to be transferred through the opening into the cold zone by convection. In the hot zone the temperature near the partition at $x/L=0.4643$ in the region from $z/H=0.33$ to $z/H=0.83$ is even higher than those near the hot wall. It is due to the air coming from the upper part of the door opening in the hot zone and from both side-walls in the y direction, where the temperature is higher than that at $x/L = 0.0375$ and from $z/H = 0.33$ to 0.83. In the cold zone, for the similar reason, the temperature near the door opening (curve 3) in the range from $z/H=0.12$ to $z/H=0.37$ is lower than that adjacent to the cold wall (curve 4). These phenomena can be observed only in the three-dimensional airflow modeling.

The unit of the maximum velocity vectors shown in the Figures is meter per second.

5.1.5 Conclusions

The effects of the door height and location, and the partition location in a room on the airflow pattern and the inter-zone convective heat transfer rate are investigated by the numerical model.

For two-zone enclosures in which two end-walls (parallel to the partition) maintain different isothermal temperatures while the other boundaries are well insulated, one may draw the following conclusions:

(1) The airflow pattern is very sensitive to the change in the door
height and its location in the partition and to the change in the partition location.

(2) The heat transfer rate is sensitive to the change in the door height and its location on the partition, but not sensitive to the change in the partition location.

(3) The neutral level of the velocity (velocity in the x direction is zero) in the hot zone is lower than that in the cold zone.

5.2 Three-dimensional Analysis of Airflow Pattern and Contaminant Dispersion in a Ventilated Two-zone Enclosure

Outline

The pattern of an isothermal air flow caused by infiltration and ventilation in a two-zone enclosure is investigated. The two zones are separated by a partition with a door opening. Two types of boundary conditions for air supply are considered: 1) the outside air uniformly infiltrates through an end-wall parallel to the partition into the enclosure and leaves through a ceiling-mounted exhaust opening; and 2) the ventilation air flows into the enclosure through a rectangular supply opening near the floor on an end wall parallel to the partition, and leaves the enclosure through a exhaust opening on the ceiling. For each type of the boundary conditions, two different exhaust opening

locations, each with three door positions, are studied. Contaminant concentration distributions for different cases are also presented to illustrate the influence of the flow pattern on the removal of the contaminant generated in one of the two zones. The results show that the location of the door not only guides the direction of the air movement but also affects the strength of the air circulation in the downstream zone, while the upstream zone is less influenced.

5.2.1 Problem description

An enclosure having the same geometrical configuration as described in natural convection study is used here. The difference between the two enclosures is that the one used in the present study has openings of air supply and exhaust on a wall and the ceiling as illustrated in Figure 5.2.1. Two types of boundary conditions for air flow are considered. In the first type, the outside air uniformly infiltrates into the enclosure through wall W, at a velocity of 0.01 m/s, and leaves the enclosure through a rectangular exhaust opening placed on the ceiling. In the second type, the fresh air flows into the enclosure through a rectangular supply opening located on wall W, and leaves the enclosure through the exhaust opening on the ceiling. The air velocity at the supply opening is taken as 2.0 m/s (5 ach). A contaminant source with a constant emission rate (assumed unity) is placed at the height of z_s/H = 0.125, right under the exhaust opening for all cases.

The dimensions of the supply, exhaust and door openings are listed in Table 5.2.1. In this study, these dimensions remain unchanged. The locations of the partition and the supply opening are also fixed for all

cases, while the exhaust opening and the contaminant source are placed in zone A and zone B respectively as specified in Table 5.2.2.

In order to simplify the problem, the following assumptions are made: 1) The thickness of the partition is relatively small compared to the length of the enclosure and may be neglected; 2) The buoyancy force in a ventilated enclosure has a negligible effect on the flow field and may be neglected; 3) the contaminant source is considered to be a point source, namely, it does not have any physical volume; 4) The contaminant emission rate is relatively small compared to the air infiltration rate and to the ventilation airflow rate, and, therefore, may be neglected; and 5) a one-phase flow is assumed in this study, that is, both the air and the contaminant have the same velocity.

Generally speaking, the air flow in a ventilated enclosure is turbulent. In this study, the Reynolds number, Re, is over 3.6×10^4 with u_I=2.0 m/s, therefore, the flow is turbulent (Gosman et al., 1980). With the isothermal flow assumption, the governing equations for this problem are relatively simple. There is no need to solve the energy equation. The conservation equation for the contaminant concentration does not affect the solution of velocities and turbulent properties. It is a passive variable, and may be solved after the convergent flow field is achieved. The variables to be solved are u, v, w, c, k, and ε, respectively.

The boundary conditions are as follows:

For wall W with infiltration:

$$u = u_{IF} \qquad (5.2.1)$$

$$v = w = 0 \qquad (5.2.2)$$

$$k = 0 \tag{5.2.3}$$

$$c = 0 \tag{5.2.4}$$

The zero turbulent energy is taken at the infiltration wall. It is out of the consideration that a uniform air infiltration through the wall is similar to air flowing through a filter. For such a case, the turbulence would be very small.

For the supply opening (the second type only),

$$u = u_I \tag{5.2.5}$$

$$v = w = 0 \tag{5.2.6}$$

$$k = k_I = \frac{3}{2} u_f^2 \qquad (\text{ where } u_f = 0.05\ u_I) \tag{5.2.7}$$

$$\varepsilon = \varepsilon_I = C_\mu\ k_I^{1.5} / l \tag{5.2.8}$$

$$c = 0 \tag{5.2.9}$$

and for the exhaust opening,

$$w = w_E = u_{IF} H\ W/A_E \qquad \text{for the first type of air supply} \tag{5.2.10}$$

$$w = w_E = u_I A_I / A_E \qquad \text{for the second type of air supply} \tag{5.2.11}$$

$$u = v = 0 \tag{5.2.12}$$

$$c = c_E = e/(\rho u A_E) \tag{5.2.13}$$

$$\frac{\partial k}{\partial z} = 0 \tag{5.2.14}$$

$$\frac{\partial \varepsilon}{\partial z} = \text{constant} \tag{5.2.15}$$

At the other solid surfaces,

$$u = v = w = 0 \tag{5.2.16}$$

$$k = 0 \tag{5.2.17}$$

$$c = 0 \tag{5.2.18}$$

5.2.2 Numerical treatment

The numerical computation is performed on 20x14x14 uniform control volumes. The air velocities at the supply and exhaust openings are considered to be uniformly distributed over the entire areas of the openings. The wall function method is employed for the grid nodes near all solid surfaces. However, there is an exception for the first type of the air entering condition: wall W, because, with the air penetration, the boundary layer near this wall does not exist.

5.2.3 Results

Two types of the air entering conditions, as described above, are considered. For each type, six cases with different exhaust and door opening locations are examined. A total of twelve cases studied are listed in Table 5.2.2.

It should be noted that in the classification of the cases, the first number denotes the type of air entering condition; the following capital letter indicates the zone where the exhaust opening is placed, and the last number represents the location of the three different door positions.

5.2.3.1 First type of air entering

For the first type, the outside air enters the enclosure through entire wall W in zone A by uniform infiltration.

Exhaust and Contaminant Source in Zone B ($x_E/L=0.75$, $y_E/W=0.71$):

Figure 5.2.2 indicates that in zone A, the air flow is nearly one-dimensional and uniform, regardless of the location of the door opening. Only in the region near the partition the velocity component in y direction becomes comparable with that in x direction.

In zone B, however, the air flow pattern is obviously dependent on the position of the door. In case 1B-1 (Figure 5.2.2a), the air in zone B forms a large anti-clockwise vortex, centering about the exhaust opening. This vortex occupies the entire area of zone B. In case 1B-2 (Figure 5.2.2b), there exist two large circulations in zone B, one clockwise at the south-east corner, and the other anti-clockwise at the north-east corner. In case 1B-3 (Figure 5.2.2c), the door opening at $y_D/w = 0.75$ is closer to the exhaust opening. The air, after passing through the door opening, would be expected to have a short way to leave the enclosure through the exhaust opening, and consequently the air movement in zone B would become weaker. However, in comparing Figure 5.2.2c with Figure 5.2.2a, there is no significant decrement of the air movement in zone B. The air still travels the entire region of zone B before leaving. A large, clockwise circulation appears in case 1B-3.

Figures 5.2.2d and 5.2.2e present the contours of the contaminant concentration in the horizontal plane at z/H=0.63 for cases 1B-1 and 1B-3 respectively. Following the path of the air movement, the contours of contaminant concentration are also in circulation forms. In case

1B-3, the source position is located at the upstream region (close to the door opening), and the contaminant is directly diluted by the fresh air, and removed away through the exhaust vent. Thus, the average concentration in Figure 5.2.2e is lower than that in Figure 5.2.2d.

Exhaust and Contaminant Source in Zone A (x_E/L=0.19, y_E/W=0.71):

Generally speaking, the outside air is not likely to constantly infiltrate into a building in a fixed direction. In order to examine the flow pattern subject to the air infiltration in the opposite direction, instead of changing the direction of the air infiltration, we simply move the exhaust opening from zone B to zone A.

Figure 5.2.3a demonstrates the velocity vectors for case 1A-1 in the vertical plane at y/W=0.17. Figures 5.2.3b, c, and d demonstrate the velocity vectors in the horizontal plane at z/H=0.38 for cases 1A-1, 1A-2, and 1A-3, respectively.

From Figures 5.2.3b, c and d, it can be seen that in zone A, the air flow pattern and the magnitude of the velocity are not significantly changed by varying the position of the door opening. The explanation of this is that, in a steady state, the location of the exhaust opening is more responsible for controlling the air movement in zone A than that of the door opening because of the mass continuity. It is seen that only a small portion of the infiltrating air has the chance of going to zone B through the door opening while the rest of the air forms a vortex in the northern region in zone A. Thus, the velocity in zone B is relatively low.

Figure 5.2.4a shows the distribution of the contaminant concentration in the horizontal plane at z/H=0.38 for case 1A-3. In this case, the contaminant source (x_S/L=0.19, y_S/W=0.71) and door opening

(centered at $y_D/W=0.75$) are very close to each other, and the contaminant seems to have a higher probability of moving into zone B. However, the contaminant dispersion is restrained by the air vortex in zone A (refer to Figure 5.2.3d), therefore the contaminant can hardly enter zone B. In Figures 5.2.4b and 4c, it is noticed that the contours at the plane of $z/H=0.96$ for cases 1A-3 and 1A-1 are almost the same. This is attributed to the similarity of the flow patters in these two cases.

5.2.3.2 Second type of air entering

For the second type, the ventilation air enters the enclosure through the supply opening, whose position is fixed on wall W near the floor ($y_I/W=0.13$, $z_I/H=0.042$) for all cases. The exhaust opening and the contaminant source are placed either in zone B (cases 2B-1, 2B-2 and 2B-3) or in zone A (cases 2A-1, 2A-2 and 2A-3).

Exhaust and Contaminant Source in Zone B ($x_E/L=0.75$, $y_E/W=0.88$):

Figure 5.2.5 illustrates the velocity vectors for cases 2B-1, 2B-2 and 2B-3. In zone A, the flow pattern does not show much difference with the variation of the door position (Figures 5.2.5a, c and d). An anti-clockwise air circulation in zone A is observed. The center of the circulation moves towards wall W as the horizontal plane rises to $z/H=0.96$ (Figures 5.2.5a and b).

At the horizontal section $z/H=0.29$, the air vortexes in zone B are all clockwise regardless of the change of the door position.

The distributions of the contaminant concentration of case 2B-1 for different horizontal levels are presented in Figures 5.2.6a, b and c. At the lower level, $z/h=0.13$, the contaminant has not yet been widely

spread. When the horizontal level rises to z/H=0.29 or above, the entire area in zone B is polluted. In case 2B-3 (Figure 5.2.6d), the contaminant concentration in the region near the partition is higher than that in case 2B-1, because the source is at the upstream, and the air flowing into zone B is already contaminated before reaching the region near the partition.

Exhaust and Contaminant Source in Zone A (x_E/L=0.19, y_E/W=0.88):

Figures 5.2.7a, c and e present the flow patterns at the horizontal section of z/H=0.29 for different door locations when the source and the exhaust opening are placed in zone A. It is seen that in zone A, the airflow forms an anti-clockwise vortex, and the flow pattern is almost not affected by the change of the door location. This phenomenon is also supported by Figure 5.2.7b and d. They show that the airflow in the vertical section at y/W=0.88 for case 2A-1 and 2A-3 are very much alike, even though Figure 5.2.7d contains the door opening, while Figure 5.2.7b does not.

In zone B, which is no longer an active zone, the air velocity is significantly reduced. For case 2A-1, since the door is not as close to the exhaust opening as the other two cases, the effect of the suction from the exhaust on the air movement at the door opening is not strong. It makes the air easier to enter zone B. As a result, the air movement in zone B is relatively strong in case 2A-1.

Figure 5.2.8a illustrates the contours of the contaminant concentration at z/H=0.29 for case 2A-1. As described above, for case 2A-1, more air with contaminant has the chance flowing into zone B, therefore the contaminant concentration in zone B for this case is remarkably higher than that in case 2A-3 (Figure 5.2.8b). Figures 5.2.8b

and 5.2.8c show the contaminant distributions of case 2A-3 at two horizontal levels. At the lower level z/H=0.29, zone B is almost free of contaminant. However, at the higher level z/H=0.96, where the two zones is completely separated by the door soffit, there are some contaminants accumulate in the region near the ceiling of zone B.

5.2.4 Validation of forced convection

In forced convection studies, since there is no experimental data available, a comparison of the results predicted by this numerical model with those computed by Chen (1990d) through PHOENICS code was carried out (Jiang and Haghighat, 1990).

The configuration in the compared case is similar to the one shown in Figure 5.2.1 (second type of air supply with exhaust located in zone B), except that the door is located at y_D/W=0.83 near the northern wall, and the ventilation flow rate at supply opening is 1m/s. The contaminant source is placed in zone A at

$$x_s/L = 0.25 \qquad y_s/W = 0.46 \qquad z_s/H = 0.46.$$

The velocity distributions in two vertical sections at the door opening predicted by this model and by PHOENICS code are presented in Figure 5.2.9.

For two-zone enclosure, the door opening can be consider as an exhaust for upstream zone and as a supply for down-stream zone. Therefore, the velocities at the door opening are crucial, and are chosen for comparison.

The overall contaminant concentrations in zones A and B are also

compared, and listed as follows.

Average contaminant concentration in each zone

	zone A	zone B
predicted by the present model	10.212	9.929
predicted by PHOENICS code	10.023	9.588

From above list and Figure 5.2.9, it is seen that the agreements of both the velocity distributions and the average contaminant concentrations in each zone computed by this numerical model and by PHOENICS code are very good.

5.2.5 Conclusions and discussion

The effects of the door location on the air flow pattern and on the contaminant dispersion induced by natural infiltration and mechanical ventilations in a two-zone enclosure are investigated. The door location not only guides the direction of the air flow, but also affects the strength of the air circulation. The flow pattern and the contaminant dispersion in the two-zone enclosure demonstrated in this case study can be summarized as follows:

(1) The air flow pattern in the upstream zone, zone A (where either the air infiltration or the mechanical ventilation supply takes place) is not significantly influenced by the door location, while in the downstream zone, zone B, both the direction and the magnitude of the air circulation are dependent on the door location.

(2) When the exhaust opening and the contaminant source are located in the upstream zone, a partition combined with a local exhaust can efficiently prevent the downstream zone from being contaminated if the door opening is properly arranged. In the upstream zone, the contaminant may be lowered by a proper arrangement of the supply and exhaust openings.

(3) When the contaminant source is in the downstream zone, the door location significantly affects the distribution of the contaminant concentration in this zone. The positions of the exhaust, the contaminant source, and the door opening should be carefully planed to reduce the contaminant concentration in the downstream zone. A reasonable arrangement can be achieved from the comprehension of the air movement.

In this study, the temperature distribution is not considered, and the buoyancy effect is not taken into consideration. The buoyancy term must be added into the momentum equation whenever a contaminant source is also a heat source, such as a stove in a kitchen. For the cases of the first type of the air entering condition, the infiltration through the wall is assumed to be uniform. It may not be met in practice. However, as long as the velocity of the infiltration air can be considered to be one-dimensional, this assumption will not make a significant difference in the flow pattern and in the contaminant distribution.

The results obtained from this study have a practical relevance, and give a clear picture and qualitative information about the ventilation air circulations and the contaminant distributions in two-zone enclosures.

5.3 Influence of Air Infiltration on Isothermal Ventilation Airflow and Contaminant Field in a partitioned enclosure

Outline

The influence of air infiltration on the isothermal airflow and the contaminant distribution in a ventilated two-zone enclosure are examined. The direction of the infiltration airflow is considered to be in the opposite direction of the air velocity at the ventilation supply. The enclosure and the layout of the openings are the same as the one used in section 5.2 except that the exhaust opening and the contaminant source are fixed in zone B. The infiltration air flows uniformly into zone B (infiltration zone) through the end-wall opposite to the supply-located wall, and leaves through the exhaust. Three different values of air infiltration rate are considered. In the analysis of the combined influence of door opening position and infiltration on the air movement, the door opening is placed at three positions, namely, y_D/W=0.167, 0.5 and 0.833 respectively. The results indicate that a local exhaust will effectively limit the transportation of the contaminant from the infiltration zone into the ventilation zone, and the effect of the infiltration on the contaminant migration into the ventilation zone may be negligibly small, if the door opening and the exhaust are properly placed.

5.3.1 Problem description

This case study is a continuation of the study in the last section. The purpose of the present case study is, (1) to examine the effect of

the air infiltration on the isothermal airflow and the contaminant distribution in a ventilated two-zone enclosure, and (2) to investigate the effect of the door position on the contaminant migration in the ventilation zone, zone A. In Figure 5.2.1, Wall E is considered to be an exterior wall through which outside air uniformly infiltrates into the enclosure. The sizes and positions of the door, the supply and exhaust are listed in Table 5.3.1.

When there is no air infiltration from wall E into the enclosure, zone A is almost free from the contaminant, because the contaminant source is located in zone B, the downstream zone of the ventilating airflow. However, when the air infiltration takes place at wall E, the contaminant may be blown into zone A by the infiltrating air, if the infiltration airflow is large enough in comparison with the ventilation airflow. In this case, a counterflow would appear at the door opening. It may be expected that, for different door locations, the effect of infiltration airflow on velocity distribution at door opening is different.

5.3.2 Results

5.3.2.1 Effect of air infiltration rate on airflow pattern and contaminant distributions

In order to examine the effect of the infiltration on the airflow patterns, three air infiltration velocities, U_{IF}= 0.005 m/s (1.8 ach), 0.01 m/s (3.6 ach) and 0.03 m/s (10.8 ach), are considered, while the ventilation air velocity is kept at U_I= 1.0 m/s (2.5 ach), and the door position is fixed at y_D/W = 0.167.

Figure 5.3.1 illustrates the airflow pattern at the vertical section y/W=0.46 where the airflow is blocked by the partition. The flow patterns in zone A do not seem to be quite different although the air infiltration flow rate at wall E in zone B increases considerably (Figures 5.3.1a through 5.3.1c). In zone B, the increment of the air infiltration results in increment of area having one-dimensional tendency. This is attributed to the uniform and one-dimensional infiltration assumption. When U_{IF} increases to 0.03 m/s, infiltration air flow dominates in zone B, and the air vortex area is significantly restricted by infiltration air flow (Figure 5.3.1c).

The velocity vectors in two horizontal sections, z/H=0.29 and z/H=0.79, are shown in Figure 5.3.2. The airflow pattern and the strength of the air circulation in zone A are similar for the two different infiltration rate as in the vertical section. It means that the infiltration exerts little influence on the air movement in zone A. In zone B, the effect of the infiltration is not apparent at the lower section, z/H =0.29. Since the supply is located at lower position, the momentum of the ventilation flow at the lower section is larger than that of infiltration, despite the total flow rate by infiltration is close to that by ventilation. When the horizontal plane rises to z/H=0.79 (Figures 5.3.2c and d), the influence of the ventilation flow on the flow pattern becomes smaller than that at section z/H=0.29, while the momentum of the infiltration flow keeps the same as that at lower section. The air movement for the case with U_{IF}=0.03 is seen to be completely dominated by air infiltration as shown in Figure 5.3.2d.

Corresponding to Figure 5.3.2, Figure 5.3.3 presents the distributions of the contaminant concentration in the horizontal

sections, z/H=0.29 and 0.79. As described earlier, at the section z/H =0.29, where the infiltration momentum is small in comparison with the ventilation momentum, the contaminant dispersion at this section is mainly controlled by the ventilation airflow. Therefore the increment of the infiltration from U_{IF}=0.01 to 0.03 does not cause a big difference in the contaminant concentration distribution as shown in Figure 5.3.3a and b. However, at the higher level, z/H=0.79, where the infiltration prevails over the ventilation flow, the average contaminant concentration with U_{IF}= 0.01 is higher than that with U_{IF}= 0.03 in both zones.

The distributions of the air velocity component in the x direction at the axis of the door opening for the three infiltration velocities are shown in Figure 5.3.4a. Since the supply is located near the floor, air movement caused by ventilation is relatively strong at the lower part of the door opening, and the infiltration airflow cannot compete with it. At the upper part of the door opening where the airflow caused by the ventilation becomes relatively weak, the resultant velocity component in the x direction has a negative value. This indicates that the airflow induced by the infiltration has a chance to enter zone A. When the infiltration flow rate increases, the negative velocity at the upper part of the door opening becomes larger. To ensure the mass balance, the positive mass flow rate at the lower part of the door opening must increase.

The average contaminant concentrations in each zone with the different air infiltration rate from wall E are presented in Table 5.3.2. It indicates that the increment of the air infiltration rate lowers the average concentration in both zones.

5.3.2.2 Effects of door position on airflow pattern and contaminant distribution

To investigate the effects of the door position on the airflow pattern, three door positions, y_D/W=0.167, 0.5 and 0.833 are examined. The velocity of the ventilation air at supply opening remains 1.0 m/s. The infiltration air velocity is taken as 0.03 m/s to model an extremely strong infiltration.

The airflow patterns at the vertical section, y/W=0.46, for the three door positions are illustrated in Figure 5.3.5. In zone A, there exist two vortex flows, a large clockwise vortex flow is near the center of the lower part of zone A, and a small counter-clockwise vortex flow is at the upper-right corner. The infiltration action in zone A can hardly be seen, and the flow pattern is not sensitive to the position of the door opening. However, the velocity level in zone A is lower when the door opening is at y_D/W=0.167, and the action of ventilation airflow in lower area of zone B is stronger than the other two cases. It is because that the ventilation air is easier to enter zone B in this case than in the other two cases.

Figures 5.3.6 and 5.3.7 demonstrate the flow patterns at the horizontal sections, z/H=0.29 and 0.79 respectively. In Figures 5.3.6b and 5.3.6c, since the door openings are away from the supply, the circulation in zone B is relatively weaker that that in Figure 5.3.6a, the infiltration airflow seems to dominate the flow field, and the flow patterns are similar. In Figure 5.3.6a, the infiltration effect is less strong for the reason explained earlier.

At the section z/H=0.79, where zone A and zone B are completely separated by the door soffit, the effects of door position on flow

pattern can be seen neither in zone A nor in zone B. The ventilation flow is dominant in zone A, while in zone B, the infiltration flow is more pronounced.

The contaminant concentrations corresponding to Figure 5.3.6 are illustrated in Figure 5.3.8. Once again, it is observed that the concentration distributions in Figures 5.3.8b and c are similar form, and that the zone A is almost free from being contaminated in the two cases. The contaminant concentration in zone B presented in Figure 5.3.8a is higher than those in Figures 5.3.8b and c, and there is a small portion of the contaminant migrated into zone A from zone B.

The distributions of the velocity component in the x direction at the axis of the door opening under the infiltration velocity 0.03 m/s are presented in Figure 5.3.4b for two different door locations. With the centrally located door opening, the velocity component in the x direction is more uniform than that with the door opening close to the northern wall and close to the exhaust opening. The suction at the exhaust causes a low pressure, which acts as a sink term for the momentum equation in the x direction. Comparing Figure 5.3.4b with Figure 5.3.4a, for the same infiltration flow rate, there is a counter-airflow from zone B to zone A only when the door opening is at y_D/W=0.167. The reason may be as follows. The exhaust is closer to the door opening when y_D/W is equal to 0.5 or 0.833, thus, the influence of the suction at exhaust opening would be stronger in these cases than in the case with y_D/W = 0.167. It enhances the air movement from zone A to zone B.

5.3.3 Conclusions

The infiltration effect on the ventilation airflow is examined by numerical simulation. The infiltration flow rate varies from $0.06 m^3/s$ to $0.36\ m^3/s$, while the ventilation flow rate and door position are fixed. The door position effect on the flow pattern and contaminant dispersion is investigated by placing the door opening at y_D/W=0.167, 0.5 and 0.833 respectively. For a two-zone enclosure with a layout similar to the one being studied, the conclusions may be summarized as follows:

(1) When the ventilation air is introduced into zone A and released from zone B, the infiltration flow from the end-wall of zone B does not affect the airflow in zone A significantly, even if the infiltration flow rate is higher than the ventilation flow rate. It is because that, with the assumption of air infiltration uniformly distributed on entire wall E, the momentum of the infiltration flow is much smaller than that of the ventilation flow.

(2) The flow pattern in zone B is more sensitive to door opening location than that in zone A. This is due to the effect of the local exhaust system placed in zone B, which weakens the infiltration air flow before it reaches the door opening.

(3) When there is a local exhaust above the contaminant source and when the door opening is properly placed, the chance for contaminant in the infiltration zone to be transferred into the ventilation zone can be greatly reduced.

(4) The increment of air infiltration rate could lower the average contaminant concentration in both zones.

In the attempt to make a reasonable overall arrangement with the

openings of the supply, exhaust and door, it is obvious that detailed information about the airflow pattern and contaminant distribution is required when the ventilation airflow is affected by the infiltration. The results predicted give a clear picture and qualitative understanding on the infiltration influence on the airflow pattern in a ventilated, partitioned enclosure .

5.4 Investigation on Ventilation Effectiveness in a Two-zone Enclosure

Outline

The contaminant transportation and the air age distribution in a ventilated two-zone enclosure are investigated. The air age distribution under variable positions of the door, supply, and exhaust are compared for a ventilation rate of 2.5 ach. Correlations between the average contaminants in each zone and each of the main parameters, such as the door location, supply and exhaust positions, are illustrated in terms of diagrams, and the average air ages in both zones are shown as a function of the door position. It is found that the average air age in the upstream zone is less affected by the door position than that in the downstream zone, and that the door position near the side-walls gives a better air circulation. It is also found that the positions of supply and door positions affect the contaminant concentration in zone A significantly, while the exhaust location has little effect on the average concentration in both zone A and zone B.

5.4.1 Problem statement

The two-zone enclosure used in this case study has the same size and configuration as that used in previous case studies. The dimensions of the openings are also the same as shown in Table 5.2.1, but with a different arrangement of the openings as presented in Table 5.4.1.

A contaminant source having a unity emission rate is placed in zone A. The contaminant is removed by the ventilation air supplied to zone A, passing through the door opening, and leaving the enclosure through the exhaust opening in zone B. The amount of the contaminant remained in each of the zones will be affected by the locations of door, supply, and exhaust. Thus, the average contaminant concentration in each zone may be used as an indicator of the ventilation effectiveness..

The purpose of this investigation is twofold: (1) to examine the air age distribution in the ventilated partitioned enclosure with a door located at the middle of the partition; and (2) to investigate the effects of the location of the door, supply, and exhaust on the contaminant removal in each zone.

To accomplish the second purpose, various positions of the door, supply, and exhaust are used in computation. The door and supply are moved in the y direction to five different positions. The change of the exhaust location is in the x direction within zone B. Note that when one parameter is changing, the other parameters remain fixed as in the basic model shown in Table 5.4.1.

The ceiling, floor and walls are considered to be well insulated, therefore an isothermal airflow could be assumed. It is also assumed that the thickness of the partition is negligibly small in comparison

with the length of the enclosure. The air velocity at the supply opening is considered to be 1.0m/s. It provides a ventilation rate of 2.5 ach. For the basic model described in Table 5.4.1, the average contaminant, with five different ventilation rates are computed as well.

When the perfect mixing cannot be expected, a proper description of the transport properties of a ventilation system is required. That is so-called the effectiveness of the system. It is usually measured by its capability to provide fresh air uniformly and remove the contaminant within an enclosure. Thus, the freshness of the air in a ventilated enclosure may be taken as an indicator of the effectiveness of the ventilation system. Sandberg and Sjoberg (1983) introduced the concept "age of air" to assess the average ventilation system performance. The age distribution provides useful information about the uniformity of the air freshness within an enclosure.

The local mean age of the air at an arbitrary point is defined as the time, τ, that has elapsed (on average) since the molecules passing this point entered the enclosure. There are two methods determining the local mean age numerically (Davidson and Olsson, 1987): (1) Step-up, at time t=0, a fraction of the supply air is labelled with contaminant. The contaminant concentration at each point is computed for each time-step. (2) Step-down, fresh air is supplied into an enclosure which is initially filled with a uniform concentration of contaminant. The decay of concentration at each point is computed for each time step. In this study, the Step-down method is adopted, and the local mean age of air is determined in the following form .

$$\tau_p = \frac{1}{c_0} \int_0^\infty c_p(\tau)\, d\tau \qquad (5.4.1)$$

where c_0 is the initial contaminant concentration of the enclosure, and $c_p(\tau)$ is the local concentration at time τ, which is determined by its own conservation equation. Actually, it is not necessary to carry out the integration to infinity. The transient concentration decays exponentially in the form of

$$c(\tau)/c_0 = \exp(-\lambda\tau) \qquad (5.4.2)$$

Therefore the computation can stop when the decay slope reaches a constant value at time τ_λ, and the rest of integration can be calculated through $c(\tau)/(2\lambda c_0)$ (Davidson and Olsson, 1987).

The average air age of each zone is calculated as

$$\tau = \frac{1}{V} \int_v \tau_p dV \qquad (5.4.3)$$

where V represents the volume of a zone.

5.4.2 Numerical treatment

A 20×14×14 mesh system is used. The iteration number used to compute the transient concentration at each time step in Equation (5.4.1) is 25, while 20s of time is taken as one time step. $\Delta\tau$=15s and 25s are also tested for comparison. It is found that, with 25 iterations, there is not much difference between the resultant contaminant concentrations for $\Delta\tau$=15s and $\Delta\tau$=20s. Therefore, it is unnecessary to take a time step less than 20s.

5.4.3 Results

The air age is normalized by a reference time τ_n, the time needed to replace the air in the enclosure;

$$\tau_n = \frac{\text{the volume of the enclosure}}{\text{the volume flow rate of supply air}}$$

Figure 5.4.1 illustrates the air age distributions in the vertical and horizontal sections for the case with the door at the middle of the partition while the supply flow rate is 2.5 ach. The air age in zone A decreases when the horizontal level rises from z/H=0.04 to 0.79, or the vertical section moves from south, y/W = 0.13 to north, y/W =0.88. This indicates that the air circulation at the lower level or in the southern part of the zone is not as good as that at the higher level or in the northern part. In zone B, the local air age at the lower level is smaller than that at the higher level since the exhaust opening is located on the ceiling, where the air age is always higher than in other areas. It is noted that in the region near the southern wall, the air age in zone B is quite uniform.

Figure 5.4.2 demonstrates flow patterns and age distributions at the vertical section y/W=0.13, for the door location at y_D/W=0.17, 0.50 and 0.83 respectively. The flow patterns in the upstream zone, zone A, strongly resemble each other, as observed in Haghighat et al (1990a). As a result, the air age distributions in this zone are similar to each other. The local age is increased from ceiling to floor. In the downstream zone, zone B, the average air age in this section for y_D/W=0.17 is lower than that for the other two cases. The reason is that with door at y_D/W=0.17, the vertical section crosses the door opening,

so the air enters zone B more freshly, without traveling a long way in this zone.

The flow patterns and the air age distributions at the horizontal section near the floor, z/H=0.04, are shown in Figure 5.4.3. In zone A, there is an increase in the local air age from the partition towards the western wall in zone A for all the three cases. The average age of zone A in this section rises when the door opening is moved from north to south. This is due to the fact that the exhaust opening is located near the northern wall, and the air in zone A is sucked into the exhaust with less resistance when the door opening is close to the exhaust (y_D/W=0.83). In zone B, the local air age increases from the partition to the eastern wall for y_D/W=0.17. In the other two cases, the air age in the central areas is higher than that in the periphery, since the air movement is in a rotation form.

The average air ages in the two zones for five different door locations are presented in Figure 5.4.4. The average air age in zone A is much smaller than that in zone B for all the cases. In zone A, the average air age decreases when the door opening is moved from the position y/W=0.17 to y/W=0.833. In zone B, the average air age has its largest value when the door is located in the middle of the partition. The average air age decreases as the door opening moves from the central position towards the side-walls.

Figures 5.4.5, 5.4.6 and 5.4.7 illustrate the average contaminant concentrations in zone A and zone B as a function of the locations of the door opening, supply, and exhaust respectively. Note that when one parameter varies, the other parameters remain unchanged. In Figures 5.4.5 and 5.4.6, it is observed that the average concentration in zone B

almost retains constant when the door position is moved along the partition from south to north, or when the supply position is moved in the y direction on the western wall. In zone A, however, the door and supply positions do affect the average concentration in this zone. It is due to the fact that (1) the supply location affects the air vortex flows in zone A, and, therefore, the ability of the contaminant removal; (2) although the door location does not affect the airflow pattern in zone A significantly, the relative position between the contaminant source and the door opening contributes to the contaminant removal. From Figure 5.4.7, it can be seen that the change of the exhaust location on the ceiling in zone B does not seem to influence the average concentration in zone A and zone B.

An increase of the ventilation air flow rate results in the rapid decrease of the average contaminant concentrations in both zones as shown in Figure 5.4.8. However, the average concentrations are not inversely proportional to the supply airflow rate. When the ventilation flow rate is higher than 4 ach, the decrease of average concentration slows down. For the purpose of energy saving, an appropriate ventilation rate for each ventilation system needs to be predicted.

5.4.4 Conclusions

The airflow pattern, the contaminant removal, and the air age distribution in a ventilated partitioned enclosure with various arrangements of the door, supply and exhaust are predicted by numerical simulation. For the two-zone enclosure examined in this case study, the following conclusions are applied:

(1) The average air age in the upstream zone is much lower than that

in the downstream zone.

(2) The change of door location influences average air age in both Zones A and B.

(3) The average contaminant concentration in zone A is greatly affected by the door location and by the supply location, but the average concentration in zone B is not.

(4) The change of the exhaust location on the ceiling in zone B does not seem to influence the average concentration in zone A and zone B.

5.5 Thermal Comfort and Indoor Air Quality in a Partitioned Enclosure with Mixed Convection

5.5.1 Introduction

In a ventilated room, the buoyancy effect cannot be neglected if the room is not well insulated or if there is a heat source (which need not necessarily be a stove or fire place—computers and occupants generate heat constantly and can thus be so considered). In this last instance, the ventilation system functions not only to supply fresh air and remove contaminants, but also to maintain thermal comfort for occupants.

Field studies (Thorshauge 1982 and Hanzawa et al., 1987) have identified turbulence intensity to be around 30 to 60 percent in spaces subject to traditional mixed convection. The turbulence of the airflow is considered to have a significant impact on the sensation of draft. Drafts are usually defined as unwanted local cooling of the human body

caused by air movement, a common complaint in many air-conditioned rooms. The gradients of air velocity and temperature caused by buoyancy may have a significant influence on thermal comfort. Predicting the percentage of dissatisfied people is a necessary element in the estimation of thermal comfort.

The risk of draft rises with increasing air velocity and decreasing air temperature. The fluctuation of air velocity also contributes to the sensation of drafts.

In order to predict thermal comfort in enclosures under mixed convection conditions, a few models have been developed (ISO 1984). However, the influence of turbulence intensity has not been emphasized in most of the models. A new thermal comfort equation introduced by Fanger (1989) takes the turbulence intensity into account, and has been applied to estimate the thermal comfort in enclosures under mixed convection condition. It is expressed by

$$PD = (34 - T_a)(V - 0.05)^{0.62}(0.37\ V\ I + 3.14) \qquad (5.5.1)$$

(for V<0.05m/s insert V=0.05m/s, for PD>100% use PD+100%).

where PD = the percentage of dissatisfied people due to draft (%)

T_a = local air temperature

V = local mean air velocity

I = local turbulence intensity

Turbulence intensity usually indicates the velocity fluctuations, which can be calculated by

$$I = 100\ (2\ k)^{0.5} / V \qquad (5.5.2)$$

where k is the turbulent energy.

Chen et al. (1990c) applied this model to predict thermal comfort in a furnished office, and pointed out the necessity of including the relative humidity and temperature gradients in thermal comfort estimations.

For the present case study, a two-zone enclosure similar to that illustrated in Figure 5.2.1 is considered. The layout of the ventilation openings and door position is shown in Table 5.5.1. The eastern wall of the enclosure is assumed to be exposed to a hot environment, simulated by a 300W constant heat flux from this wall. A computer in zone B is represented by a point heat source of 100W combined with a contaminant source having a unity emission rate.

The temperature of the supply air is considered to be 18°C, 19°C and then 20°C, and the air velocity is assumed to be 1m/s at the supply opening, giving a flow rate of 2.5 ach. The Archimedes numberis about 3.6×10^{-2} in this study. The ceiling, the floor, the partition, and all but the eastern walls are assumed to be well insulated. The average percentage of dissatisfied people and the contaminant concentration in each zone are computed. The field distributions of temperature and the percentage of dissatisfied people resulting from three different door locations are examined as well.

5.5.2. Results

Figures 5.5.1 through 5.5.9 illustrate the distributions of the air velocity, temperature, and PD due to draft in three cases with different door locations. The supply air temperature and velocity are fixed at 18°C and 1m/s respectively.

(a) Case 1: Door Opening at $y_D/W = 0.17$

Figure 5.5.1 shows the velocity vectors at vertical sections y/W=0.13 and 0.63, and at horizontal sections z/H=0.042 and 0.46. At vertical section y/W=0.13, an air circulation loop dominated by natural convection is seen in zone B. The air movement near floor is much stronger than that in the upper region; this is attributed to the suction caused by the natural convection in this zone. At the upper part of the door opening, there is a counterflow from zone B to zone A. At vertical section y/W=0.63, a strong air movement near the ceiling in zone A is caused by airflow from the nearby supply opening. The upward movement of air entering zone A from zone B is due to the higher air temperature in the latter. About mid-height of the enclosure where the head of an occupant sitting down might be, air velocity is predicted to be at an acceptable level (Figure 5.5.1d). Figures 5.5.1c and d illustrate that only the air near the partition enters zone B from zone A; this can also be seen in Figure 5.5.1a. The rest part of air circulates in zone A. In the region near the floor (z/H=0.042), the air in zone A moves mainly towards the western wall because of an upward air movement there. Higher, at level z/H=0.46, there are two large air circulations: clockwise in zone A and counter-clockwise in zone B.

Figure 5.5.2 shows that the temperature in zone A is quite uniform; it changes only in the narrow region near the partition. In zone B, the temperature stratification is more pronounced at vertical section y/W=0.13 than that at section y/W=0.79. This may cause dissatisfaction because of the noticeable temperature difference from ankle to head level. Since cool air flows mainly through the lower part of the doorway

into zone B, and is warmed up on the way to the eastern wall, the temperature gradient in the lower horizontal section is steep (Figure 5.5.2c). At a higher level (Figure 5.5.2d), the temperature is more uniform except in the small region around the heat source.

The PD distributions demonstrated in Figure 5.5.3 indicate that the risk due to the temperature draft and the turbulent intensity in zone A is higher than in zone B. However, in a small region near the floor of zone B, the PD is over 20%. Figure 5.5.3d shows a quite high PD distribution near the supply inlet because of the higher air velocity and lower temperature.

(b) Case 2: Door Opening at $y_D/W = 0.50$

It can be observed by comparing Figure 5.5.4 with Figure 5.5.1 that the velocity field in zone A does not show much difference when the door is moved from $y_D/W = 0.17$ to 0.50. However, at the lower level, the velocity field in zone B is more uniform (Figure 5.5.4b) than it is in case 1.

Figure 5.5.5 illustrates the temperature field when the door opening is in the middle of the partition. The temperature distribution in zone A is similar to that when the door is near the southern wall; this is because the airflow pattern in both cases is similar. Generally speaking, the temperature stratification in zone B is greater than acceptable. At section y/W=0.13, the temperature in zone B is about 22.2°C near the ceiling and 20.4°C near the floor. There is a sudden drop in air temperature across the door opening as shown in Figures 5.5.5b and c. Figure 5.5.5c indicates that an occupant would suffer a 2°C temperature shift at ankle-level when walking from the partition to

the eastern wall. The situation improves higher up (see Figure 5.5.5d).

Figure 5.5.6 presents the PD for vertical sections y/W=0.13 and 0.46, and for horizontal sections z/H=0.042 and 0.46. In zone A, since the supply air has a high velocity and a low temperature, the PD is much higher than for zone B, especially in the region near the supply opening (Figure 5.5.6b). It can be seen that the PD for section y/W=0.13 is lower than for y_D/W=0.167. At the horizontal section z/H=0.042, air velocity is relatively high (as shown in Figure 5.5.4c), and temperature is quite uniform in zone A, while temperature increases gradually in zone B. A higher PD distribution results than for y_D/W=0.167 (see Figure 5.5.6c). At horizontal section z/H=0.46, the most of the area is thermally comfortable. At the corner formed by the partition and the northern wall in zone A, the risk due to draft is high since air velocity is relatively high and the air temperature is low.

(c) Case 3: Door Opening at $y_D/W = 0.83$

The flow field shown in Figure 5.5.7 is completely different from both those shown in Figures 5.5.1 and 5.5.4. The directions of air circulation in zones A and B are exactly the reverse to those in Cases 1 and 2. Air velocity at section y/W=0.13 (Figure 5.5.7a) is less uniform, the maximum velocity being nearly two times as high as those in the two other cases. Geometrically, the door location here is symmetrical with respect to the supply inlet, the point heat source, and the heat source uniformly emitted from the eastern wall, to its location at y_D/W=0.17. Thus, the flow field should be geometrically symmetrical to that in Case 1 to a large extent. The actual unsymmetrical distribution of air velocity can thus be attributed to the exhaust location. At the

lower level, where the effect of the ceiling-mounted exhaust is less important, the velocity distributions are found to be very much symmetrical to those in Case 1 (comparing Figures 5.5.7c and d to Figures 5.5.1c and d).

Figure 5.5.8 presents the temperature distributions. Since the flow field in this case is to a large extent symmetrical to that in Case 1, the temperature field at vertical section y/W=0.13 (Figure 5.5.8a) is similar to that at section y/W=0.79 in case 1 (Figure 5.5.2b). Likewise, Figures 5.5.8b and 5.5.2a correspond to one another. At horizontal sections z/H=0.042 and 0.46, the temperature fields are also symmetrical to those in Case 1. For example, the temperature gradient at section z/H=0.042 is in a north-south direction instead of the south-north direction of Case 1. In zone A, the temperature is as uniform as in the other cases.

In Figure 5.5.9a, the PD gradient of zone A at section y/W=0.13 is larger, although the supply inlet from which the cool air is entered is not located here. This is because, when the variation in air temperature in zone A is negligibly small, the PD distribution is mainly dependent on air velocity and the turbulence intensity field. In zone B, the PD in the area near the floor, where there is a steep gradient in the other two cases, is equal to zero. Because section y/W=0.13 corresponds geometrically to section y/W=0.88 in Case 1, the PD distribution in Figure 5.5.9a is similar to that in Figure 5.5.3b. From Figures 5.5.9b, c and d, the PD distributions can be seen to follow the form of the air movement. Since the air movement in zone B is of boundary layer type, the PD near the floor and ceiling is always higher than in the central region. The occupant in zone B may feel uncomfortable at ankle-level in

all three cases.

In Table 5.5.2, the average percentage of dissatisfied people (PD) and the average contaminant concentration, in both zones and for different supply air temperatures and door locations are presented. At the same supply air temperature, when the door is moved from $y_D/W=0.17$ to $y_D/W=0.83$, the average PD decreases slightly in zone A and increases slightly in zone B. This indicates that the average PD in both zones A and B is not sensitive to change in the door location. The average contaminant concentrations in zones A and B are at their lowest values when the door is located in the middle of the partition, and at their highest values when the door is near the northern wall. However, since the average contaminant concentrations in each zone depend as much on the location of the contaminant source, it is usually preferable to move the contaminant source instead of the door opening to achieve better quality indoor air.

With a fixed door location, increasing the supply air temperature from 18 to 19 or 20°C results in a slight decrease in the average PD in both zones A and B. This is because people are usually more sensitive to drafts when in temperatures. Obviously, there is a limit to how much supply air temperature can be increased in order to reduce a high PD value due to draft. For a comfortable environment, the room temperature should range from 19 to 24°C when the relative humidity is 40-75%.

The average contaminant concentration does not seem to be sensitive to change in supply air temperature in the situation under consideration. This is because the forced air flow from the ventilation system is much stronger than the air movement induced by temperature

difference.

The mixed convection case here being considered is composed of a forced convection produced by mechanical ventilation and a natural convection induced by a heat source along the eastern wall and a point source representing a computer. Since the air temperature in zone B is higher than that of the ventilation air in zone A, the ventilation air is accelerated downward when entering zone B. Across the upper part of the door opening, a small amount of warm air carrying contaminants flows into zone A from zone B. The amount of the counterflow of warm air depends on the location of the door opening. When the door is closer to the exhaust ($y_D/W=0.83$), the suction at the door opening caused by the exhaust would be relatively stronger, and thus the airflow from zone A to zone B would be enhanced. However, the ventilation flow rate remains unchanged. In order to keep the overall mass continuity, the counterflow from zone B into zone A would have to be increased. This indicates that more contaminants and heat would be brought into zone A from zone B in which the contaminant and heat sources are located. As a result, in Case 3, the average contaminant concentration is relatively higher (see Table 5.5.2), and the average temperature in zone A at the section crossing the door opening (see Figure 5.5.8b) is also higher than that in case 1 (see Figure 5.5.2a).

5.5.3 Concluding Remarks

The field distributions of air velocity, temperature, and PD for a two-zone enclosure under mixed convection condition are predicted by numerical simulation. The influence of the door location and the supply

air temperature on thermal comfort are investigated. The door opening is placed near the southern wall (Case 1), in the middle of the partition (Case 2), and near the northern wall (Case 3), and for each case, three supply air temperatures, 18, 19 and 20°C, are considered.

The following conclusions may be drawn for enclosures with layouts similar to the one under study:

(1) The temperature is quite uniform for the most part throughout the enclosure, except in the region near the floor in zone B, where horizontal temperature stratification is relatively pronounced regardless of the door opening position.

(2) The PD due to draft in zone A is much higher than that in zone B for all cases investigated.

(3) The PD is higher in regions around supply and exhaust openings and near the floor. In most areas, the PD is less than 10%.

(4) When the door moves along the partition, the average PD in both zones A and B varies slightly.

(5) The average concentrations in zones A and B are at their lowest value when the door is in the middle of the partition, and at their highest when the door is near the northern wall.

(6) With door location fixed, the supply air temperature only influences the average PD but not average contaminant concentration in zone A and zone B. The reason for this is that the forced air flow from ventilation systems is much stronger than the air movement induced by temperature difference (i.e., natural convection).

CHAPTER 6

CONCLUSIONS AND RECOMMENDATIONS

6.1 Conclusions

From the point of view of concern for indoor air quality and thermal comfort, better comprehension of the indoor airflow structure and the accompanying heat and mass transfer, induced by forced ventilation systems and temperature differences, is required. Numerical simulation is a powerful tool for the study of indoor environment, and has been used by many researchers. However, the majority of the previous numerical investigations has focused on single-zone configurations. The simulation of multi-zones environments is generally based on the assumption of uniform distributions of air velocity, temperature, and contaminant concentration in each zone. This type of modeling is inadequate for advanced investigations of indoor air quality and thermal comfort. More precise analyses are required.

In this thesis, a numerical model was developed and applied to analyze indoor air movement and accompanying heat and mass transfer in three-dimensional two-zone enclosures with turbulent flow. This model was used to predict the field distributions of air velocity, temperature, contaminant concentration, turbulence intensity, and other comfort parameters, such as the percentage of dissatisfied people, for various flow configurations. For natural convection cases, the convective heat transfer rate across the connecting doorway between two

zones was presented in term of the convective coefficient. The influence of door size and location on the inter-zone heat transfer rate was shown. In force ventilated and partitioned enclosures, contaminant transportation and ventilation effectiveness were investigated. The effects of infiltration on the airflow pattern and contaminant migration were examined as well. Correlations between the average contaminant concentration and main parameters involved in the problem of specific door and ventilation supply and exhaust arrangements were obtained. For a two-zone enclosure in mixed convection circumstances, the distributions of air velocity and temperature, and the percentage of dissatisfied people due to drafts were studied. From the various case studies, the following conclusions may be drawn:

(1) For natural convection caused by a constant temperature difference between two end-walls, the inter-zone convective heat transfer rate is quite sensitive to the change in the door height, but not to the door location on the partition and the partition location itself. The neutral level of the air velocity component in the direction perpendicular to the partition is lower in the hot than in the cold zone.

(2). For forced convection caused by mechanical ventilation, when supply and exhaust openings are located in different zones, the airflow pattern in the upstream zone is not significantly influenced by door location. However, in the downstream zone, both the direction and the magnitude of the air circulation are dependent on door location. As a result, contaminant dispersion in the downstream zone changes when the location of the door changes. When the supply, exhaust, and contaminant source are placed in the same zone, the proper locations of a door in

the partition can effectively protect the other zone from being contaminated.

(3) When the ventilation air is introduced into zone A and released through zone B, air infiltration uniformly distributed on the end wall in zone B may only affect the airflow in zone B; a counterflow from zone B to zone A may be avoided when the door opening is properly placed. This is because, the momentum of infiltration air is much smaller than that from ventilation air when the former infiltrates into the enclosure through the entire end wall in zone B. Air infiltration can be considered a type of air supply. Thus, it can be understood that different air supply systems can produce quite different airflow patterns. Even for the same supply system, different modeling methods can lead to different predictions of flow field. The average amount of contamination retained in both zone is reduced when the air infiltration rate increases.

(4) For a partitioned enclosure with a ventilation supply opening located on the end wall near the ceiling in zone A, and a ventilation exhaust opening mounted on the ceiling near a side-wall in zone B, a door location closer to the exhaust opening will result in an increased ventilation effectiveness in both zones A and B.

(5). For the same arrangement of ventilation openings as described in item 4, when a constant heat flux is applied on the end-wall of zone B, and a constant point heat source is added in the central region of zone B, the air temperature in zone A is negligibly affected by the heat sources in zone B. However, the horizontal temperature gradient in the region near the floor of zone B is high, which may cause discomfort. Generally speaking the values of the PD are relatively high in the

region around the supply and exhaust openings and near the floor. The door location influences the average contaminant in both zones A and B, but not the average percentage of dissatisfied people in each zone.

Each parameter has a different effect on room airflow and thermal comfort. It is suggested that the parameters be divided into two classes. The first class of parameters consisted of those having a strong influence on airflow; for example, the location of the supply opening, the type of diffuser, the geometry of the enclosure, and so on. The location of the exhaust opening, etc, belong to the second class of parameters, those influencing room airflow less.

The results of the case studies confirmed the conclusion that the location of the supply opening is a first class parameter and that the location of the exhaust is a second class parameter. The door opening can be considered an exhaust for the upstream zone, and a supply for the downstream zone. Therefore, it exerts more effect on the flow pattern and contaminant concentration distribution in the downstream zone than in the upstream zone. However, the ventilation effectiveness (expressed by average air age) does not seem to be much affected by the door location, as described in section 5.4.

The results obtained show that proper location of supply, exhaust and door openings can be important in attempting to improve indoor air quality in each zone.

The model developed could be applied to analyze other engineering phenomena related to heat and mass transfer in Cartesian coordinate, such as cooling of electronic equipment and heat transfer through double-glass window.

6.2 Recommendations

For future research, it is suggested that the following geometrical configurations of enclosures be considered:

(1) vertically separated two-zone enclosures (multi-story configurations),

(2) three-zone enclosures in horizontal, in vertical, or in combined horizontal-vertical arrangement.

For more accurate simulations, the following modifications are recommended:

(3) a more precise formulation for air infiltration.

(4) Sources of heat and contaminant, released by both occupants and building components, should be better characterized.

(5) A more accurate description of the supply diffuser is required in order to obtain a more reliable boundary condition for ventilation air.

(6). The dynamic response of variables to the variations of the source emission rate and boundary conditions, such as the heat transfer from a time-dependent heat source or from solar radiation, should be investigated.

The development of modern super computers has created favorable conditions for numerical modeling of air movement and the convective heat and mass transfer in buildings. Large-scale computations may now be performed within acceptable costs. In these circumstances, computational prediction is expected to play a more important role in further research on indoor air quality, thermal comfort, and other heat and mass transfer phenomena in buildings.

REFERENCES

Allan, T., Kirkpatrick, A., and Hill, D.D. 1988, "Mixed Convection Heat Transfer in a Passive Solar Building", Solar Energy Vol. 40, No. 1, pp.25-34.

Barakat, S.A. 1987, "Inter-zone Convective Heat Transfer in Building: A Review", Journal of Solar Energy Engineering Vol. 109, pp.71-78.

Bejan, A. 1984, "Convective Heat Transfer", John, Wiley & Sons. Inc.

Berne and Villand, M. 1987, "Prediction of Air Movement in a Ventilated Enclosure with 3-D Thermohydraulic Code TRIO", ROOMVENT-87, Stockholm.

Boardman, C.R., Kirkpatrick, A., and Anderson, R. 1989, "Influence of Aperture Height and Width on Interzonal Natural Convection in a Full-size, Air-filled Enclosure", Proc. of 1989 National Heat Transfer Conference, ASME HTD-Vol.107, pp.273-280, Heat transfer in Convective Flow.

Bradshaw, P., Ferriss, D.H., and Atwell, N.P. 1967, "Calculation of Boundary Layer Development Using the Turbulent Energy Equation", J. of Fluid Mech., Vol.28, Part 3, pp.593-616.

Brown, W.G. and Solvason, K.R. 1962, "Natural Convection Through Rectangular Opening In Partitions, Part 1; Vertical Partition", Int. J. Heat And Mass Transfer, Vol.5, pp.859-868.

Catton, I. 1978, "Natural Convection in Enclosures", Heat Transfer, Vol. 6, Natural Research Council of Canada.

Chang, L.C., Lloyd, J.R., and Yang, K.T. 1982, "A Finite Difference Study of Natural Convection in Complex Enclosures", Proc. of 7th Int. Heat Transfer Conf., Vol. 2, pp.183-188.

Cheesewright, R. 1968, "Turbulent Natural Convection from A Vertical Plane Surface", Transactions of ASME, Journal of Heat Transfer, Feb. pp.1-8.

Chen, Q. 1988, "Indoor Airflow, Air Quality and Energy Consumption of Building", PH.D Thesis, Deft University of Technology.

Chen, Q. and Kooi, J.Van der 1988, "ACCURACY-a Program for Combined Problems of Energy Analysis, Indoor Airflow and Air Quality", ASHRAE Transactions, Vol.94, Part 2, pp.196-214.

Chen, Q., Moser, A., and Huber, A. 1990a, "Prediction of Buoyant, Turbulent Flow by a Low-Reynolds-Number k-ε Model", ASHRAE Transactions, Vol. 96. pt. 1.

Chen, Q., Moser,A., and Suter,P. 1990b, "Indoor Air Quality and Thermal Comfort under Six Kind of Air Diffusion", to be presented at ASHRAE Winter Meeting, Feb. New York.

Chen, Q., Suter,P., and Moser,A. 1990c, "Evaluation of Indoor Air Quality by a Perceived Comfort Equation", Proceedings of 5th International Conference on Indoor Air Quality and Climate: Indoor Air'90, Toronto, Canada.

Chen, Q. 1990d, Private Communication suggested by Annex 20 expert meeting, June 10-13, Oslon.

Daly, B.J. and Harlow, F.H. 1970, "Transport Equation in Turbulence", Phys. Fluid, Vol.13, pp.2634-2649.

Davidson, L. and Olsson, E. 1987, "Calculation of Age and Local Purging Flow Rate in Rooms", Building and Environment, Vol. 22,

pp.111-127.

Deardorff, J.W. 1970, "A numerical Study of Three-Dimensional Turbulent Channel Flow at Large Reynolds Numbers", J. Fluid Mech. Vol.42, pp.453-480.

Donaldson, C.P. 1972, "Calculation of Turbulent Shear Flows for Atmospheric and Vortex Motions", AIAA J. Vol.10, pp.4-12.

Driest, E.R. van 1956, "On Turbulent Flow near a Wall", J. Aeronaut. Sci. Vol.23, p.1007.

Fanger, P.O., Melikov, A.K., Hanzawa, H., and Ring, J. 1989, "Turbulence and Draft", ASHRAE Journal, Vol.31, No.7, pp.18-23.

Gadgil, A. 1979, "On Convective Heat Transfer in Building Energy Analysis", Ph.D Thesis, Department of Physics, University of California, Berkeley.

G.de Vahl Davis 1983, "Natural Convection of Air in a Square Cavity: a Benchmark Numerical Solution", Int. J. Num. Methods Fluids, Vol. 3, pp.249-264.

Gosman, A.D. and Pun, W.M. 1974, Lecture notes for a course entitled "Calculation of Recirculation Flows", Imperial College, Heat Transfer Sect., Rept.HTS/74/3.

Gosman, A.D., Nielsen, P.V., Resting, A., and Whitelaw, J.H. 1980, "The Flow Properties of Rooms with Small Ventilation Openings", Transactions of the ASME, Vol. 102, pp.316-323.

Hadjisophocleous, G.V., Sousa, A.C.M., and Venart, J.E.S. 1988, "Prediction of Transient Natural Convection in Enclosures of Arbitrary Geometry Using a Nonorthogonal Numerical Model", Numerical Heat Transfer, Vol. 13, pp.373-392.

Haghighat, F. Jiang, Z., and Wang, J.C.Y. 1989, "Natural Convection

and Airflow Pattern in a Partitioned Room with Turbulent Flow", ASHRAE Transactions, Vol. 95, Part 2, pp.600-610.

Haghighat, F., Wang, J.C.Y., and Jiang, Z. 1990a, "Three dimensional Analysis of Airflow Pattern and Contaminant Dispersion in a Ventilated Two-zone Enclosure", ASHRAE Transactions, Vol.96, Part 1, pp.831-839.

Haghighat, F., Wang, J.C.Y., and Jiang, Z. 1990b, "Development of a Three-Dimensional Numerical Model to Investigate the Airflow and Age Distribution in a Multi-zone Enclosure", Proceedings of 5th International Conference on Indoor Air Quality and Climate: Indoor Air'90, Toronto, Canada.

Hanjalic, K. and Launder, B.E. 1972, "A Reynolds Stress Model of Turbulence and Its Application to Asymmetric Shear Flows", J. Fluid Mech. Vol.52, pp.609-638.

Hanzawa, H., Melikov, A.K., and Fangar, P.O. 1987, "Airflow Characteristics in the Occupied Zone of Ventilated Spaces", ASHRAE Transactions, Vol.93, Part 1, pp.524-539.

Harlow, F.H. and Nakayama, P.I. 1968, "Transport of Turbulence Energy Decay Rate", Rep LA-3854, Los Alamos Sci. Lab., University of California.

Hill, D.D., Kirkpatrick, A., and Burns, P. 1985, "Interzonal Natural Convection Heat Transfer in a Passive Solar Building", ASME/AICH Natural Heat Transfer Conf. Denyer, Co.

Hill, D.D. and Mahajan, B.M. 1986, "Convection Between Zones with Non-linear Temperature Distribution", Proc. of the Air Movement and Distribution Conf..

Holman, J.P. 1990, "Heat Transfer", 7th edition, McGraw-Hill, New York.

Holmes, M.J. 1982, "The Application of Fluid Mechanics Simulation Program PHOENICS to a Few Typical HVAC Problems", Ove Arup and Partners, London, UK.

Horstman, R.H. 1988, "Predicting Velocity and Contamination Distribution in Ventilated Volumes Using Navier-Stokes Equations", Proc. of the ASHRAE Conference, IAQ 88, APR. 11-13, Atlanta.

ISO. 1984, "ISO Standard 7730-84, Moderate Thermal Environments-determination of PMV and PPD Indices and Specification of the Conditions for Thermal Comfort", Geneva, International Standards Organization.

Jiang, Z. and Haghighat, F. 1990, "Validation of Concordia code", a report to International Energy Agency Annex 20 Expert Meeting, Oct. 9-12, Nice.

Jones, P. and Sullivan, P.O. 1985, "Modelling of Air Flow Patterns in Large Single Volume Spaces", SERC Workshop: Development in Building Simulation Programs, Loughborough University.

Kelkar, K.M. and Patankar, S.V. 1985, "Numerical Prediction of Natural Convection in Partitioned Enclosures", Numerical Heat Transfer, pp. 63-71.

Kolmogorov, A.N. 1942, "Equation of Turbulent Motion of an Incompressible Turbulent Fluid", Izv. Akad. Nauk SSSR Ser Phys. VI, No. 1-2, 56.

Kubleck, K., Merker, G.P., and Straub, J. 1980, "Advanced Numerical Computation of Two-Dimensional Time-Dependent Free Convection in Cavity", Int. J. Heat Mass Transfer, Vol. 23, pp. 203-217.

Kuehn, T.H. 1988, "Computer Simulation of Airflow and Particle Transport in Cleanrooms", The Journal of Environmental Sciences,

Vol.31, No.5 pp.21-27.

Lam, C.K.G. and Bremhorst, K. 1981, "A Modified Form of the k-ε Model for Predicting Wall Turbulence", Journal of Fluid Engineering, ASME Trans. Vol.103, pp.456-460.

Launder, B.E. and Spalding, D.B. 1972, "Mathematical Model of Turbulence", Academic Press.

Launder, B.E. and Spalding, D.B. 1974, "The Numerical Computation of Turbulent Flows", Comput. Meth. Appl. Mech. Eng., 3, pp.269-289.

Lemaire, A.D. 1987, "The Numerical Simulation of the Air Movement and Heat Transfer in a Heated Room Resp. a Ventilated Atrium", Proc.of the Int. Conf. on Air Distribution in Ventilated Space, ROOMVENT-87, Stockholm.

Lieman, K. 1990, Master's thesis, Centre De Thermique De L'insa De Lyon.

Lin, D.S. and Nansteel, M.W. 1987, "Natural Convection Heat Transfer in a Square Enclosure Containing Water Near Its Density Maximum", Int. J. Heat and Mass Transfer, Vol. 30, No. 11, pp.2319-2329.

Mahajan, B.M. 1987, "Measurement of Inter-zonal Heat and Mass Transfer by Natural Convection", Solar Energy, Vol. 38, No.6 pp.437-446.

Markatos, N.C. and Malin, M.R. 1982, "Mathematical Modeling of Buoyancy-Induced Smoke Flow in Enclosures", Int. J. Heat Mass Transfer, Vol. 25, No. 1, pp.63-75.

Markatos, N.C. 1983, "The Computer Analysis of Building Ventilation and Heating Problems", Passive and Low Energy Architecture, pp.667-675.

Markatos, N.C. and Pericleous, K.A. 1984, "Laminar and Turbulent Natural Convection in a Enclosed Cavity", Int. J. Heat and Mass Transfer, Vol. 27, No. 5, pp.755-772.

Markatos, N.C. and Cox, G. 1984, "Hydrodynamics And Heat Transfer in Enclosures Containing a Fire Source", PH Physic-chemical hydrodynamics Vol. 5, No. 1, pp.53-66.

Murakami, S., Hibi, K., and Mochida, A. 1985, "Prediction of Room Airflow by Means of Large Eddy Simulation (part 1), Comparison between Numerical Simulation and Model Experiment", Summaries of Technical Papers of Annual Meeting of Architectural Institute of Japan, pp. 389-390 (in Japanese).

Murakami, S., Kota, S., and Suyama, Y. 1988, "Numerical and Experimental Study on Turbulent Diffusion Fields in Conventional Flow Type Clean Rooms", ASHRAE Transactions, Vol. 94, p.2.

Nansteel, M.W. and Greif, R. 1981, "Natural Convection in Undivided and Partially Divided Rectangular Enclosures", Trans. ASME J. of Heat Transfer, Vol. 103, pp.623-629.

Nansteel, M.W. and Greif, R. 1984, " An Investigation of Natural Convection in Enclosures with Two and Three Dimensional Partitions", Int. J. Heat Mass Transfer, Vol. 27, No. 4, pp.561-571.

Neymark, J., Kirkpatric, A., and Anderson, R. 1988, "High Rayleigh Number Natural Convection in Partially Divided Air and Water Filled Enclosures", Proc. of Nat. Heat Transfer Conf..

Nielsen, P.V. 1974, "Flow in Air Conditioned Rooms", Ph.D Thesis, Technical University of Denmark, Conpenhagen.

Nielsen, P.V. 1974, "Moisture Transfer in Air Conditioned Rooms and Cold Stores", Proc. of 2nd Int. CIB/RILEM Symposium on Moisture Problems in Building, Rotterdam.

Nielsen, P.V., Restivo, A., and Whitelaw, J.H. 1979, "Buoyancy-Affected Flows in Ventilated Rooms", J. Numerical Heat Transfer, Vol. 2,

pp. 115-127.

Nielsen, P.V. 1981, "Contaminant Distribution in Industrial Area with Forced Ventilation and Two-Dimensional Flow", IIR-Joint Meeting, Commission E1, Essen West Germany.

November, M. and Nansteel, M.W. 1987, "Natural Convection in Rectangular Enclosures Heated from Below and Cooled along One Side", Int. J. Heat Mass Transfer, Vol.30, No.11, pp.2433-2440.

Ostrach, S. 1982, "Natural Convection Heat Transfer in Cavities and Cells", Proc. of Int. Heat Transfer Conf., pp.365-379, Hemisphere, Washington DC.

Patankar, S.V. and Spalding, D.B. 1972, "A Calculation Procedure for Heat, Mass and Momentum Transfer in Three-dimensional Parabolic Flows", Int. J. Heat Mass Transfer, Vol.15, P.1787.

Patankar, S.V. 1980, "Numerical Heat Transfer And Fluid Flow", Hemisphere publishing corporation, New York.

Patel, V.C., Rodi, W., and Scheuerer, G. 1985, "Turbulence Models for near Wall and Low Reynolds Number flow: a review", AIAA Journal, Vol.23, No.9, pp.1308-1319.

Plandtl, L. 1926, "Ueber Dieausgebidete Turbulenz", Proceedings of the Second International Congress for Applied Mechanics, Zurich, pp.62-74.

Pun, W.M. and Spalding, D.B. 1976, "A General Compute Program for Two-dimensional Elliptic Flows", HTS/76/2, Imperial College, London.

Reynolds, O. 1894, "On the Dynamical Theory of Incompressible Viscous Fluids and the Determination of the Criterion", Phil. Trans. Roy. Soc. London, 186, 123-161.

Riffat, S.B. 1989, "Interzone Air Movement and Its Effect on

Condensation in Houses", Applied Energy, Vol.32, pp.49-69.

Rodi, W. 1984, "Turbulence Models and Their Application in Hydraulics - a State of the Art Review", Second revised edition, Karlsruhe, Federal Republic of Germany.

Sakamoto, Y. and Matsuo, Y. 1980, "Numerical Prediction of Three-Dimensional Flow in Ventilated Room Using Turbulent Models", Appl. Math. Modelling, Vol.4, pp.67-72.

Sandberg, M. 1981, "What Is Ventilation Efficiency?", Bldg Envir., Vol. 16, No.2, pp.123-135.

Sandberg, M. and Sjoberg, M. 1983, "The Use of Moments for Assessing Air Quality". Bldg Envir., Vol. 18, pp.181-197.

Scott, D., Anderson, R., and Figliola, R. 1988, "Blockage of Natural Convection Boundary Layer Flow in a Multizone Enclosure", Int. J. Heat and Fluid Flow, Vol. 9, No.2, pp.208-214.

Shaw, B.H. 1972, "Heat and Mass Transfer by Natural Convection and Combined Natural and Forced Air Flow through Large Rectangular Openings in a Vertical Partition", Proc. Int. Mech. Eng. Conf.on Heat and Mass Transfer by Combined Forced and Natural Convection, Manchester, Vol. 819, pp.31-39.

Spalding, D.B. 1972, "A novel Finite-difference Formulation for Differential Expression Involving Both First and Second Derivatives", Int. J. Num. Methods Eng., vol.4, p.551.

Thorshauge, J. 1982, "Air Velocity Fluctuations in the Occupied Zone of Ventilated Space", ASHRAE transactions, Vol.88, Part 2, pp.753-764.

Tennekes, H. and Lumley, J.L. 1972, "A First Course in Turbulence", MIT Press, London.

Wang, J.C.Y., Jiang, Z., and Haghighat, F. 1990, "Influence of Air

Infiltration on Isothermal Airflow and Contaminant Field in a Partitioned Enclosure", accepted by "Energy and Buildings".

Weber, D.D. 1980, "Similitude Modeling of Natural Convection Heat Transfer though a Aperture in Passive Solar Heated Buildings", Ph.D. thesis, Department of Physics, University of Idaho, Moscow, Idaho.

Wray, W.O. and Weber, D.D. 1979, "Last Similarity Studies; Part 1 Hot Zone/Cold Zone: A Quantitative Study of Natural Heat Distribution Mechanisms in Passive Solar Building", Proc. 4th Nat.Passive Solar Conf.,Kansas City, Vol. 4, pp.226- 230.

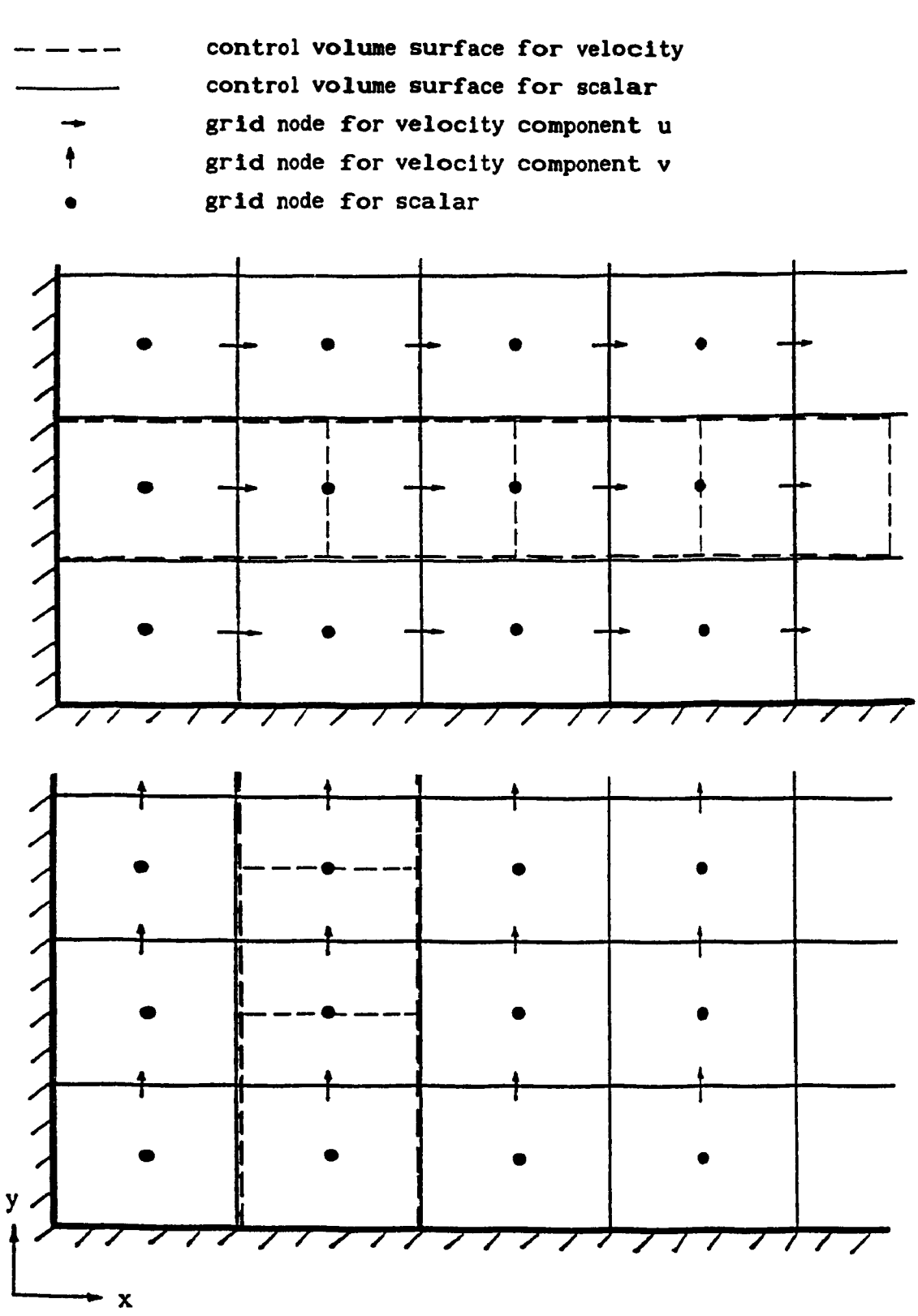

Figure 4.2.1 Structure of mesh system

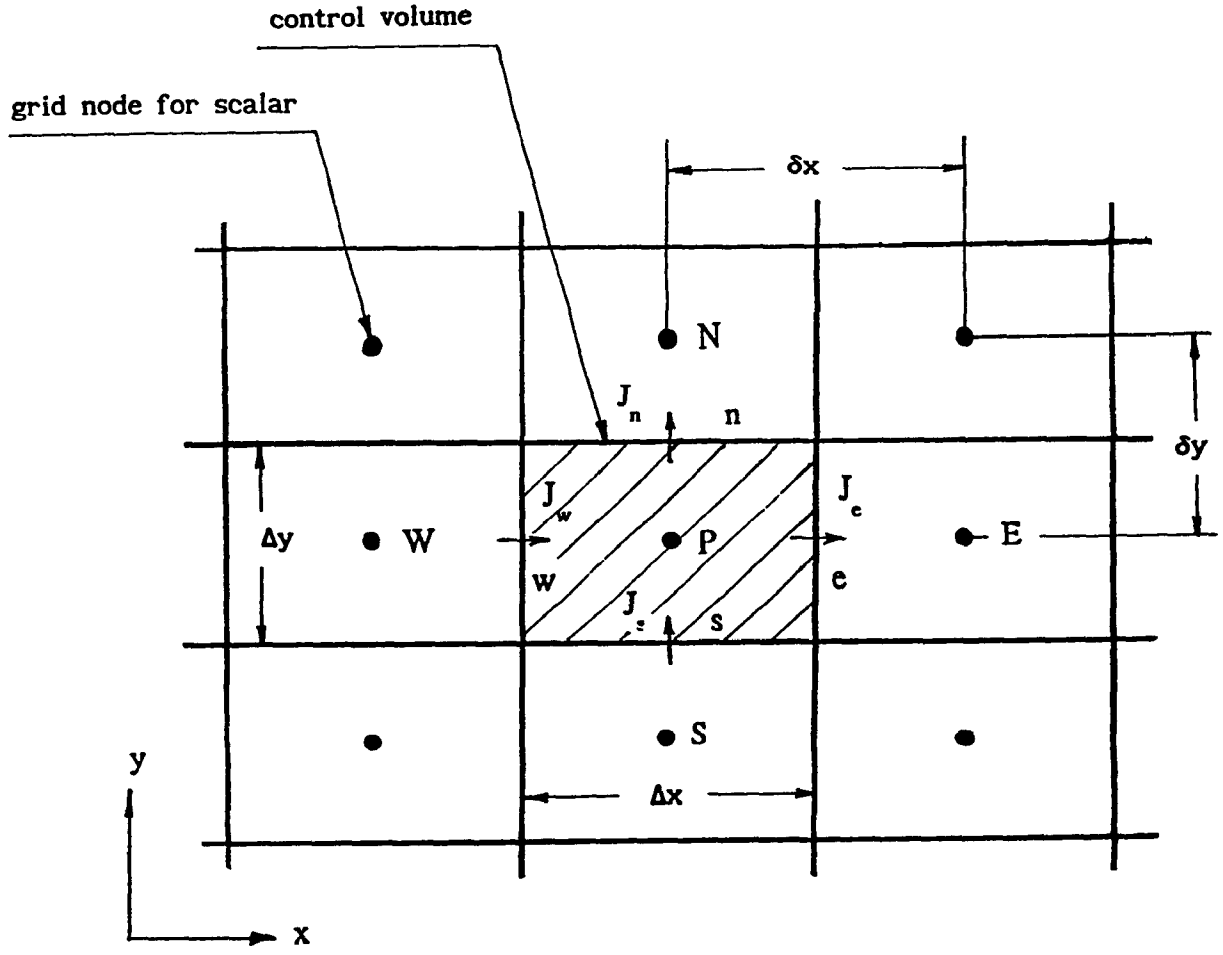

Figure 4.2.2 Flux over control-volume surfaces

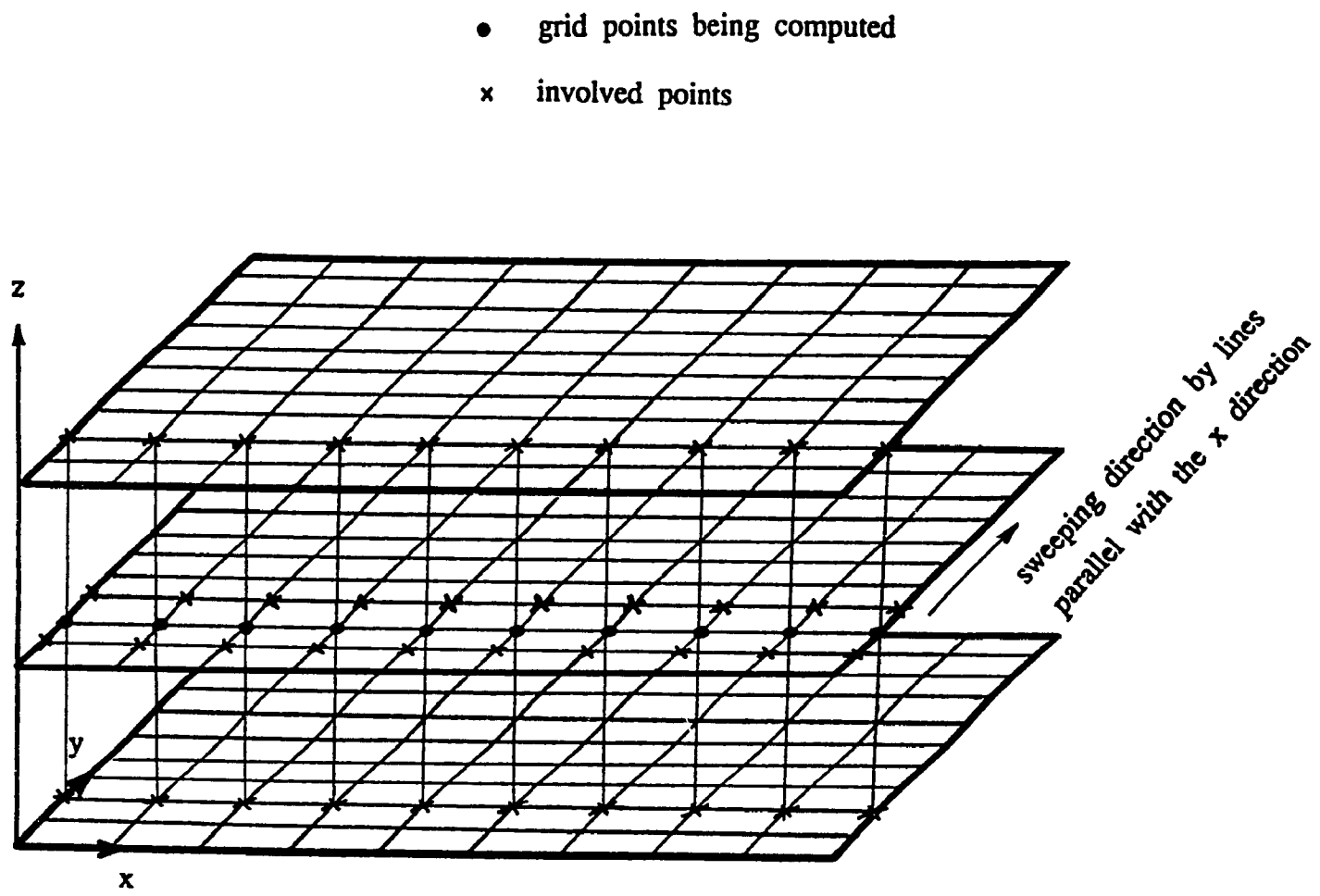

Figure 4.4.1 Line-by-line iteration

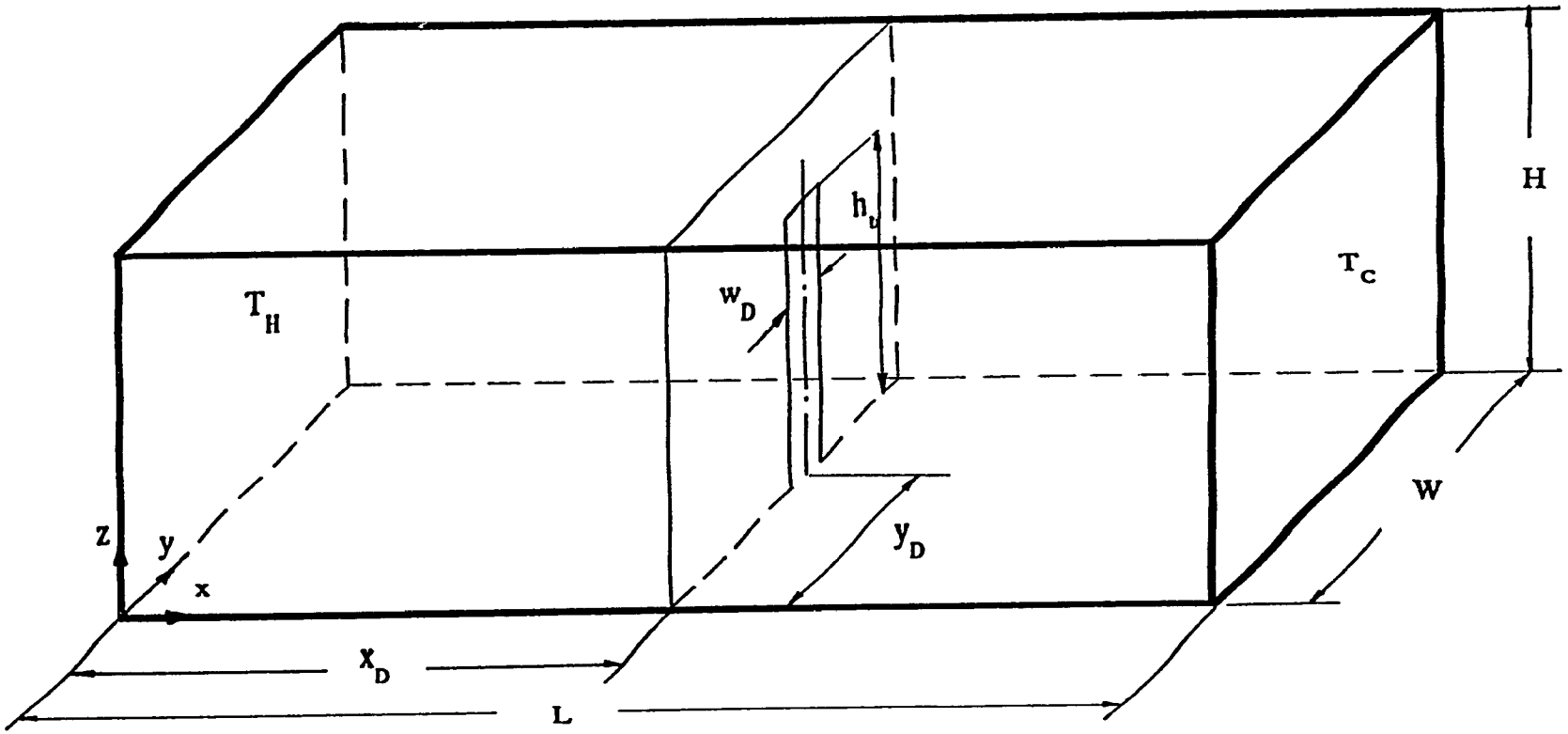

Figure 5.1.1 Configuration of a partitioned enclosure

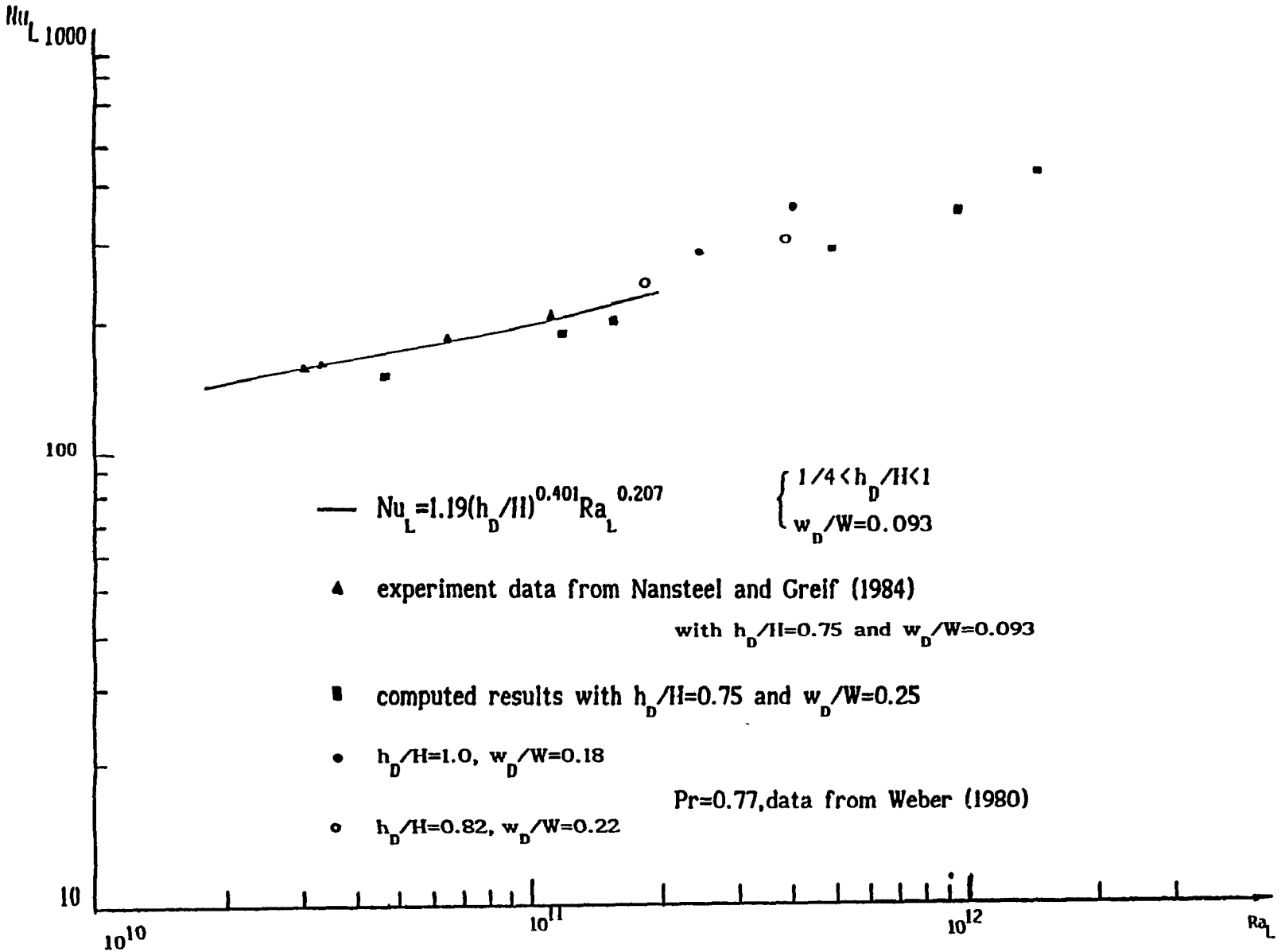

Figure 5.1.2 Comparison with experimental measurements

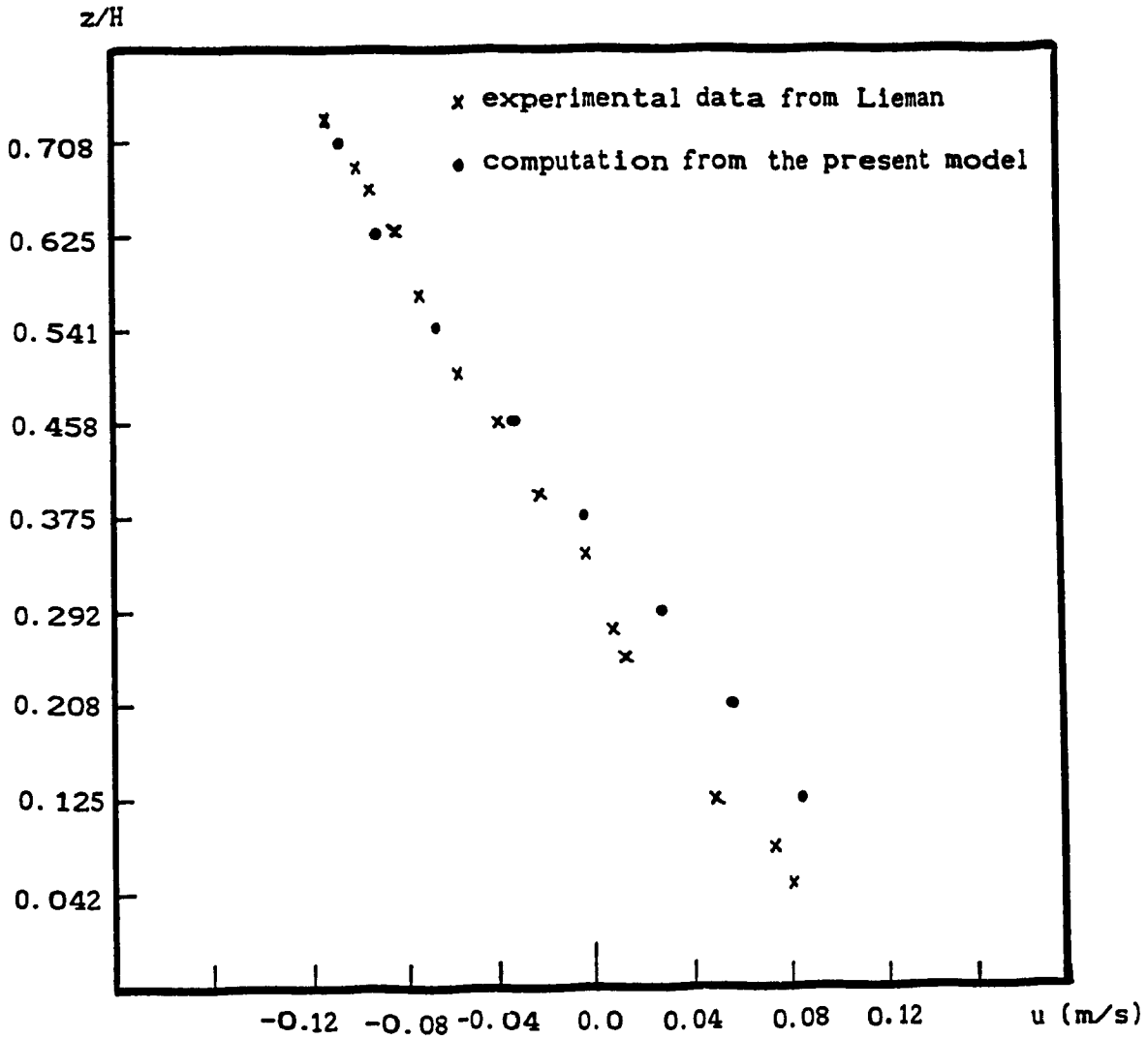

Fig. 5.1.3 Velocity distribution at the center of door opening in comparison with measurements

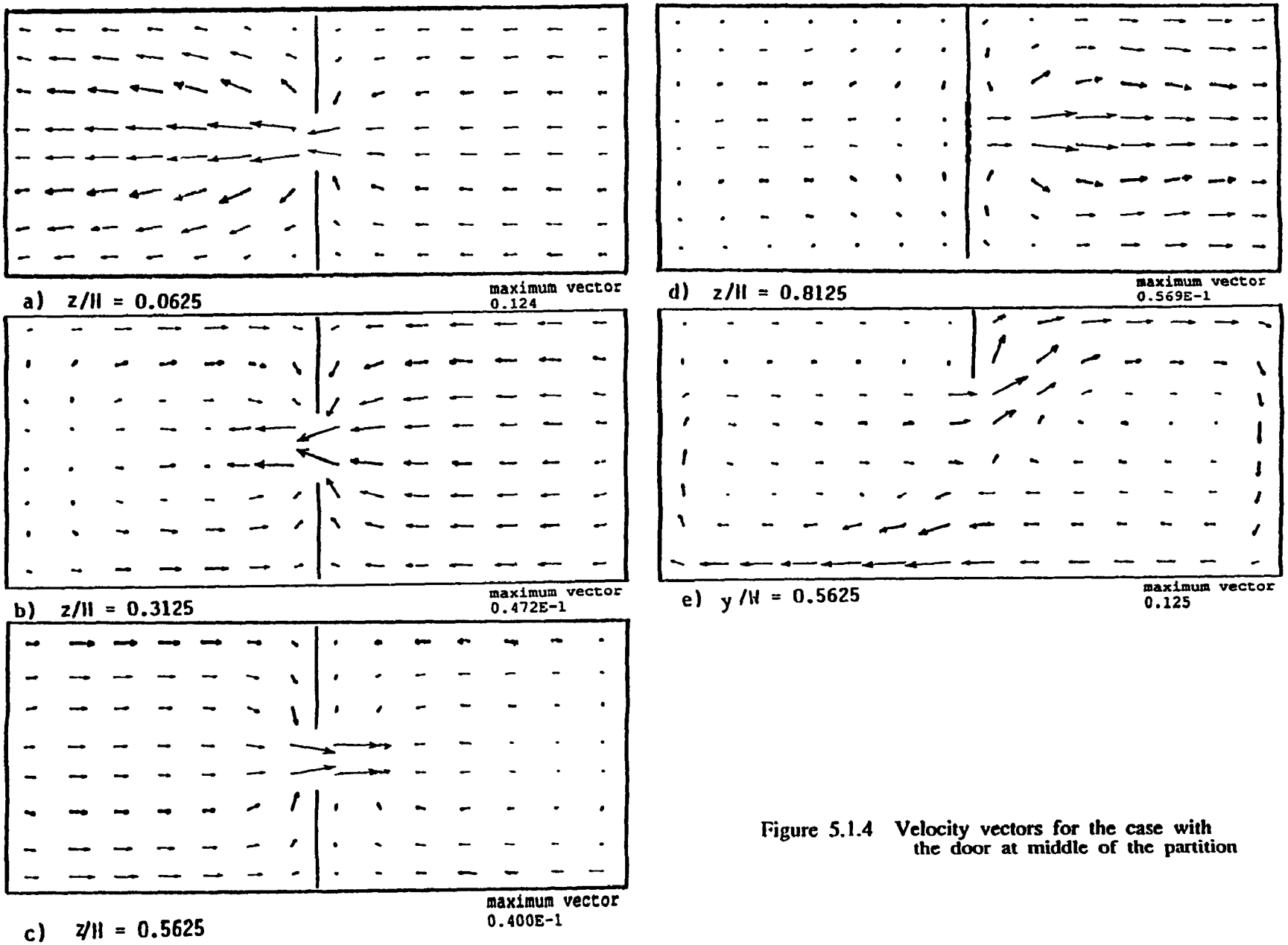

Figure 5.1.4 Velocity vectors for the case with the door at middle of the partition

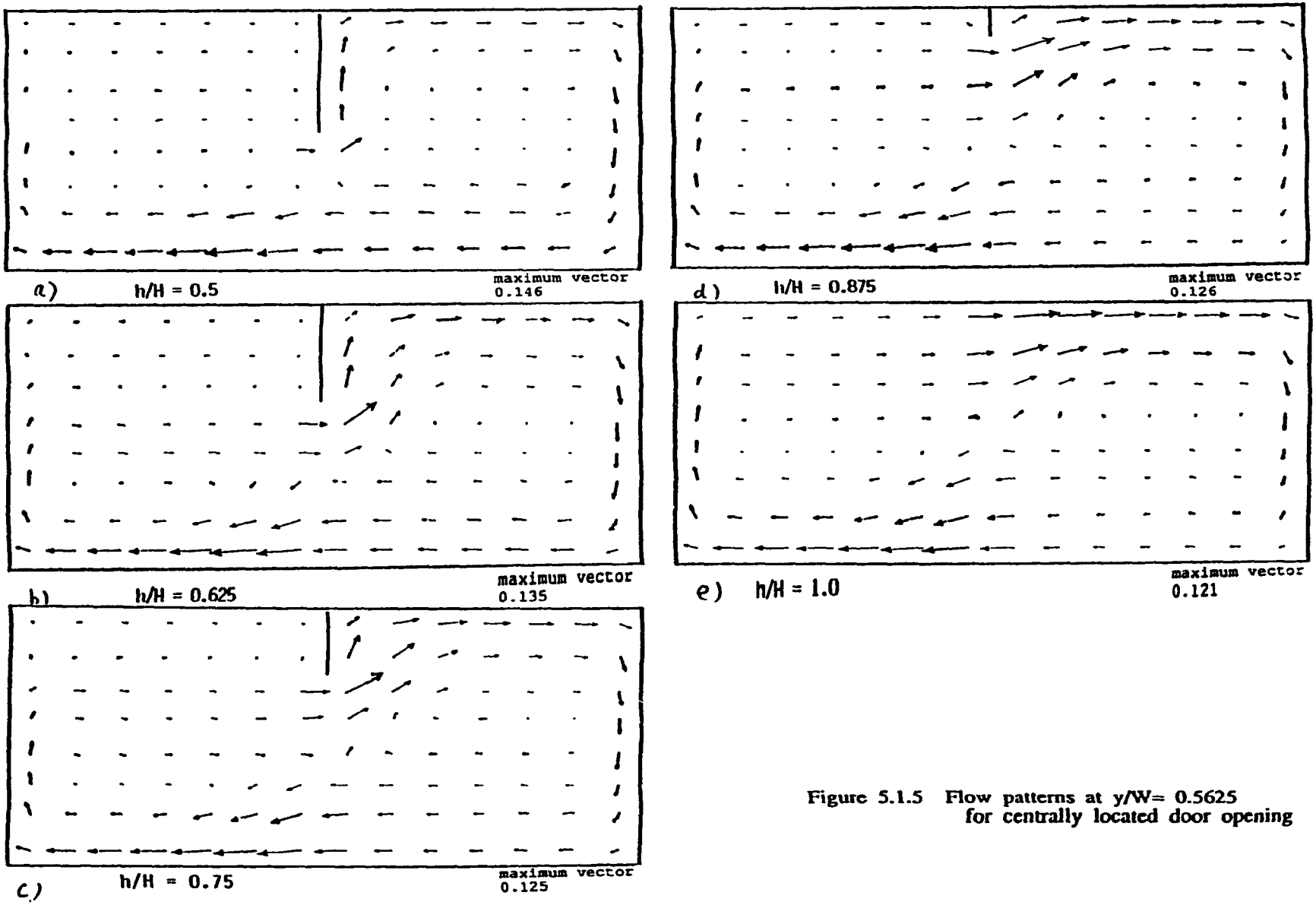

Figure 5.1.5 Flow patterns at y/W= 0.5625 for centrally located door opening

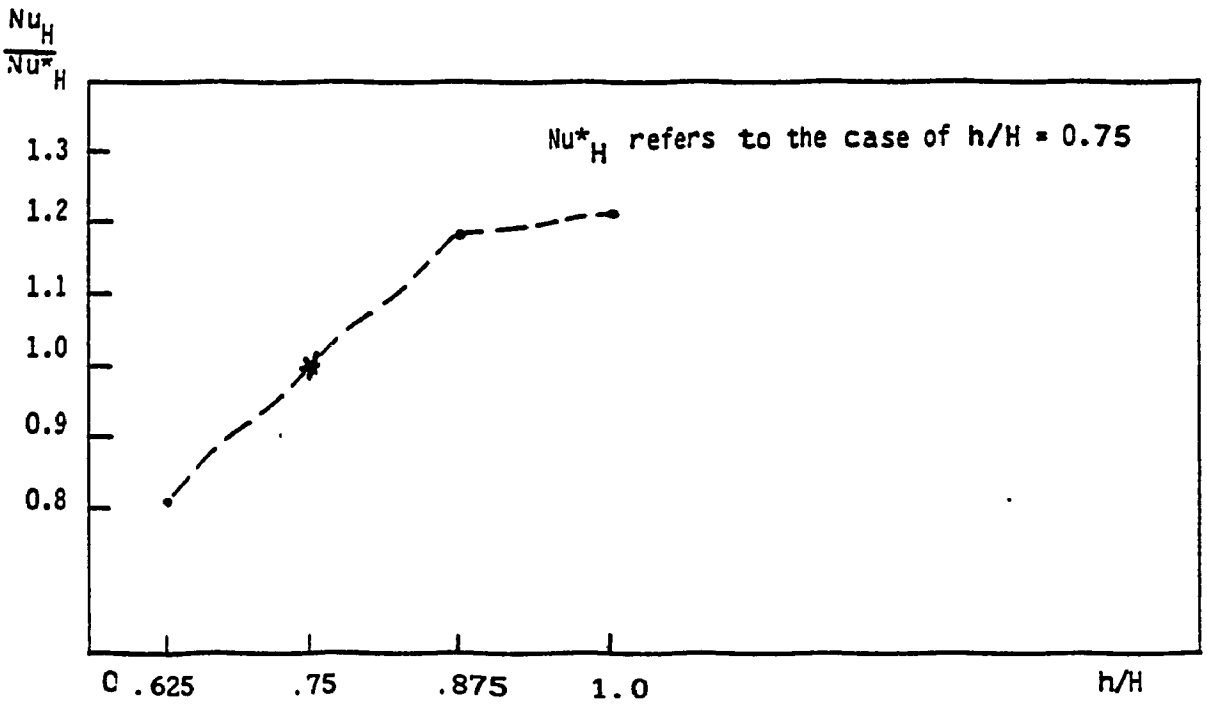

Figure 5.1.6 Nusselt number variation with door height

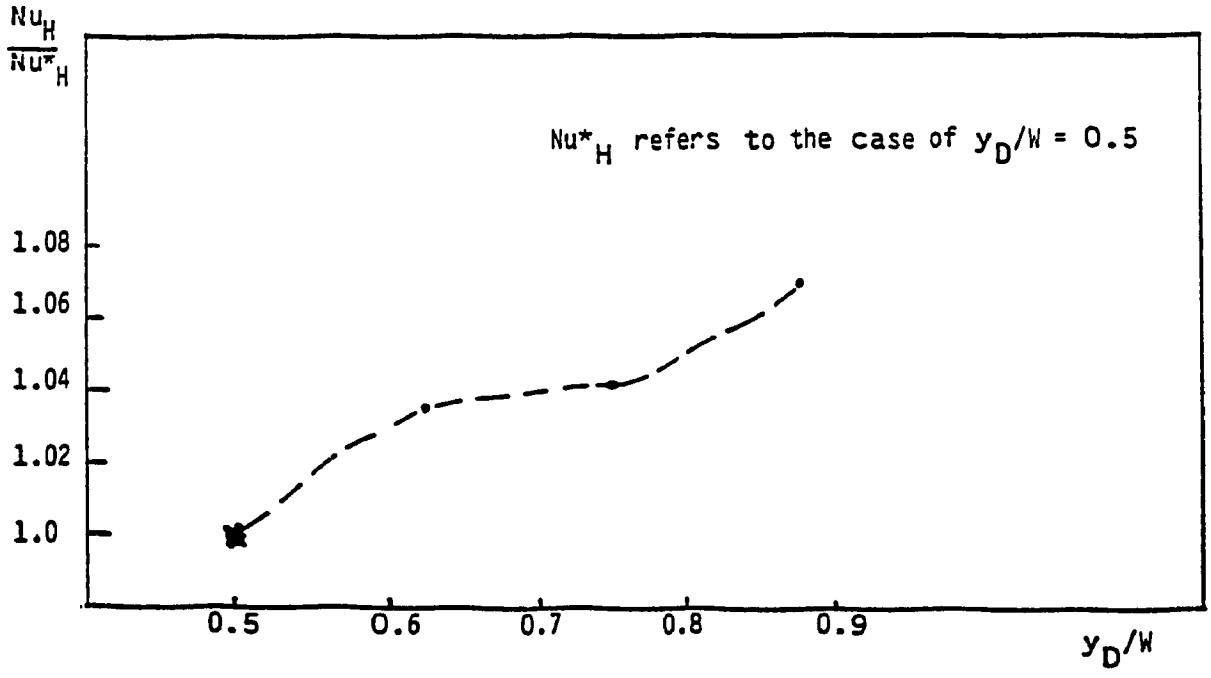

Figure 5.1.7 Nusselt number variation with door location

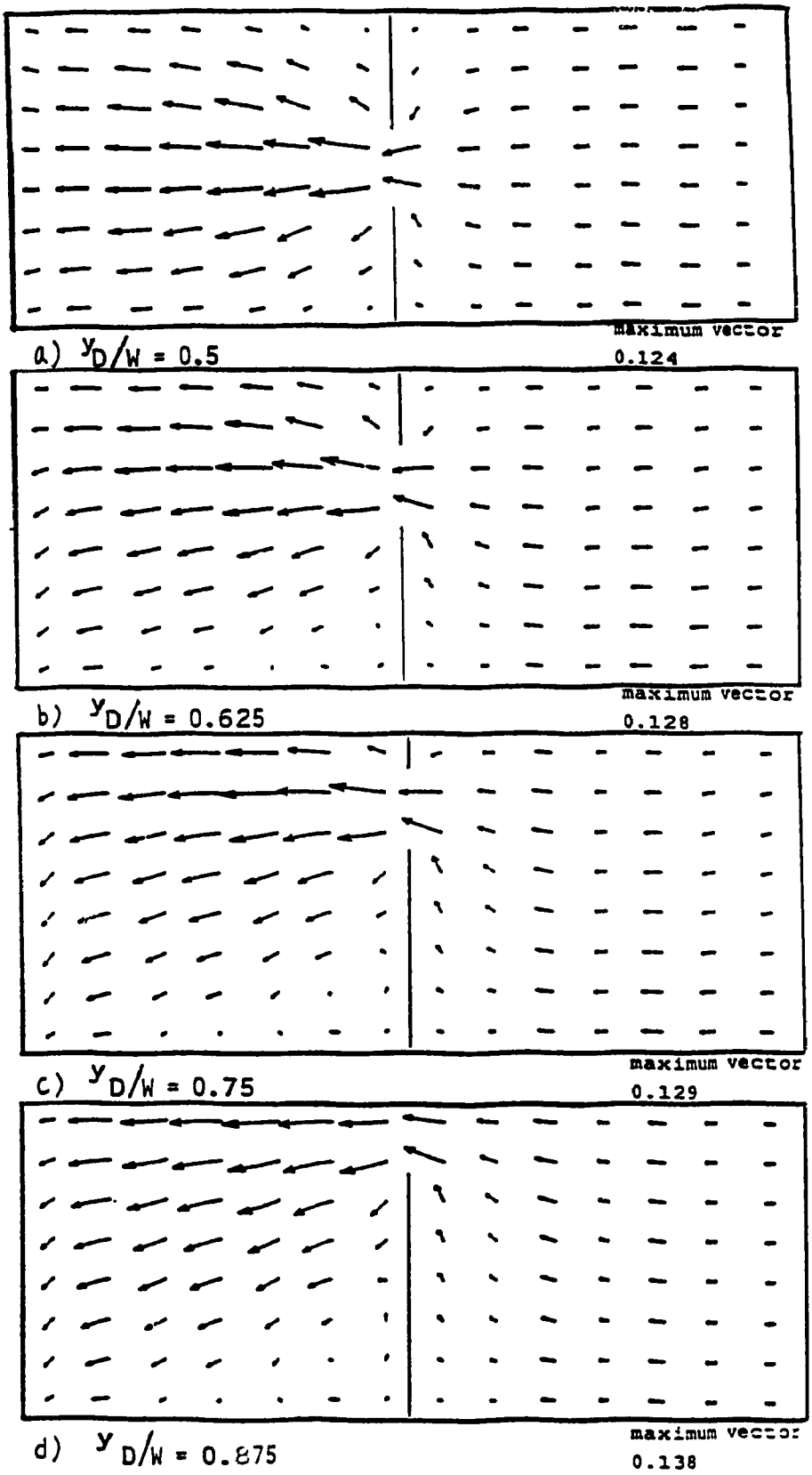

Figure 5.1.8 Variation of flow pattern at z/H=0.0625 with door location

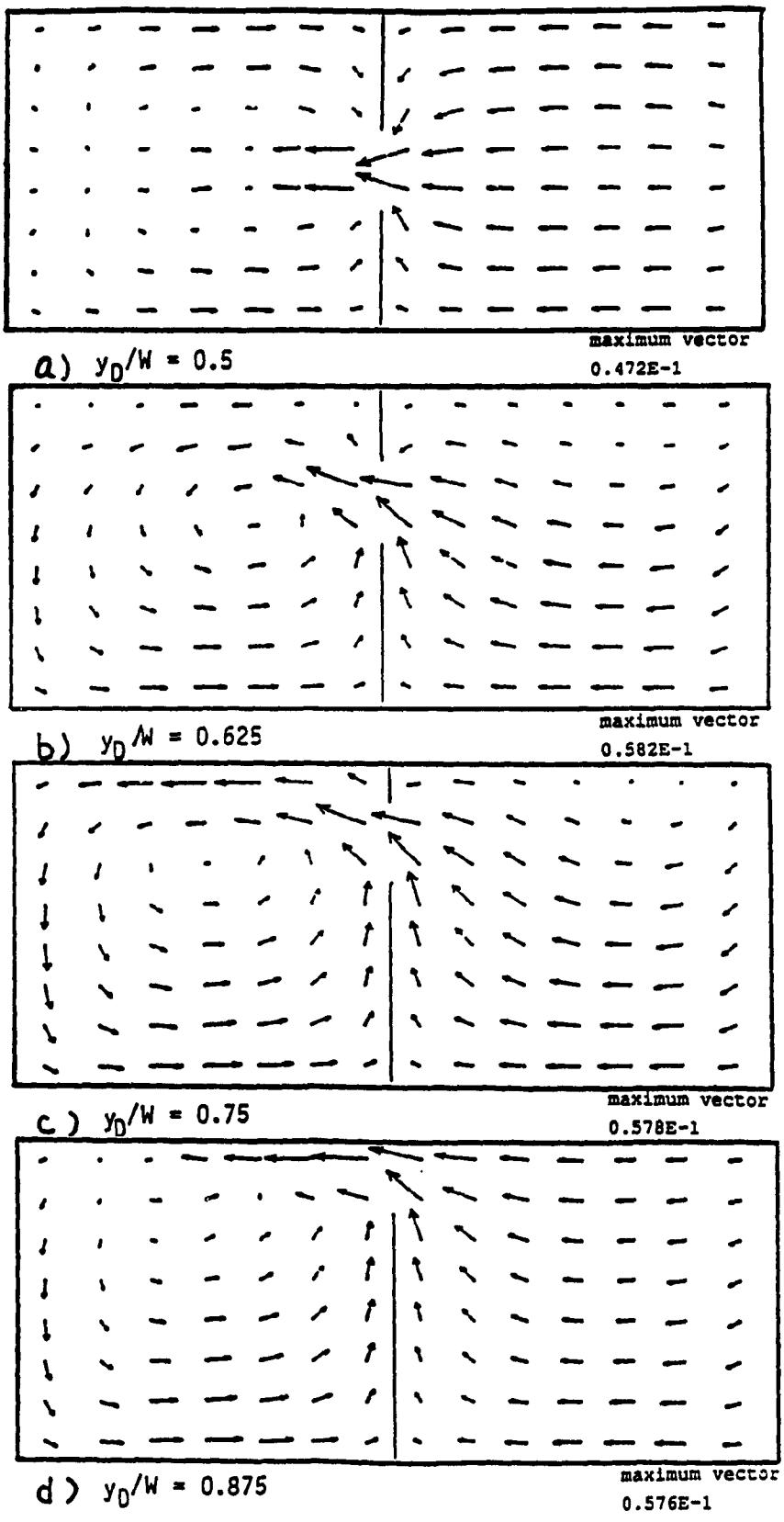

Figure 5.1.9 Variation of flow pattern at z/H=0.3125 with door location

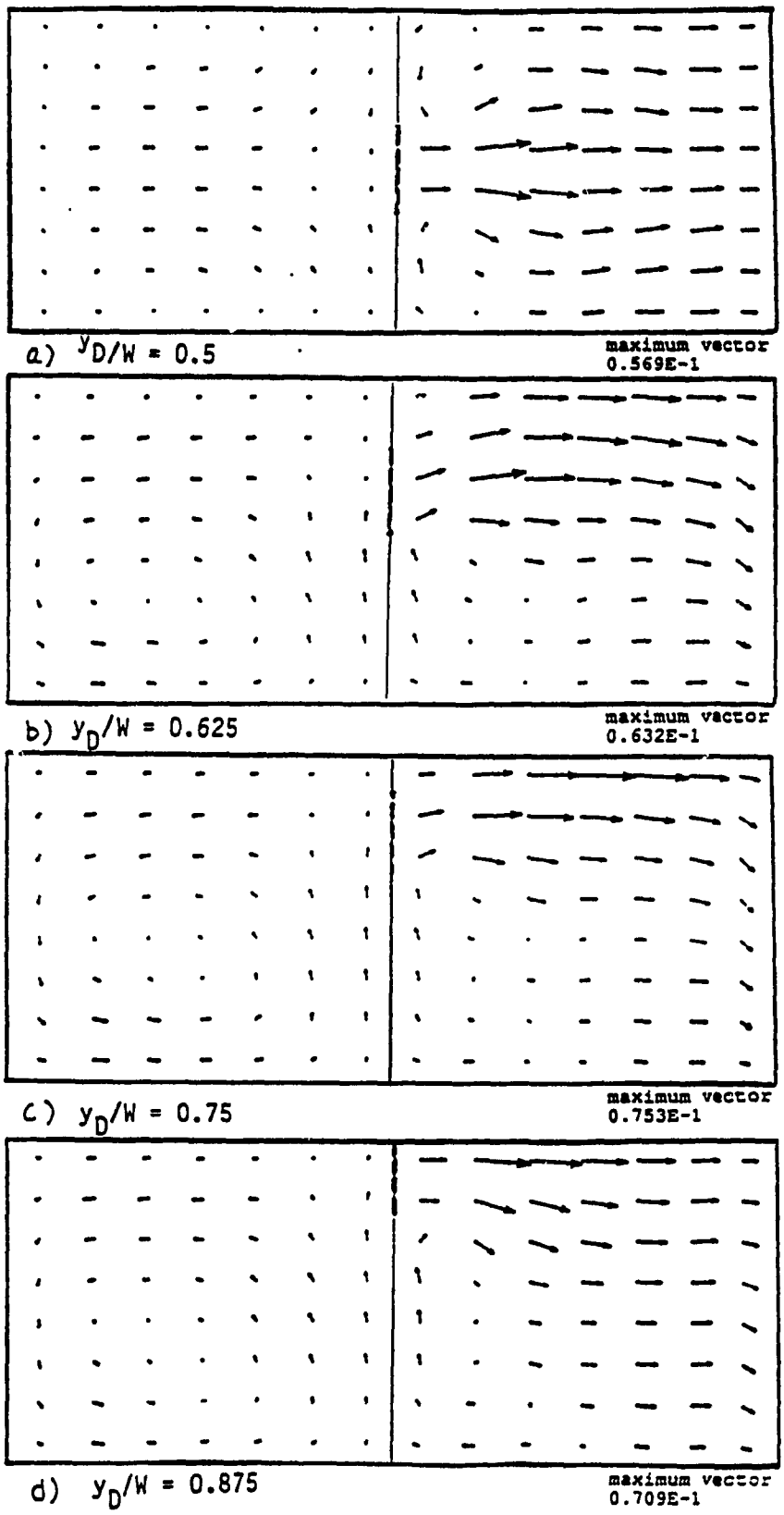

Figure 5.1.10 Variation of flow pattern at z/H=0.8125 with door location

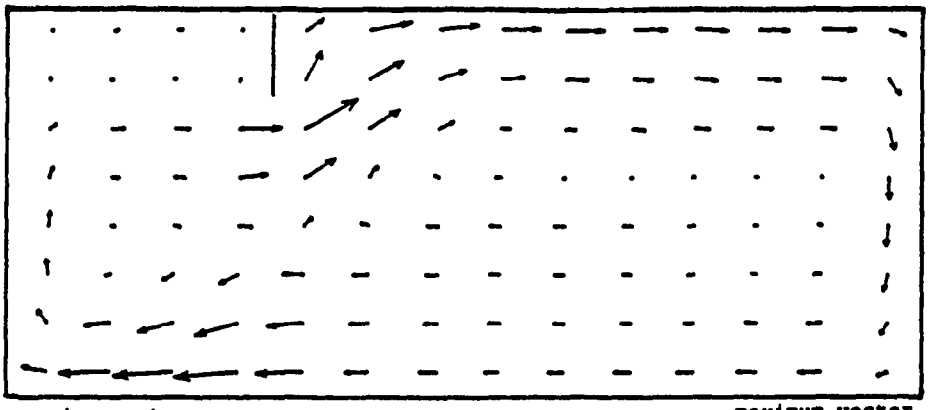

a) $x_D/L = 0.2857$

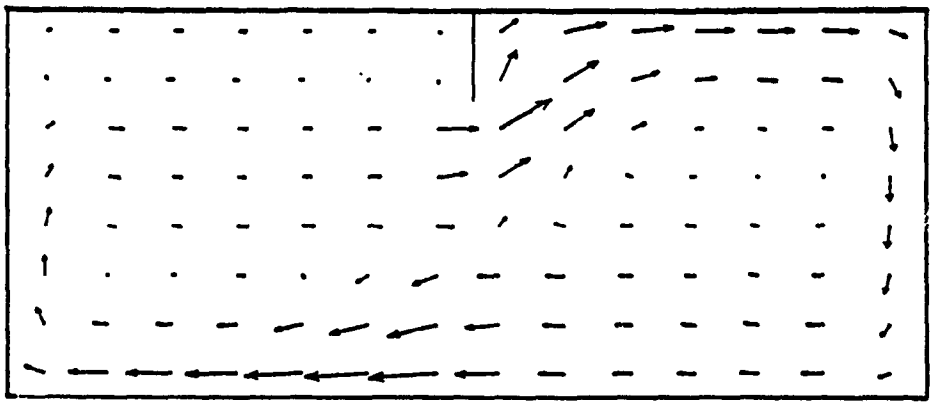

b) $x_D/L = 0.5$

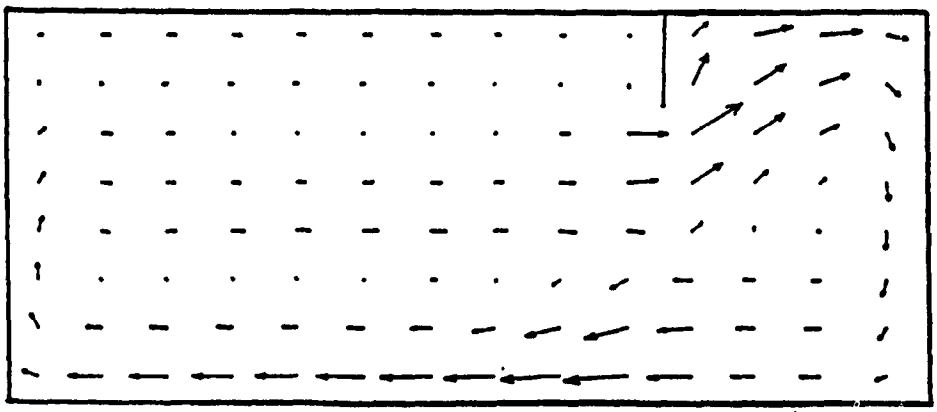

c) $x_D/L = 0.7143$

Figure 5.1.11 Velocity vectors at y/W=0.5625 (h/H=0.75)

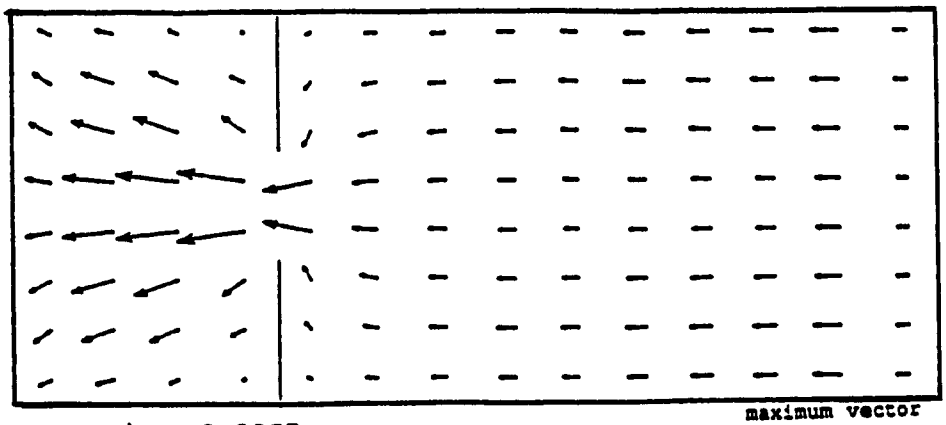

a) $x_D/L = 0.2857$

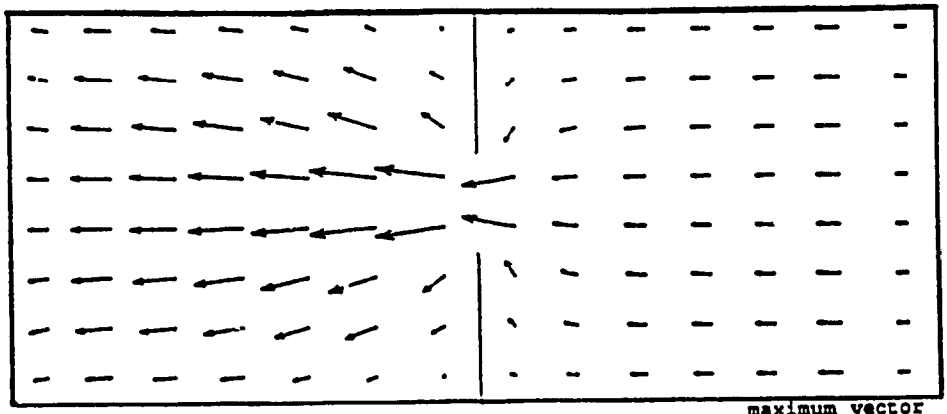

b) $x_D/L = 0.5$

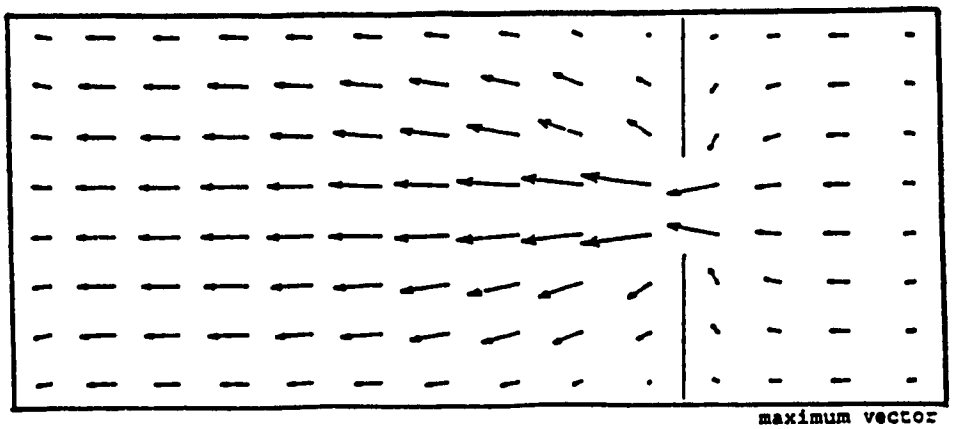

c) $x_D/L = 0.7143$

Figure 5.1.12 Velocity vectors at z/H=0.0625 (h/H=0.75)

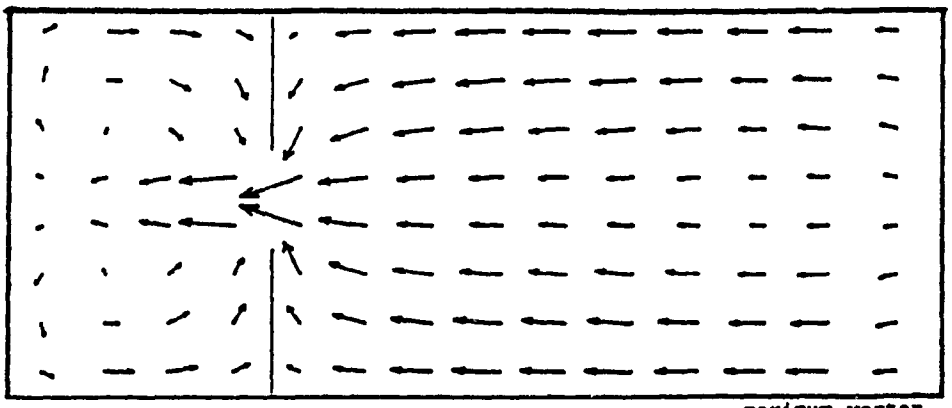

a) $x_D/L = 0.2857$

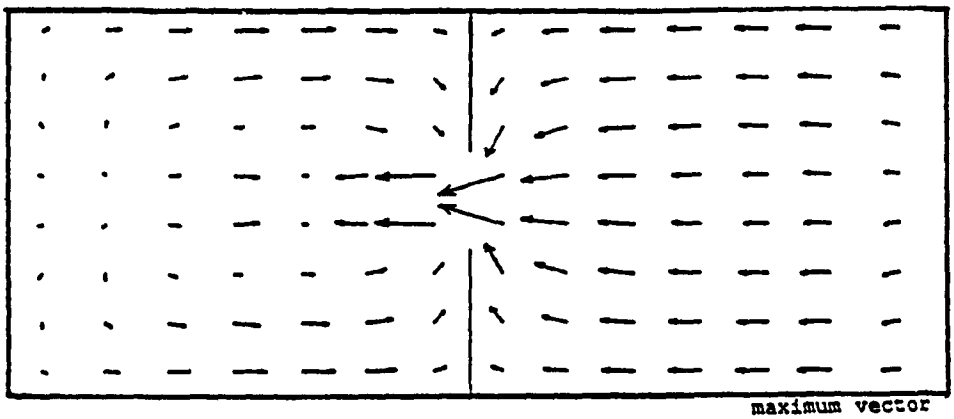

b) $x_D/L = 0.5$

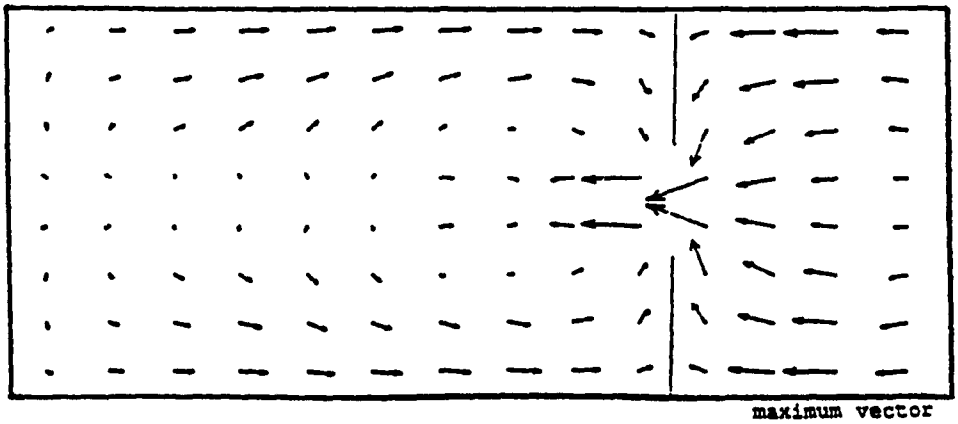

c) $x_D/L = 0.7143$

Figure 5.1.13 Velocity vectors at z/H=0.3125 (h/H=0.75)

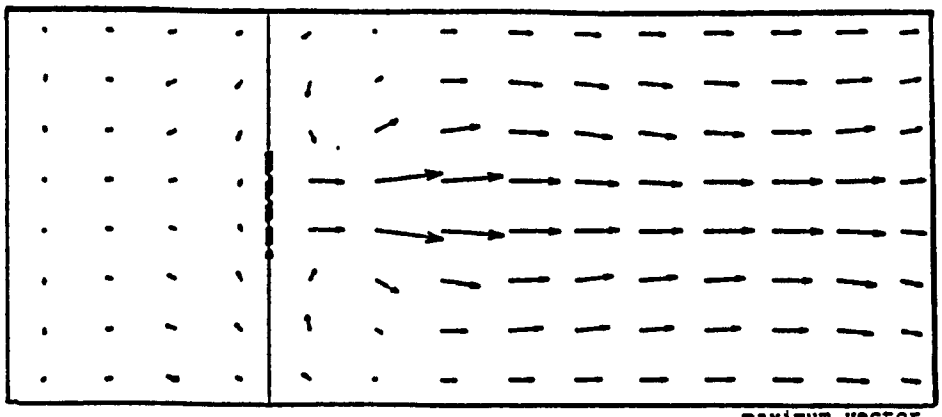

a) $x_D/L = 0.2857$

maximum vector
0.569E-1

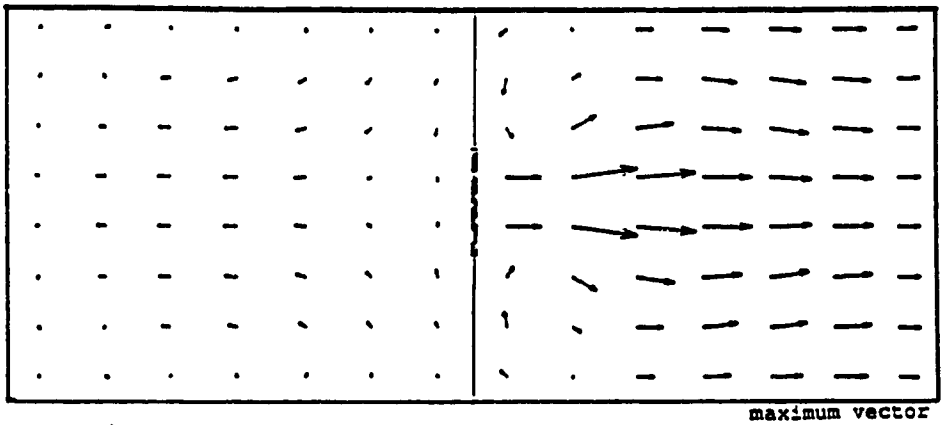

b) $x_D/L = 0.5$

maximum vector
0.592E-1

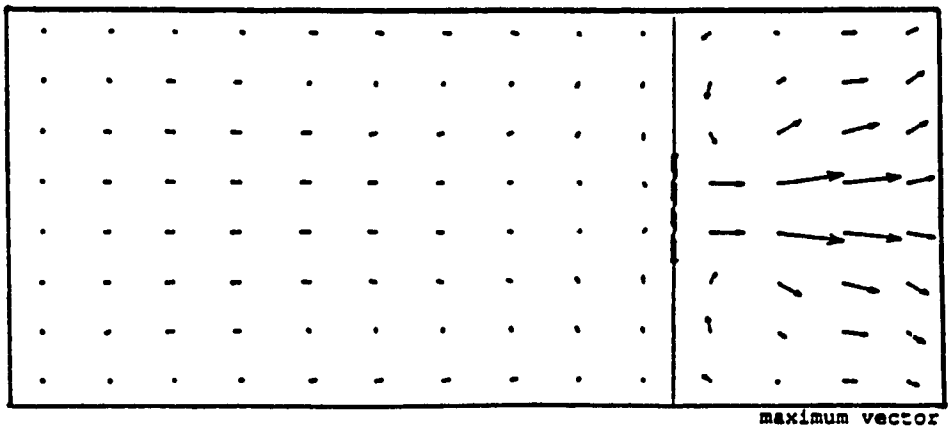

c) $x_D/L = 0.7143$

maximum vector
0.628E-1

Figure 5.1.14 Velocity vectors at z/H=0.8125 (h/H=0.75)

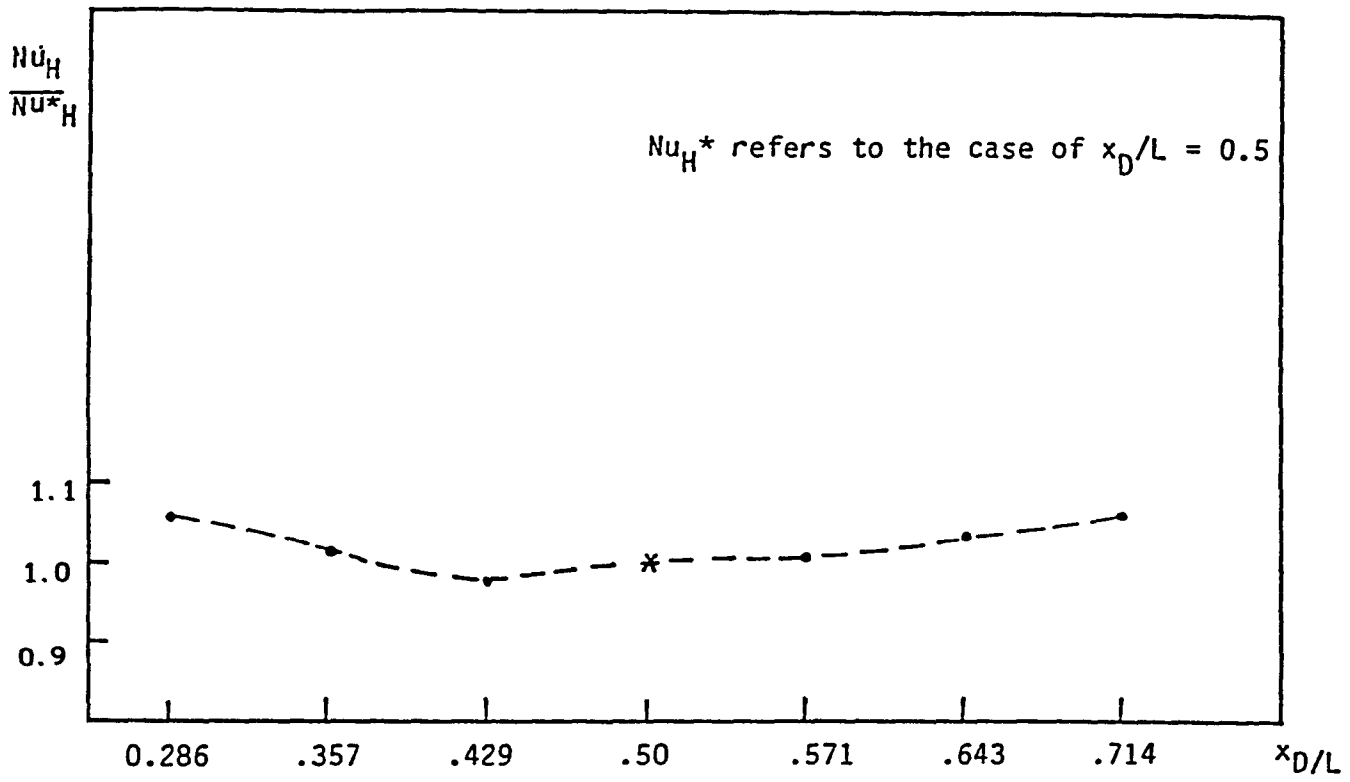

Figure 5.1.15 Nusselt number variation with partition location

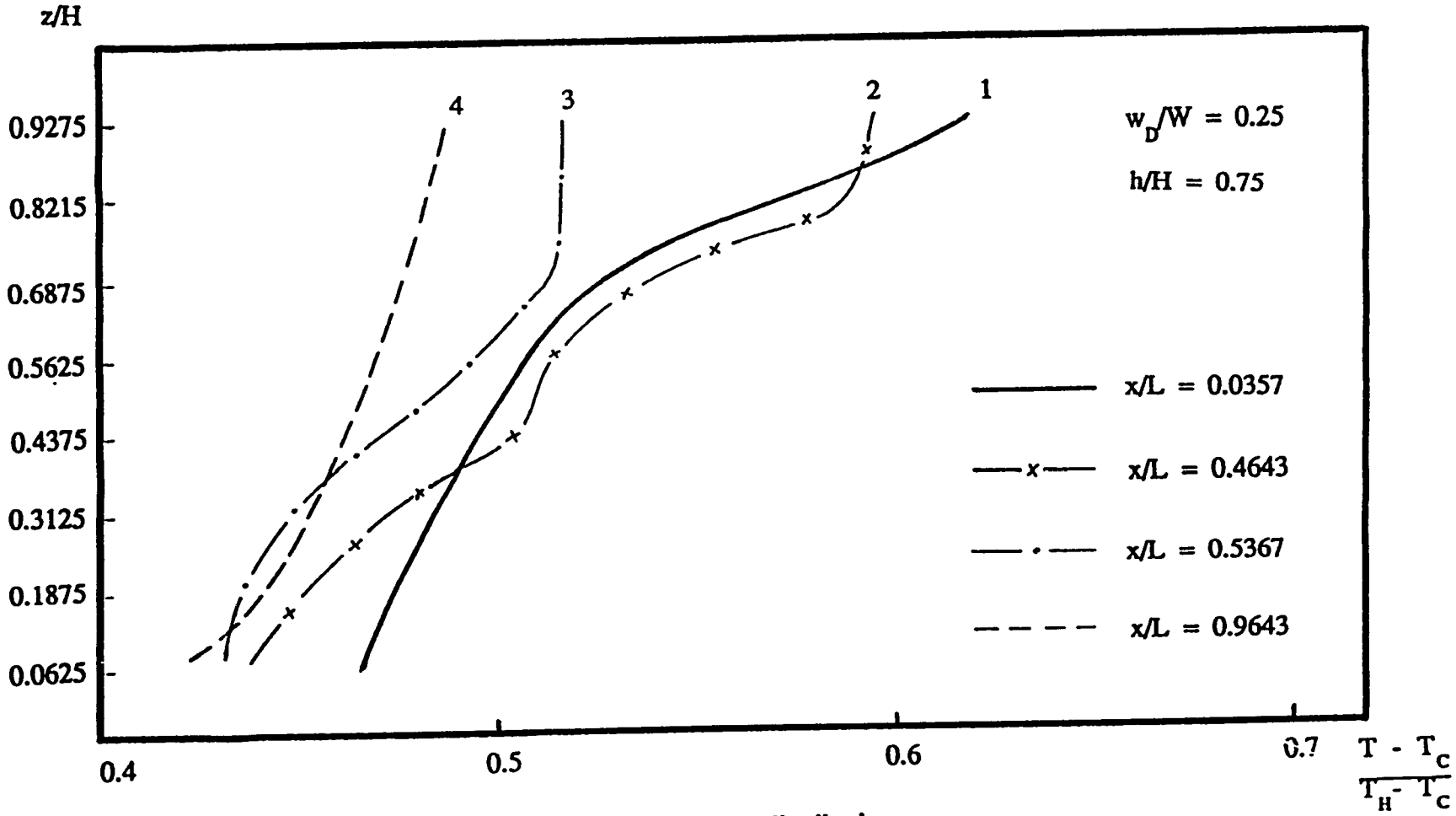

Figure 5.1.16 Vertical temperature distributions in plane y/W=0.5625 (y_D/W=0.5, x_D/L=0.5)

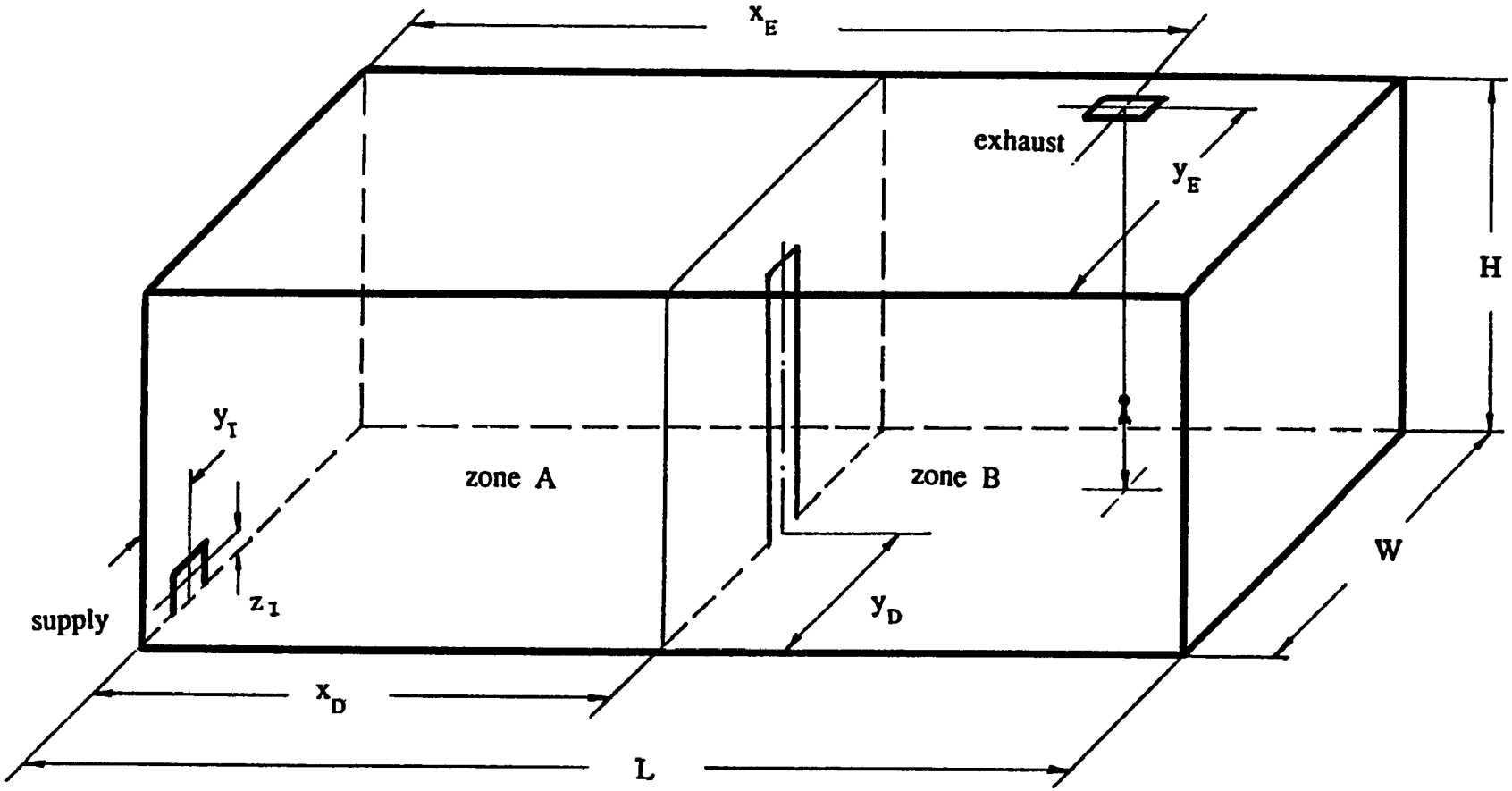

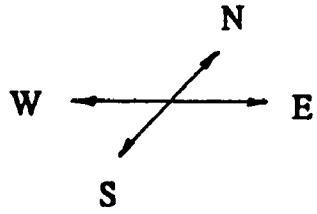

Figure 5.2.1 Configuration of a two-zone enclosure

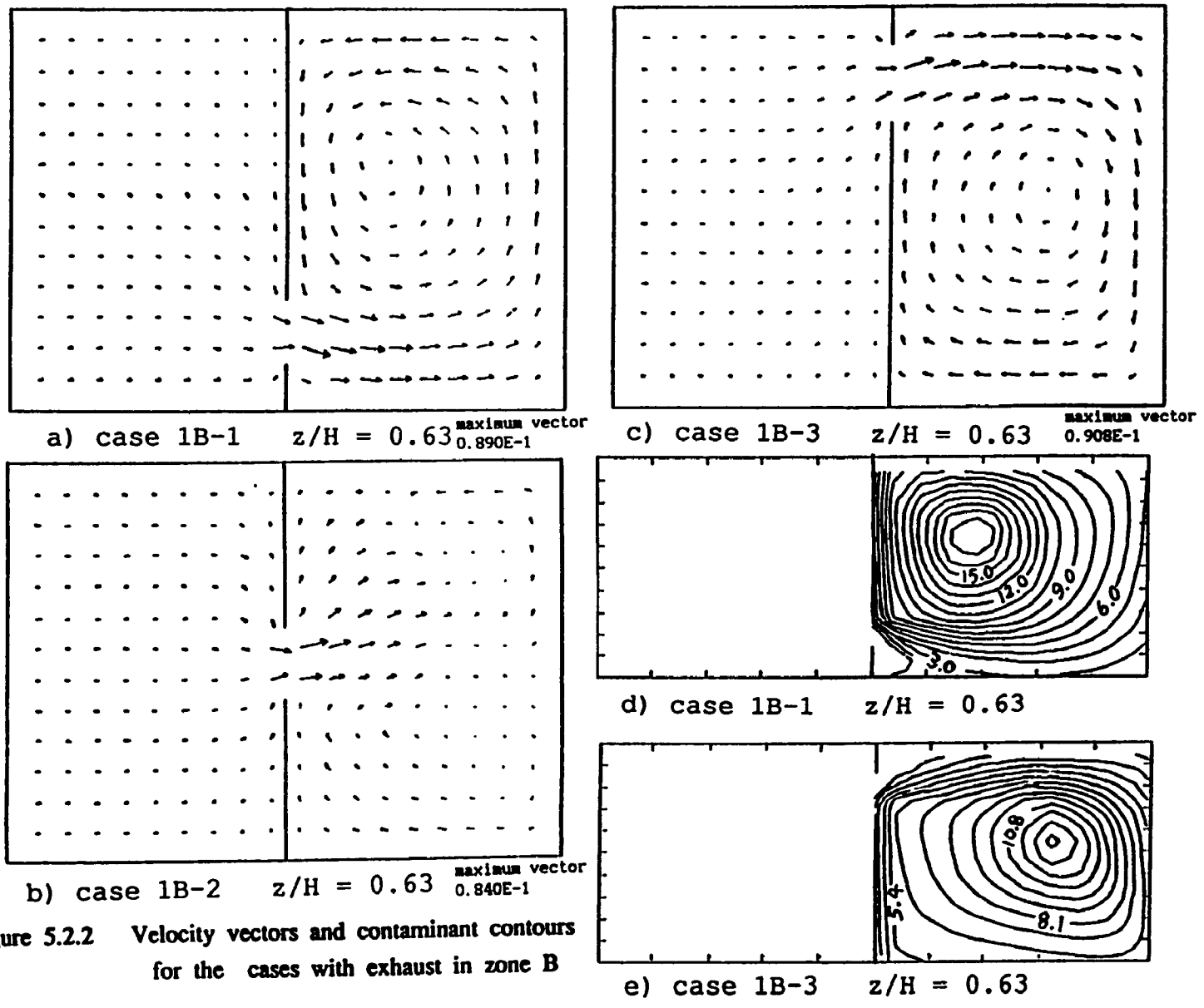

Figure 5.2.2 Velocity vectors and contaminant contours for the cases with exhaust in zone B

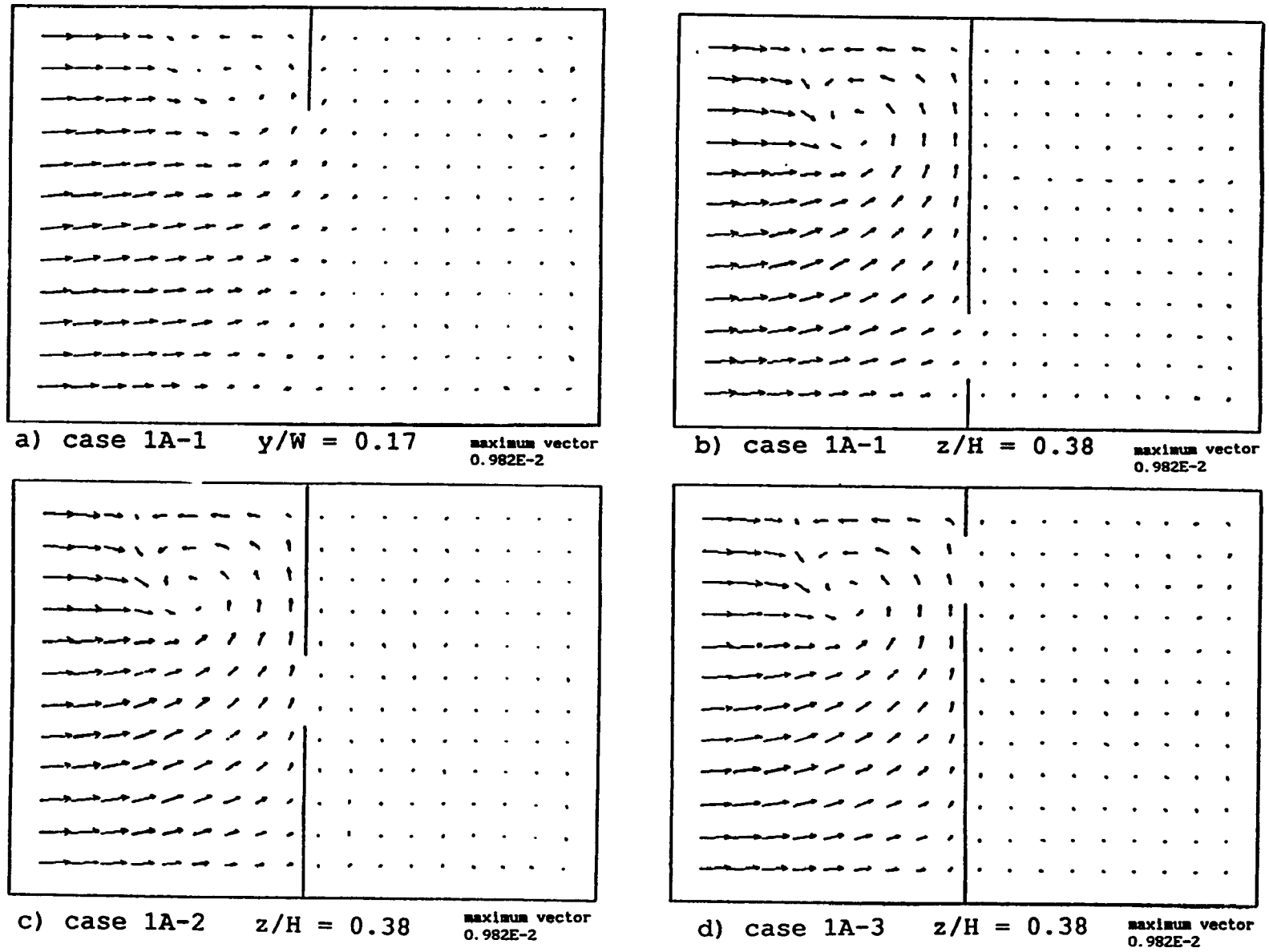

Figure 5.2.3 Velocity vectors for the cases with the exhaust in zone A

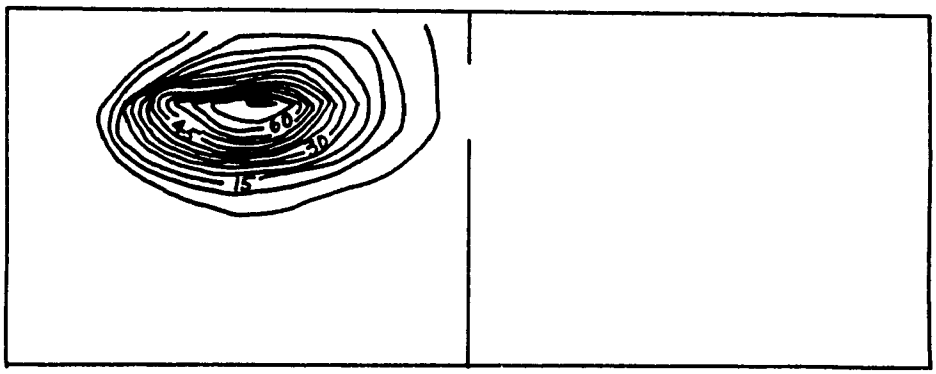

a) case 1A-3 z/H = 0.38

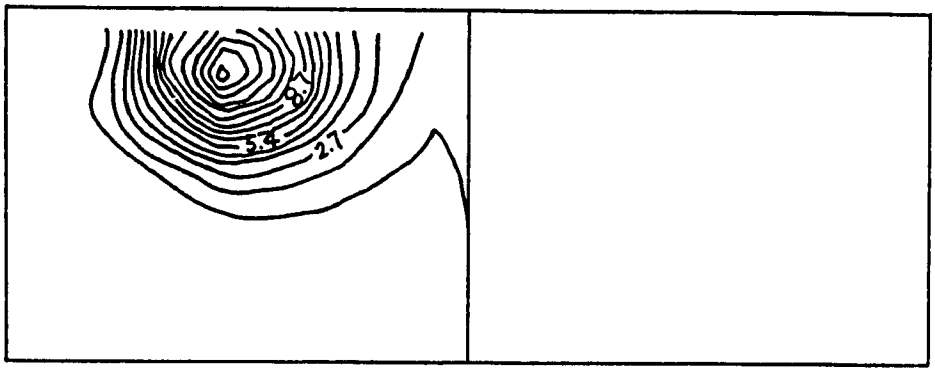

b) case 1A-3 z/H = 0.96

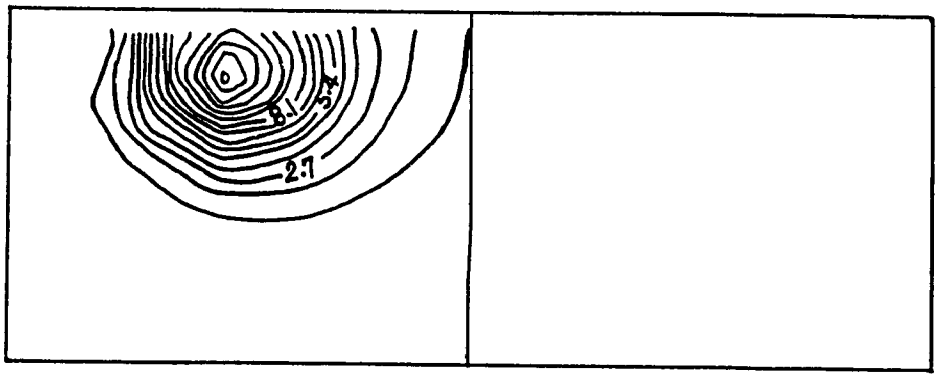

c) case 1A-1 z/H = 0.96

Figure 5.2.4 Contaminant contours for the cases with exhaust in zone A

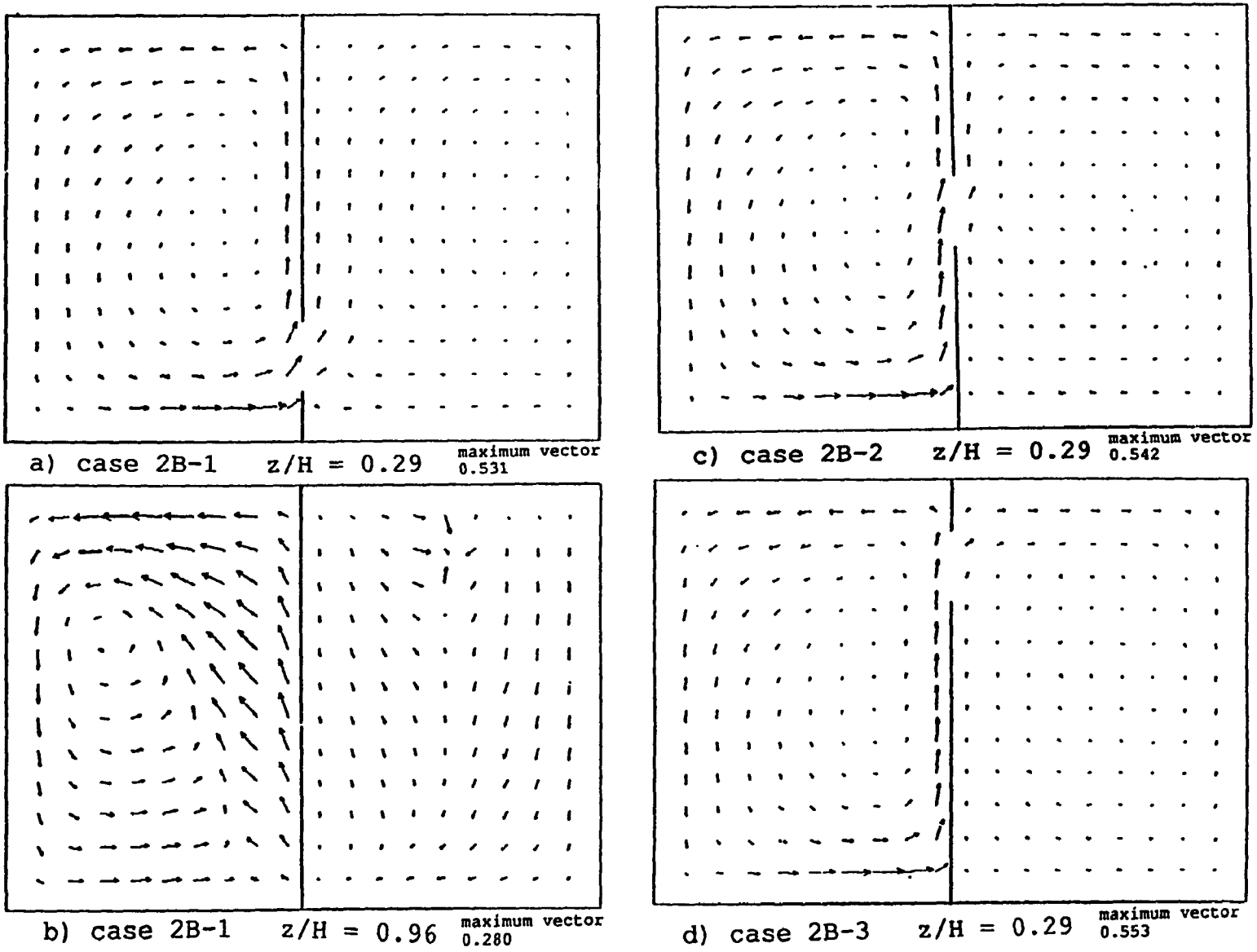

Figure 5.2.5 Velocity vectors for the cases with exhaust in zone B

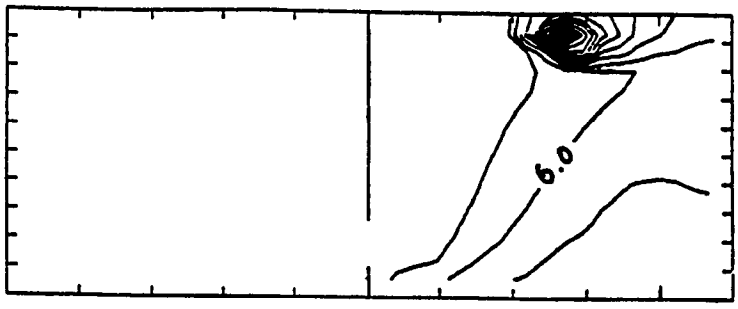

a) case 2B-1 z/H = 0.13

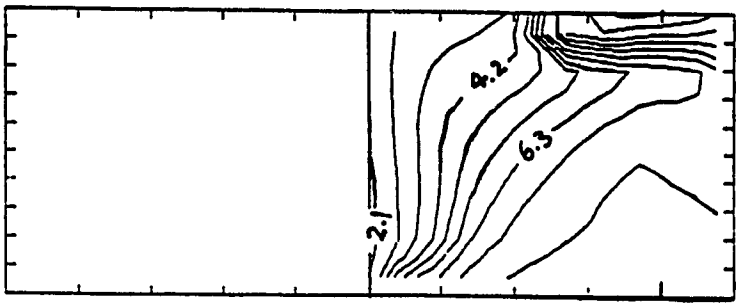

b) case 2B-1 z/H = 0.29

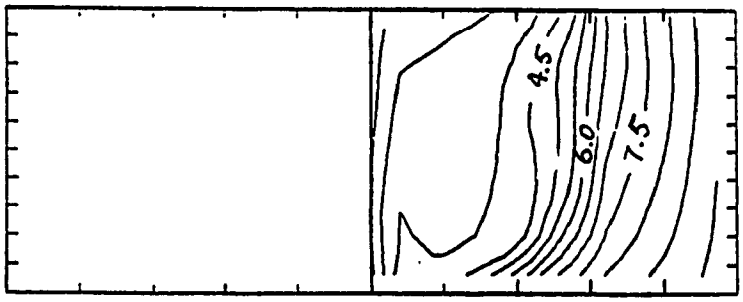

c) case 2B-1 z/H = 0.96

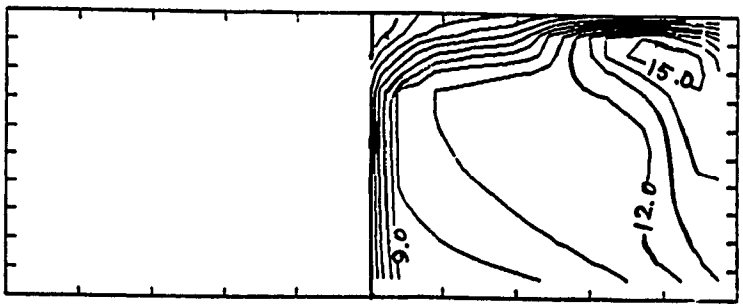

d) case 2B-3 z/H = 0.29

Figure 5.2.6 Contaminant contours for case 2B-1

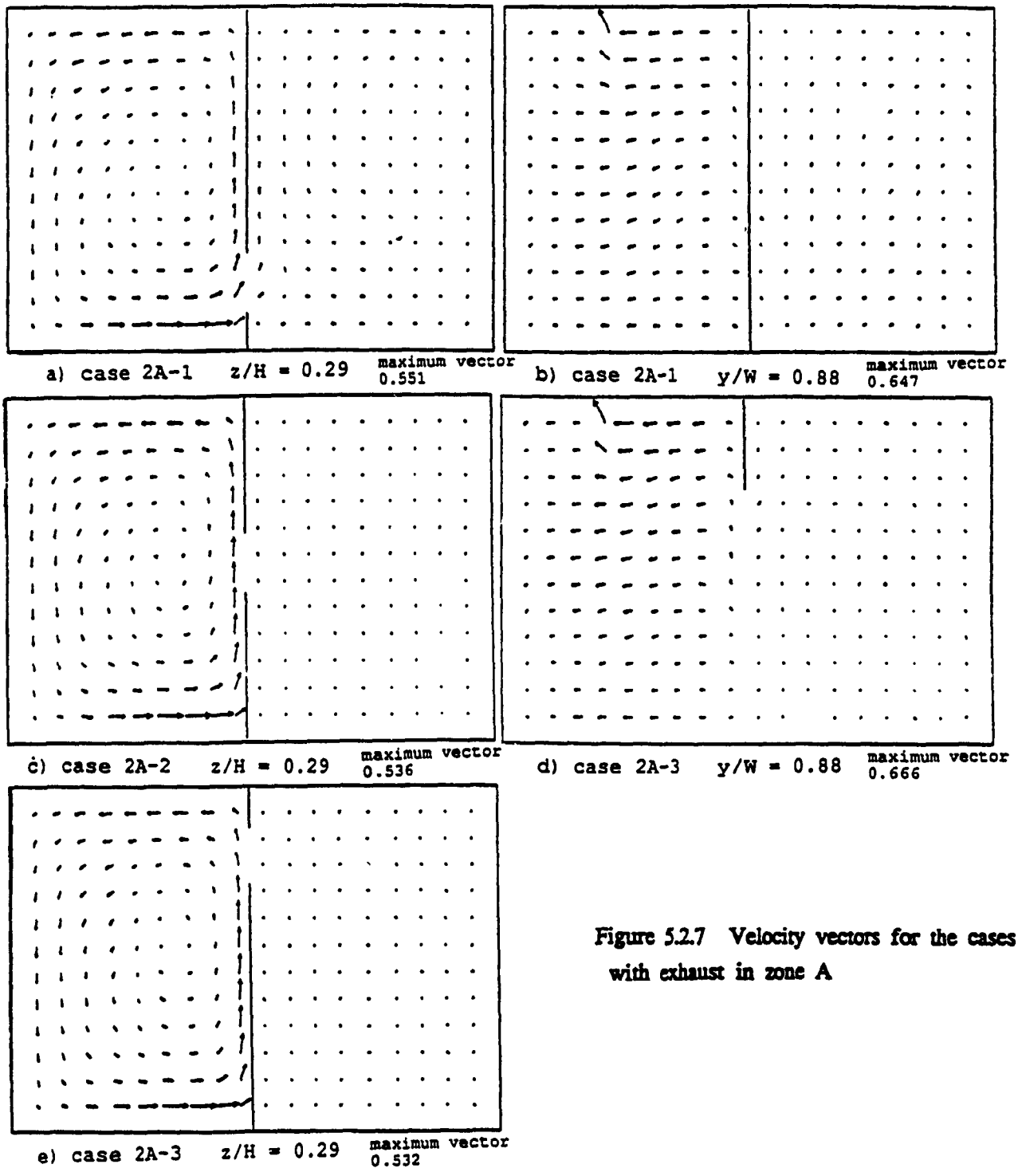

Figure 5.2.7 Velocity vectors for the cases with exhaust in zone A

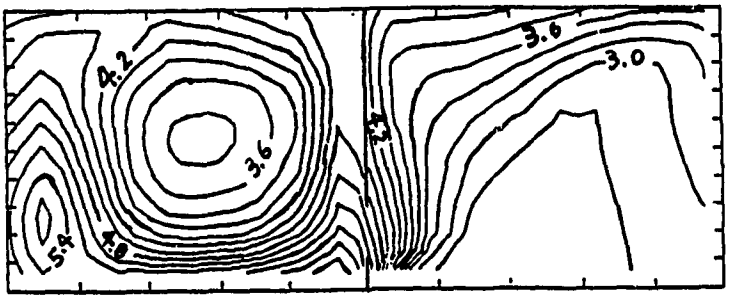

a) case 2A-1 z/H = 0.29

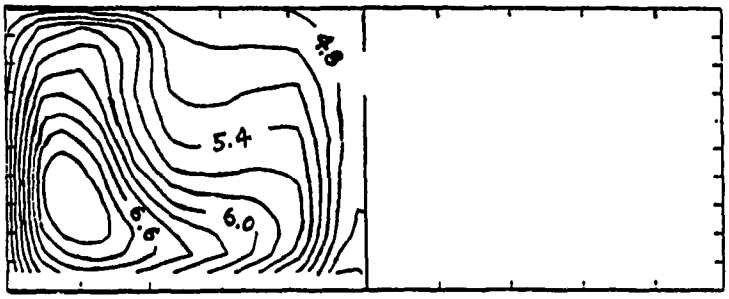

b) case 2A-3 z/H = 0.29

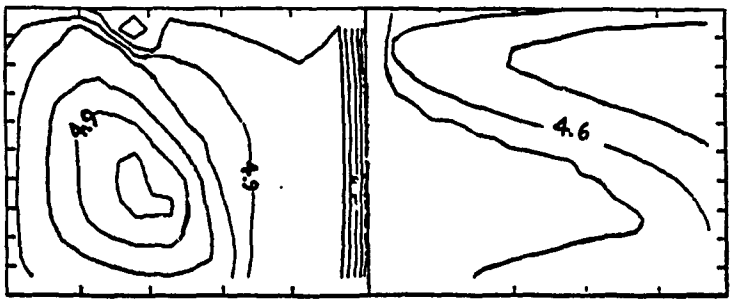

c) case 2A-3 z/H = 0.96

Figure 5.2.8 Contaminant contours for the cases with exhaust in zone A

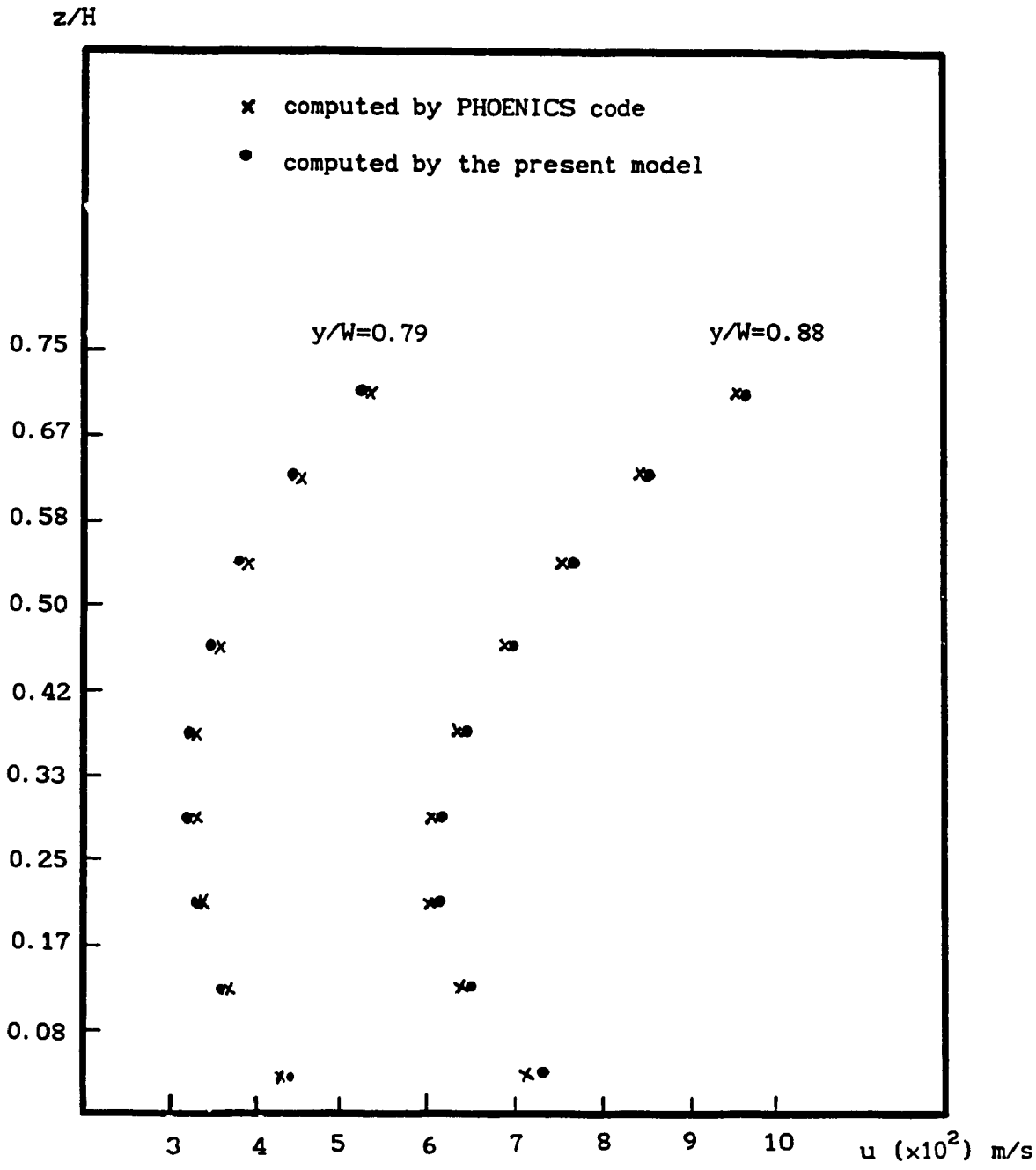

Fig. 5.2.9 Velocity distributions at door opening (x/L=0.5) in comparison with PHOENICS code

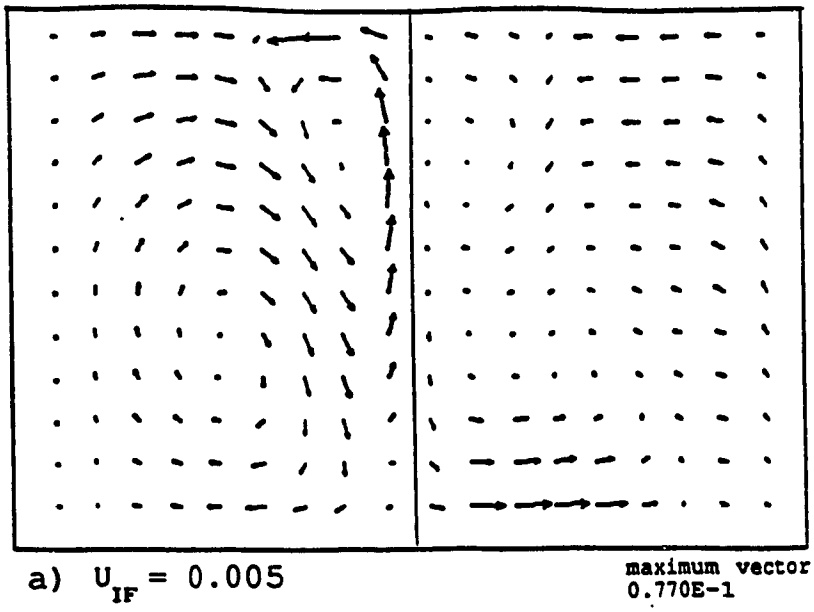

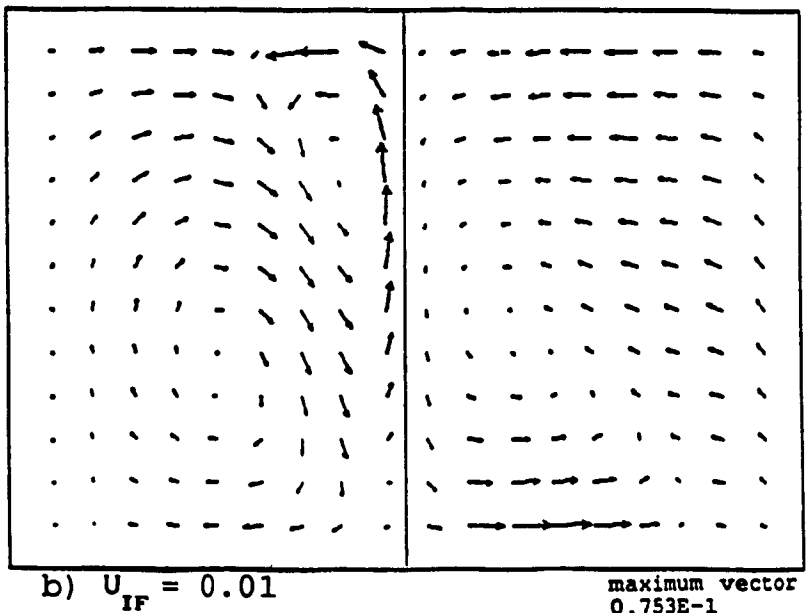

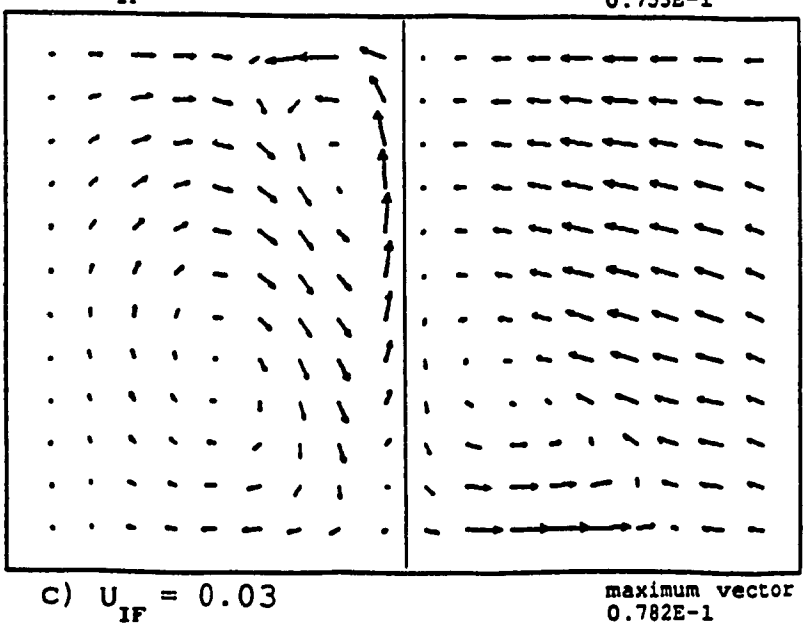

Figure 5.3.1 Velocity vectors in vertical section, y/W=0.46, for the case with y_D/W=0.167

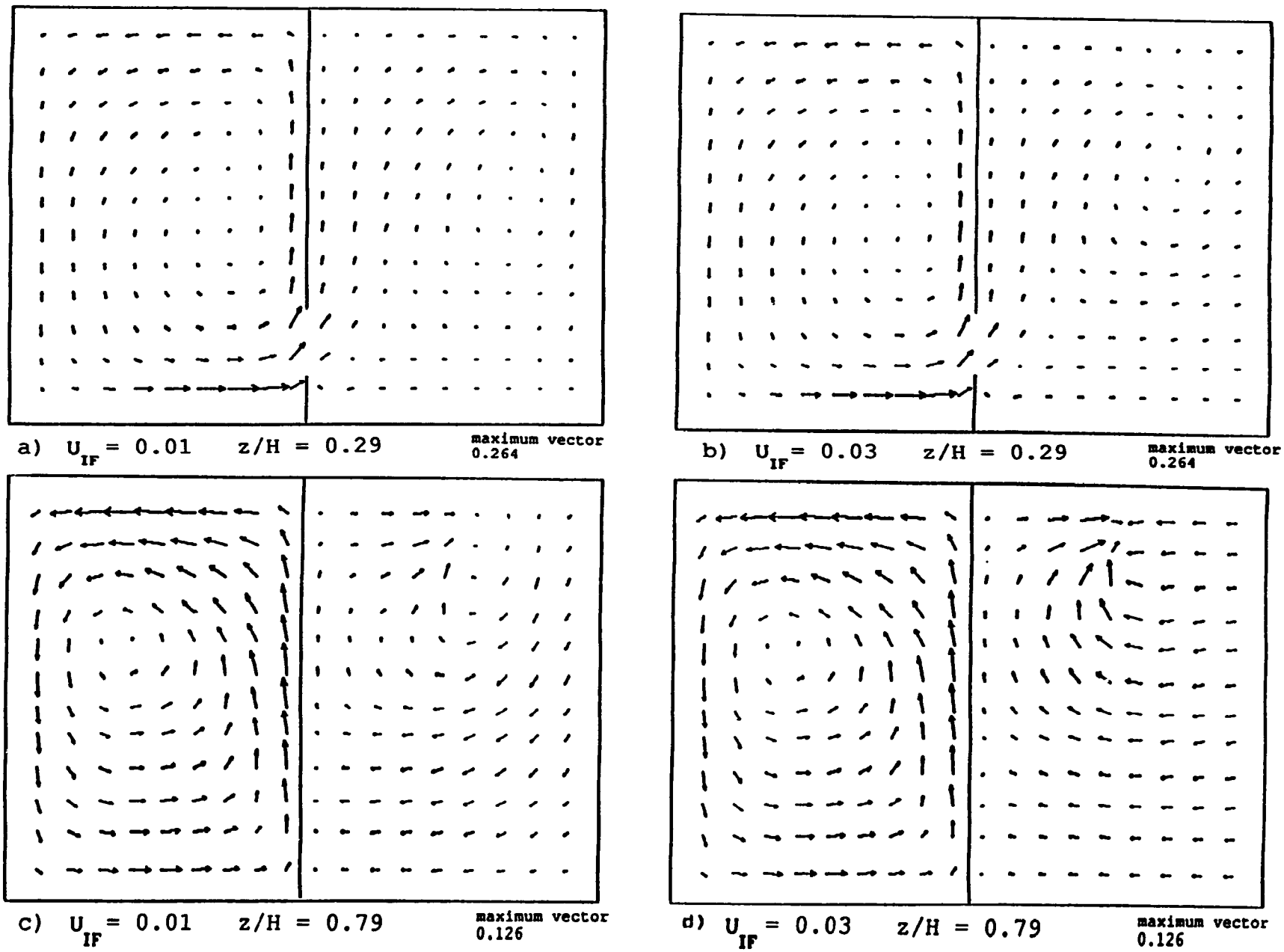

Figure 5.3.2 Velocity vectors in horizontal sections for the case with $y_D/W=0.167$

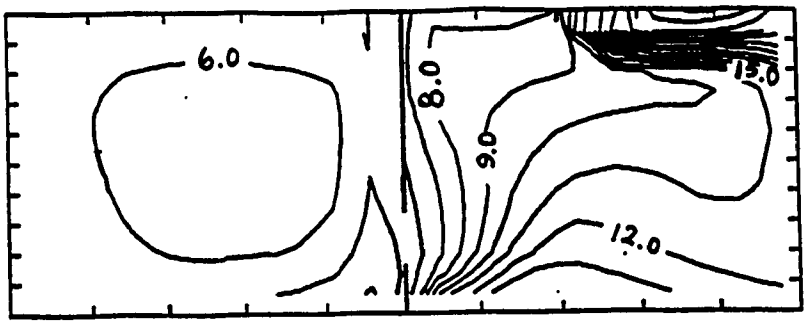

a) U_{IF} = 0.01 z/H = 0.29

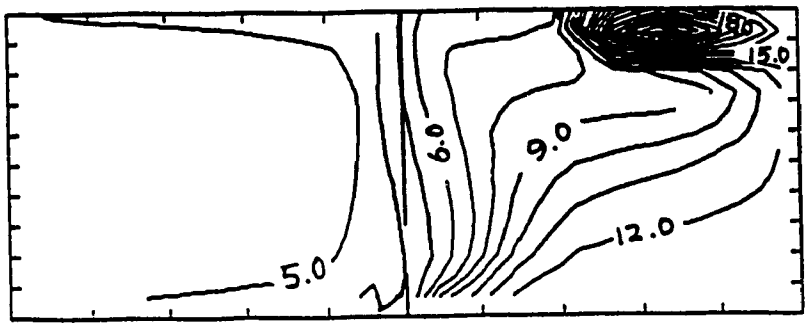

b) U_{IF} = 0.03 z/H = 0.29

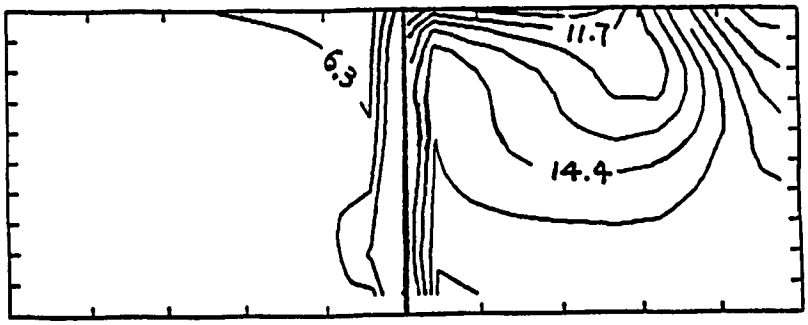

c) U_{IF} = 0.01 z/H = 0.79

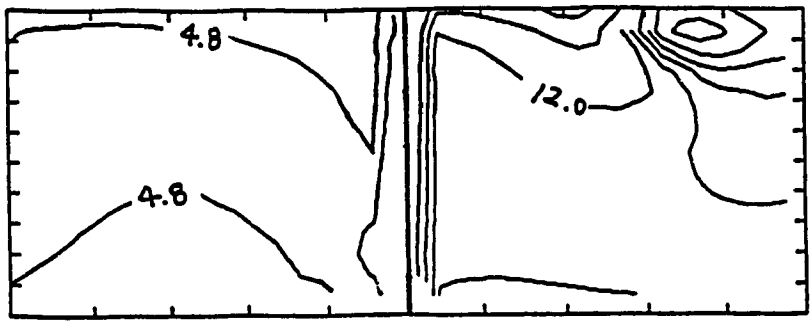

d) U_{IF} = 0.03 z/H = 0.79

Figure 5.3.3 Contaminant contours in horizontal sections for the case with y_D/W=0.167

Unit for all the contours: unit mass/kg(air)

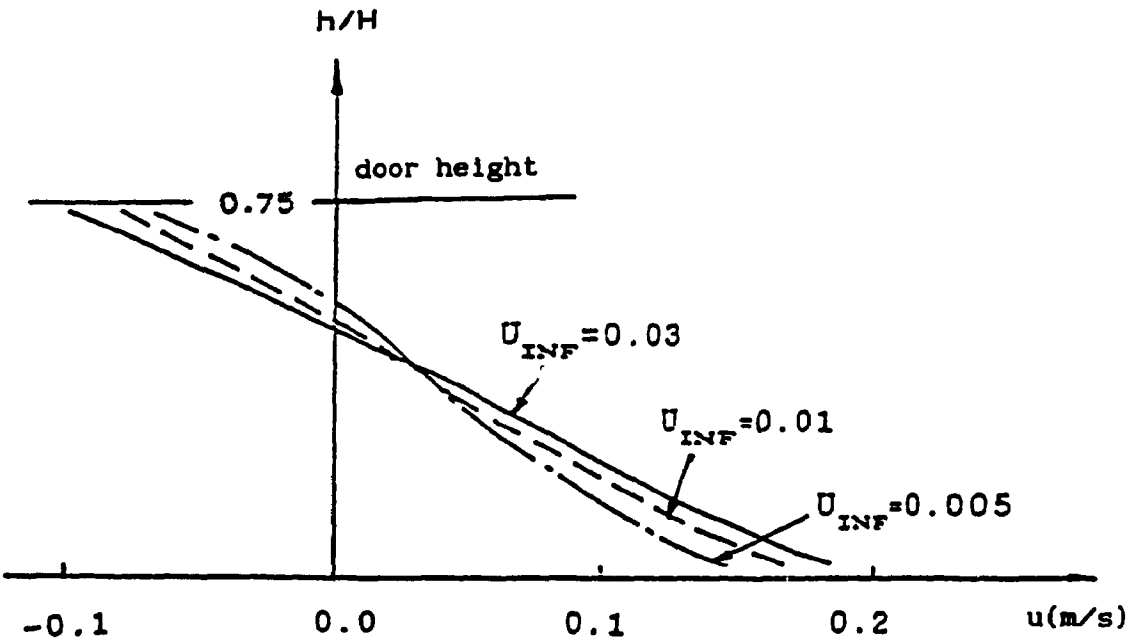

(a) Distributions of velocity component in the x direction at door opening for the case with $y_D/W = 0.167$

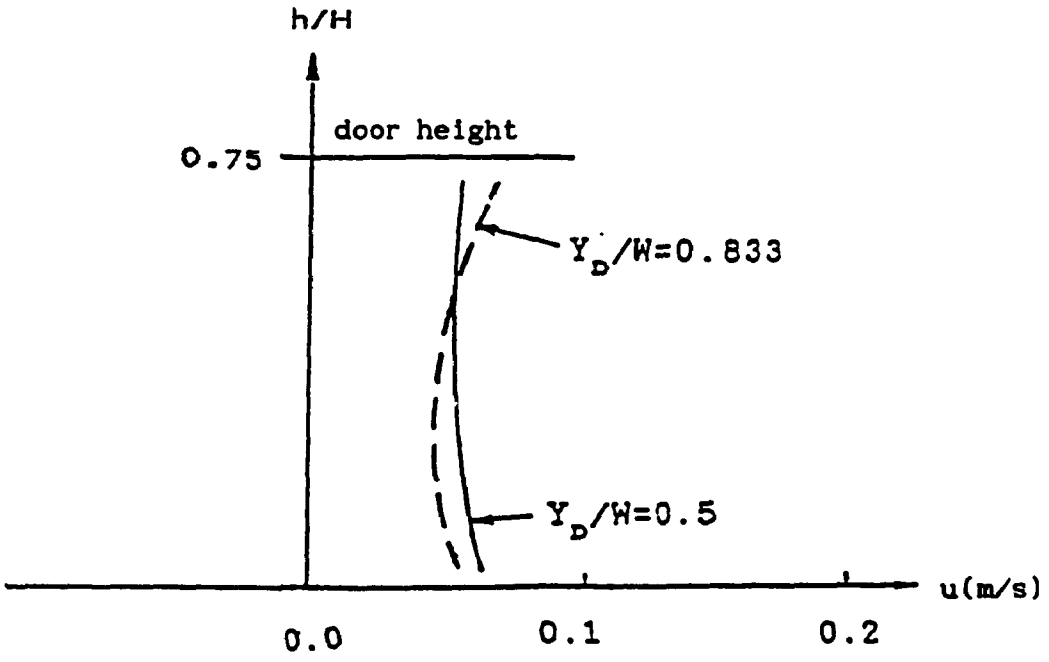

(b) Distributions of velocity component in the x direction at door opening for the cases with $y_D/W = 0.5$ and 0.833

Figure 5.3.4

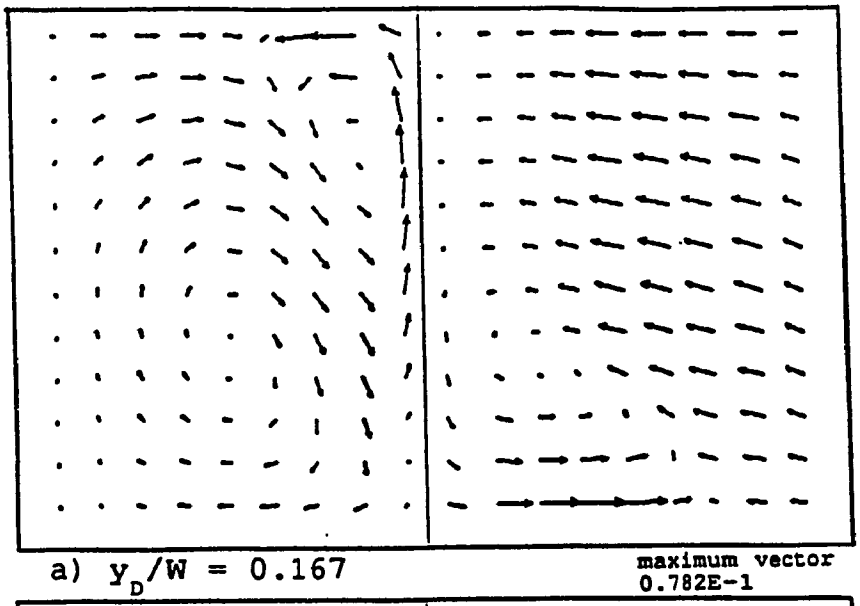

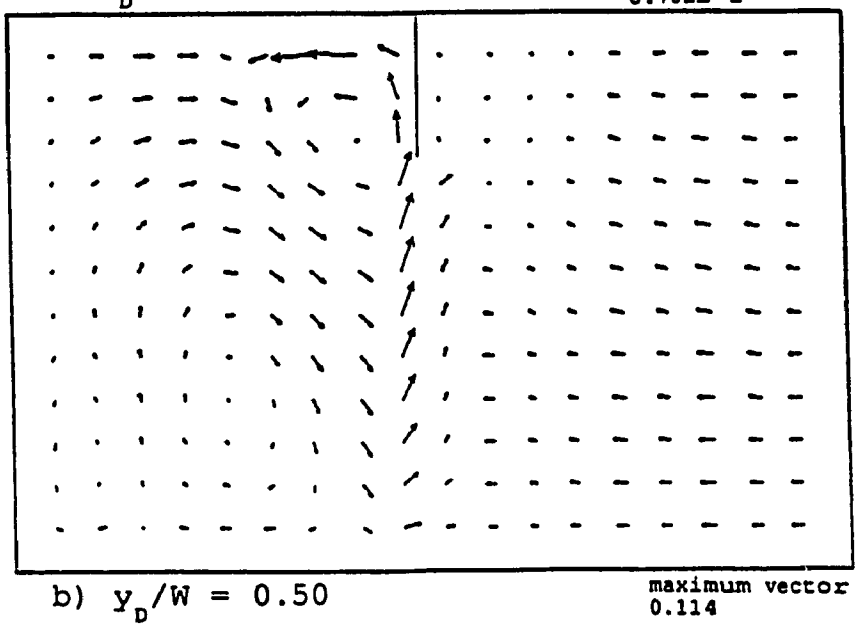

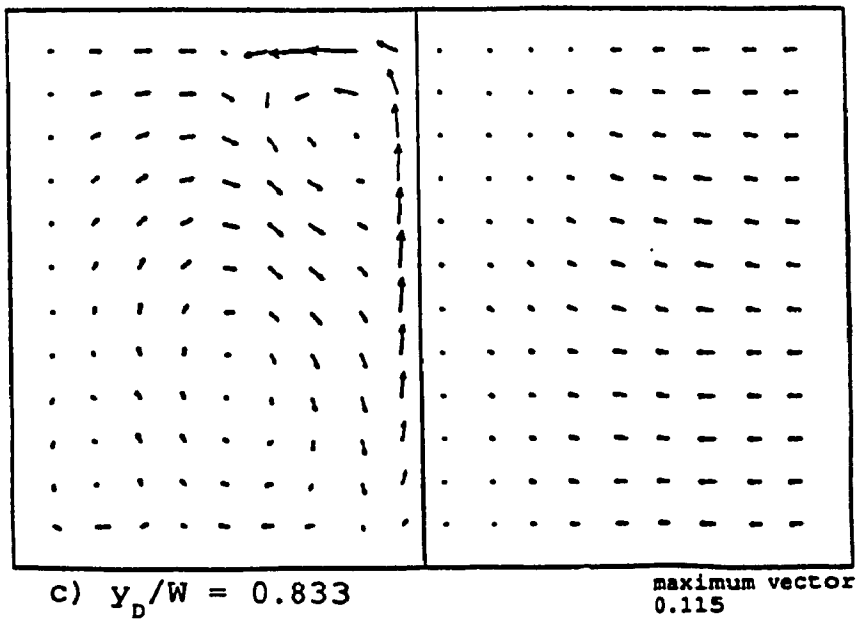

Figure 5.3.5 Velocity vectors in vertical section y/W=0.46

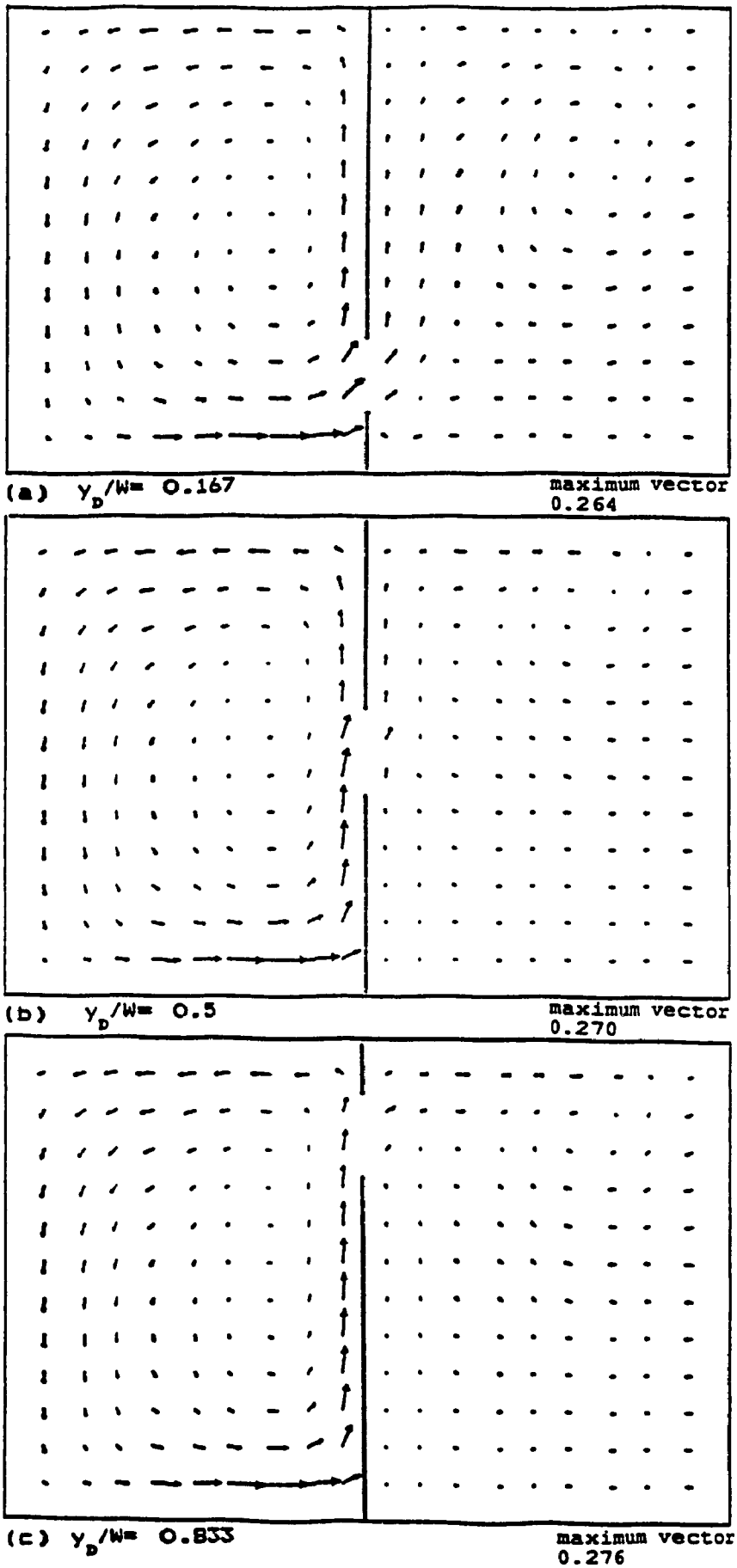

Figure 5.3.6 Velocity vectors in horizontal section z/H=0.29

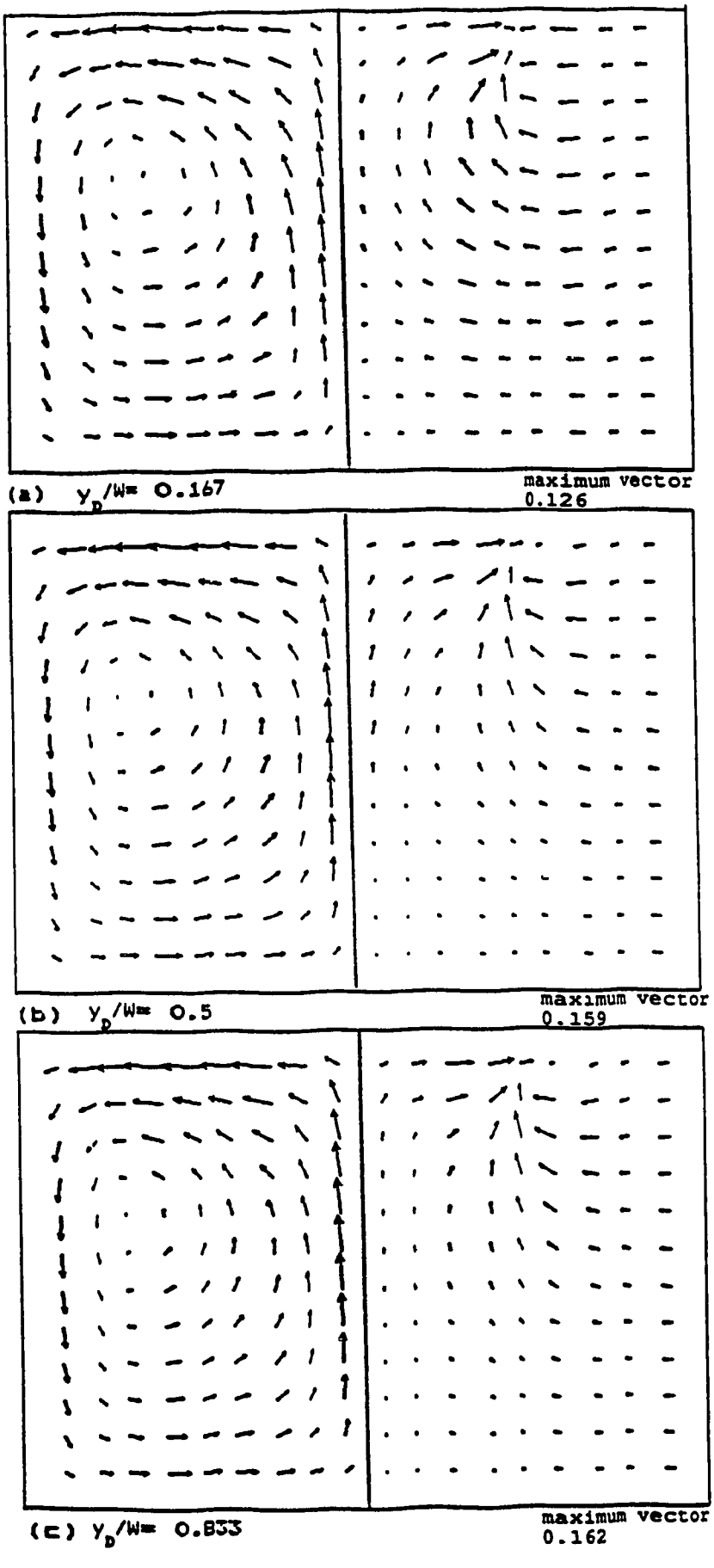

Figure 5.3.7 Velocity vectors in horizontal section z/H=0.79

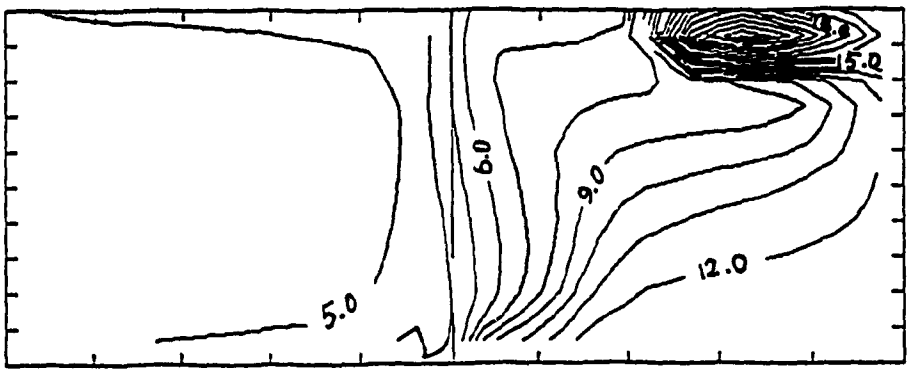

a) $y_D/W = 0.167$

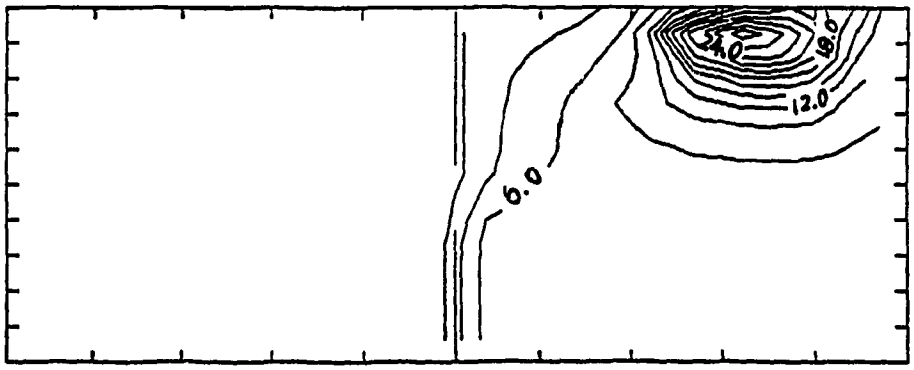

b) $y_D/W = 0.50$

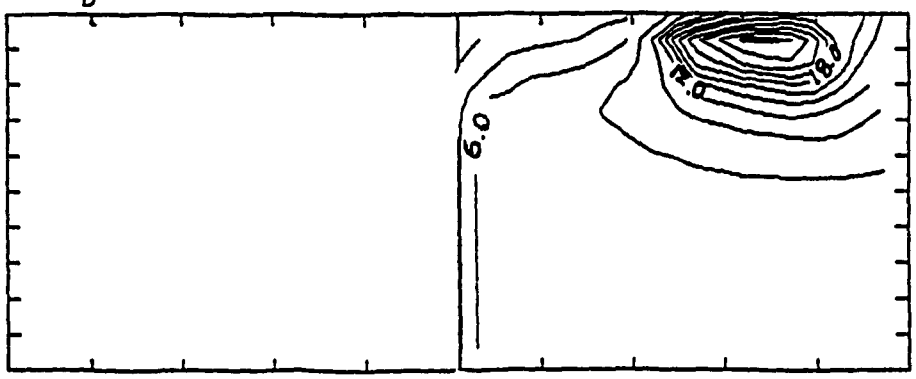

c) $y_D/W = 0.833$

Figure 5.3.8 Contaminant contours in horizontal section z/H=0.29

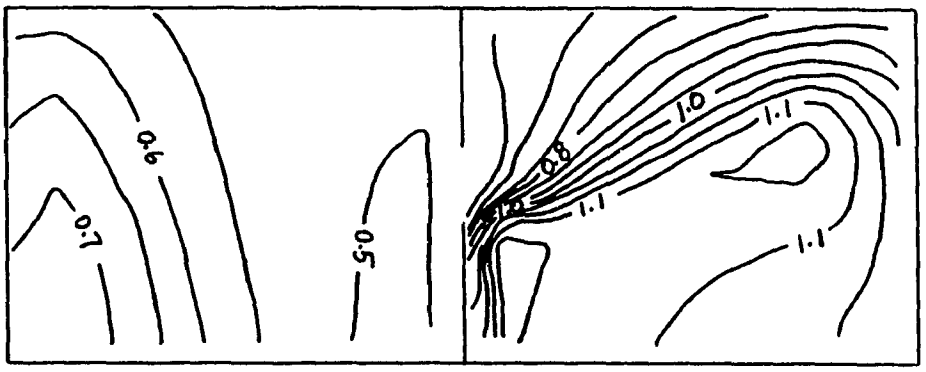

a) z/H = 0.04

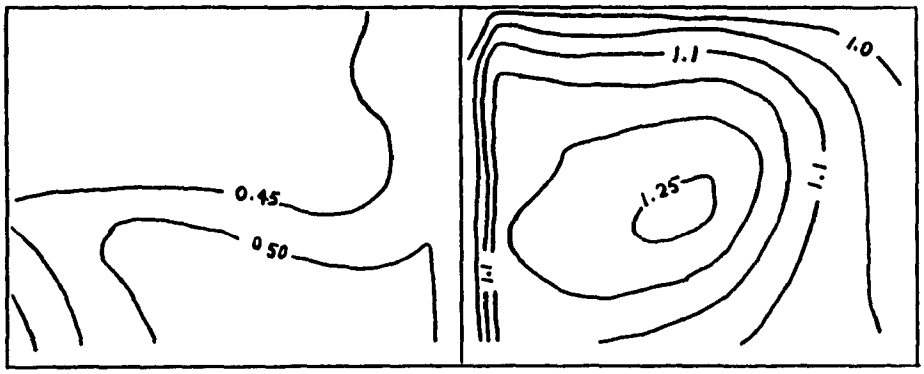

b) z/H = 0.79

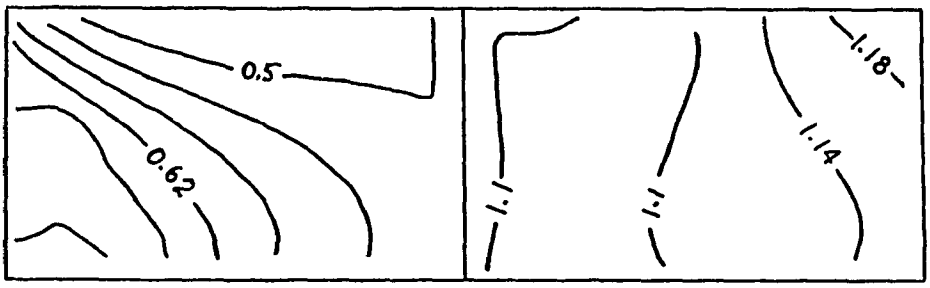

c) y/W = 0.13

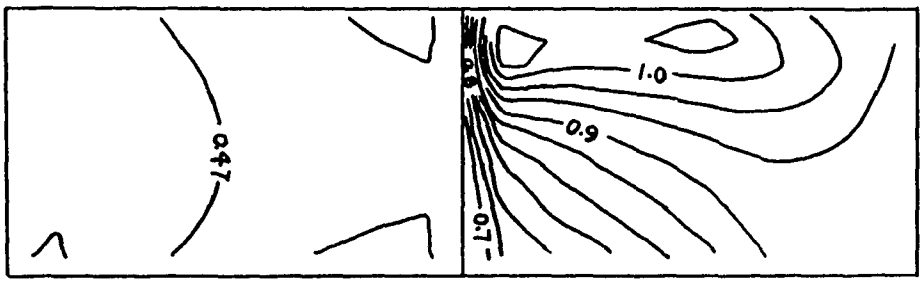

d) y/W = 0.88

Figure 5.4.1 Age contours for the case with $y_D/W = 0.5$

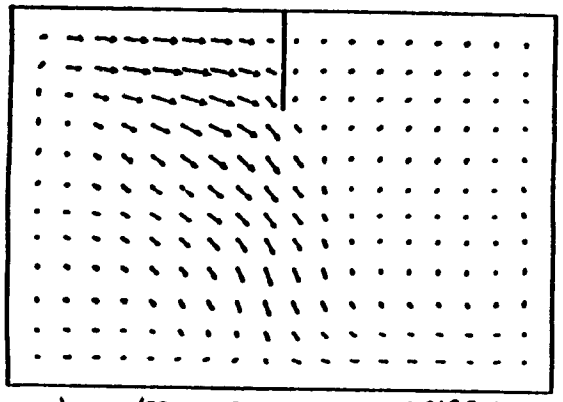

a) $y_D/W = 0.17$

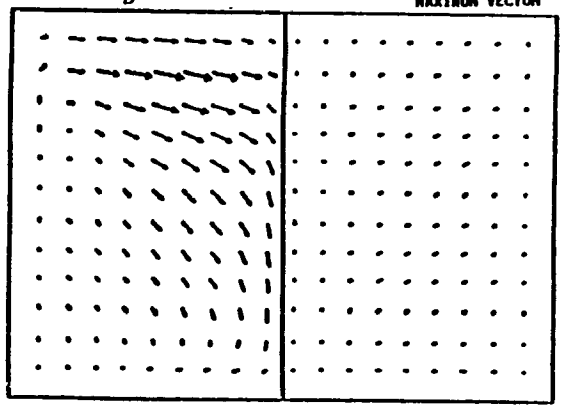

b) $y_D/W = 0.50$

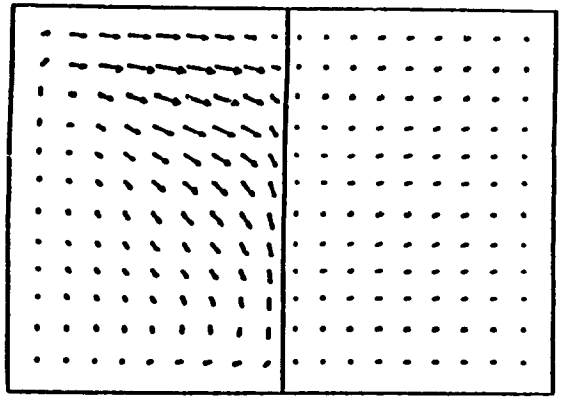

c) $y_D/W = 0.83$

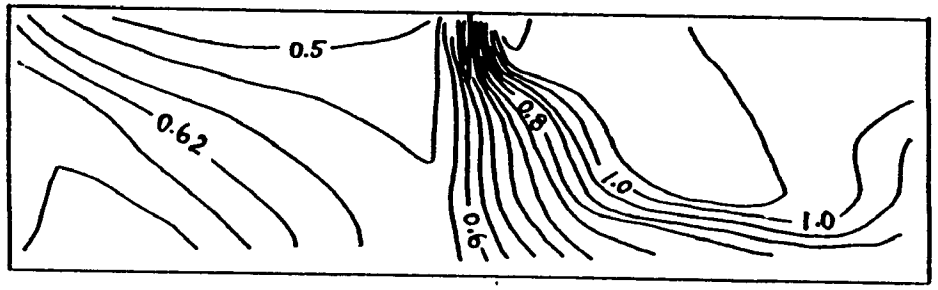

d) $y_D/W = 0.17$

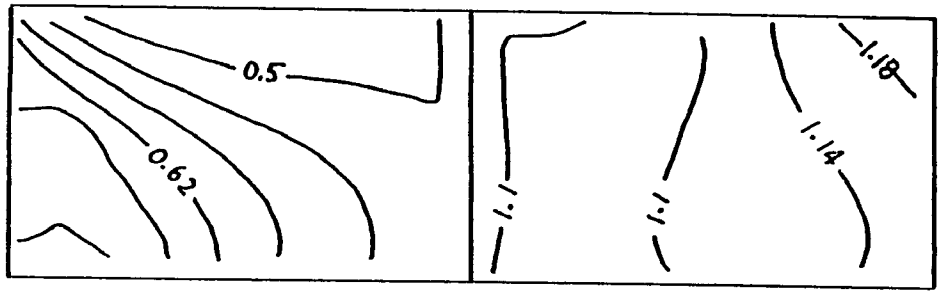

e) $y_D/W = 0.50$

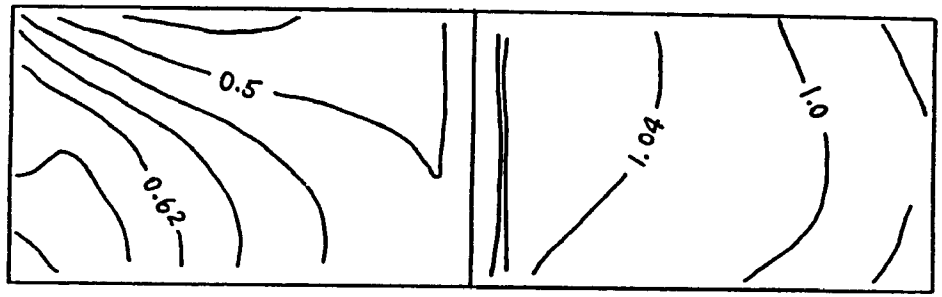

f) $y_D/W = 0.83$

Figure 5.4.2 Airflow patterns and age distributions at y/W = 0.13

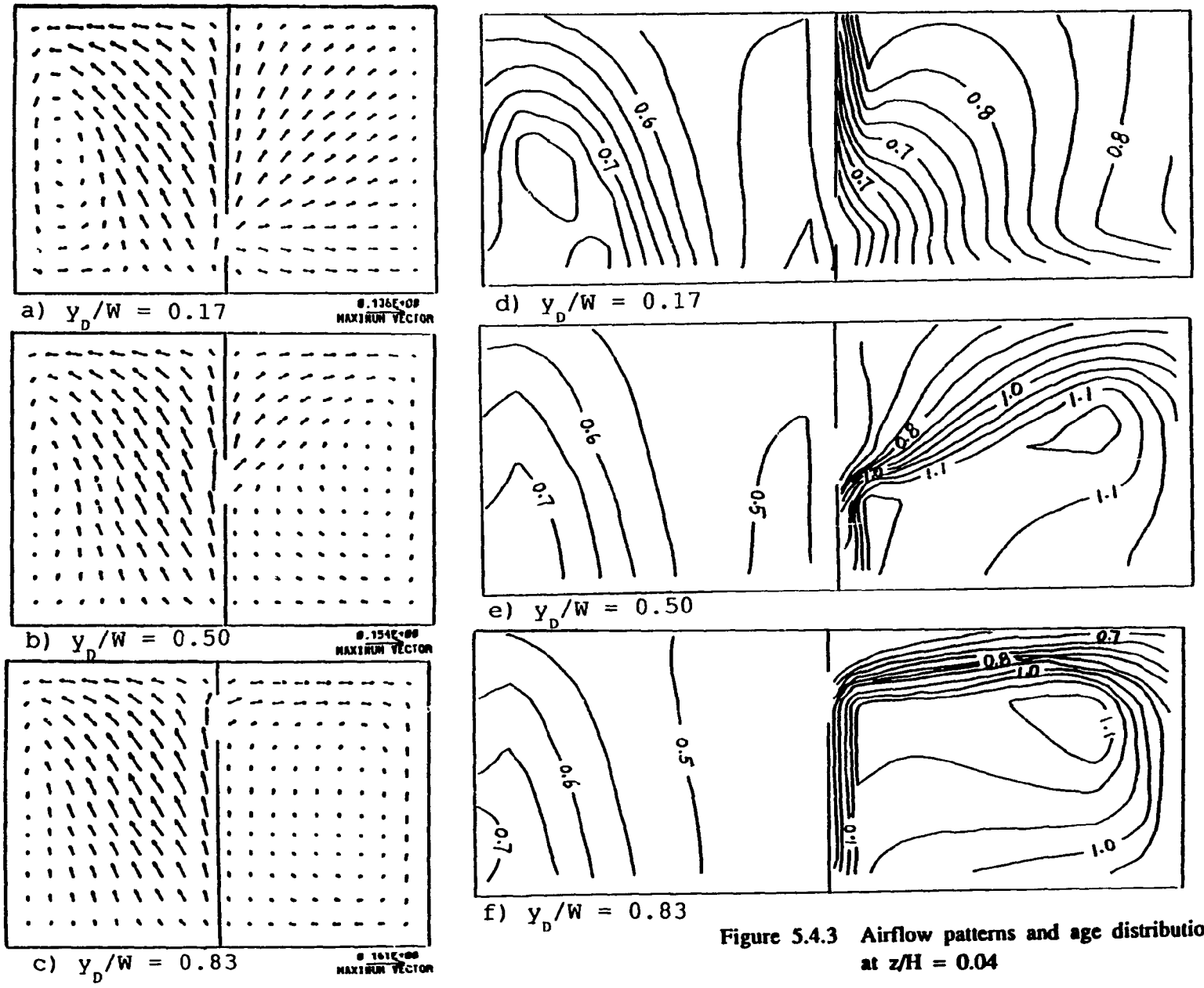

Figure 5.4.3 Airflow patterns and age distributions at z/H = 0.04

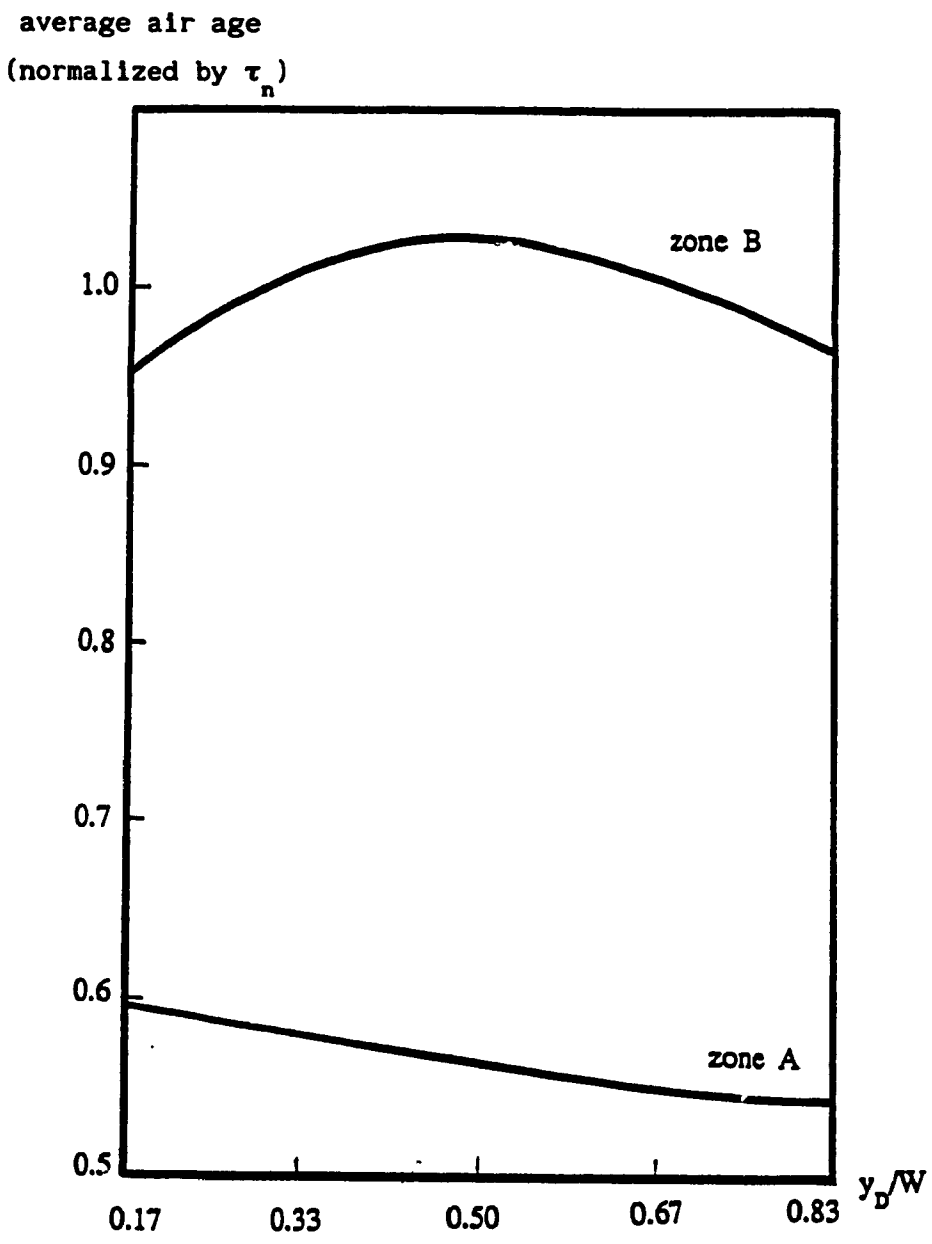

Figure 5.4.4 Variation of average age with door position

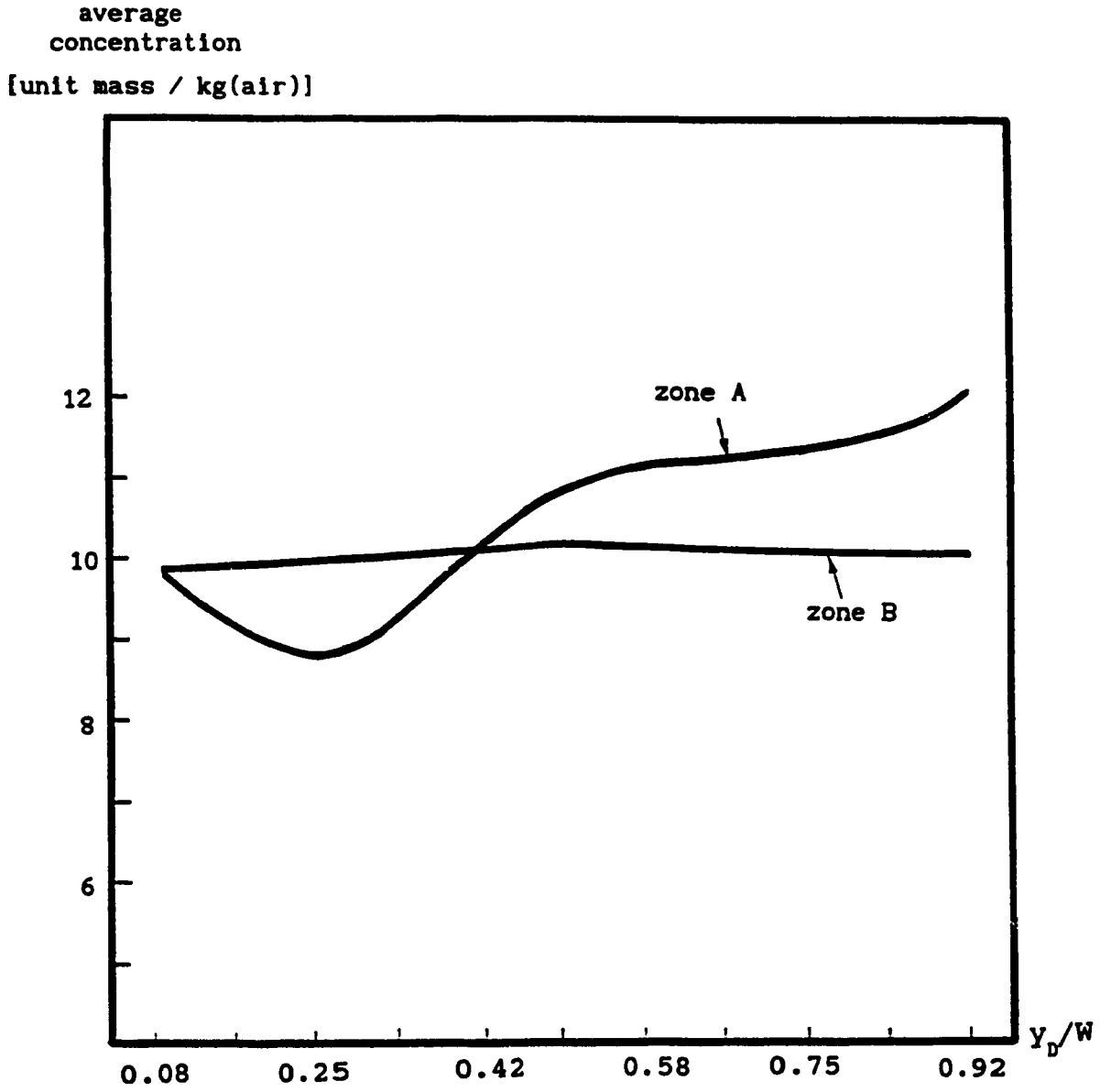

Figure 5.4.5 Variation of average concentration in each zone with door location

ventilation rate:	2.5 ach		
door location:	variable		
supply location:	$x_I/L = 0.0$	$y_I/W = 0.46$	$z_I/H = 0.88$
exhaust location:	$x_E/L = 0.75$	$y_E/W = 0.88$	$z_E/H = 1.0$

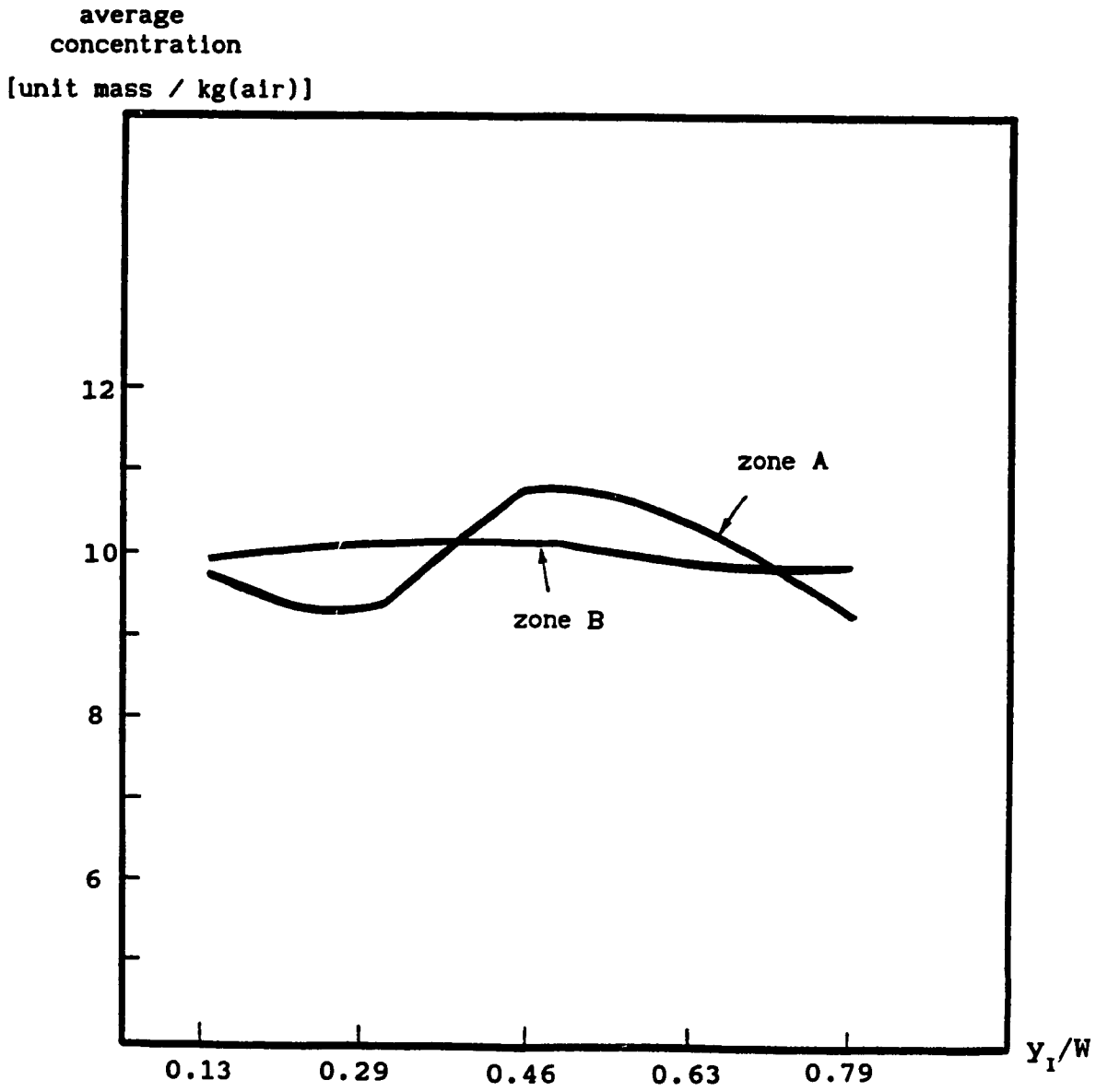

Figure 5.4.6 Variation of average concentration in each zone with supply location

ventilation rate:	2.5 ach		
door location:	$x_D/L = 0.5$	$y_D/W = 0.5$	
supply location:	variable		
exhaust location:	$x_E/L = 0.75$	$y_E/W = 0.88$	$z_E/H = 1.0$

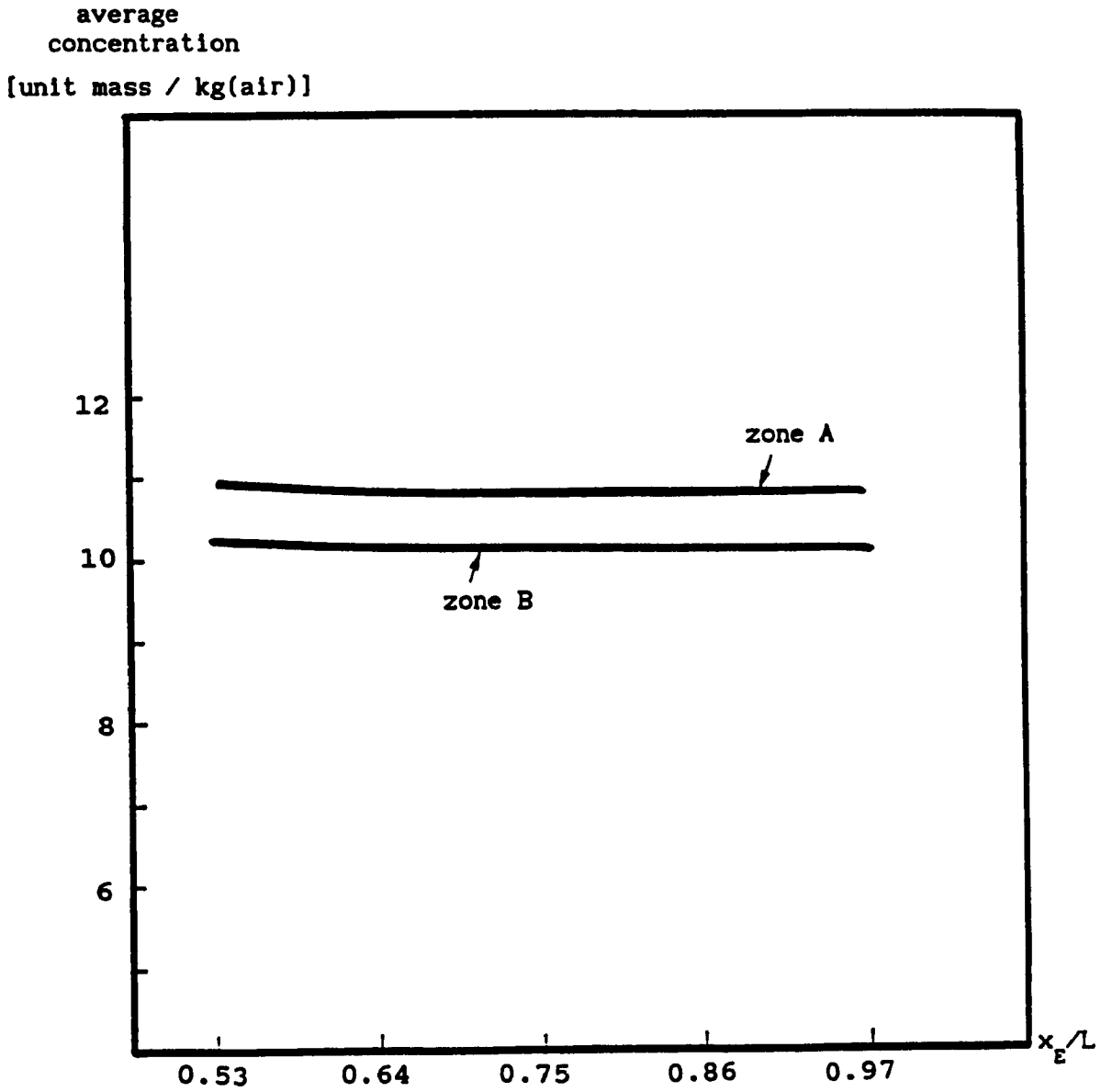

Figure 5.4.7 Variation of average concentration in each zone with exhaust location

ventilation rate:	2.5 ach		
door location:	$x_D/L = 0.5$	$y_D/W = 0.5$	
supply location:	$x_I/L = 0.0$	$y_I/W = 0.46$	$z_I/H = 0.88$
exhaust location:	variable		

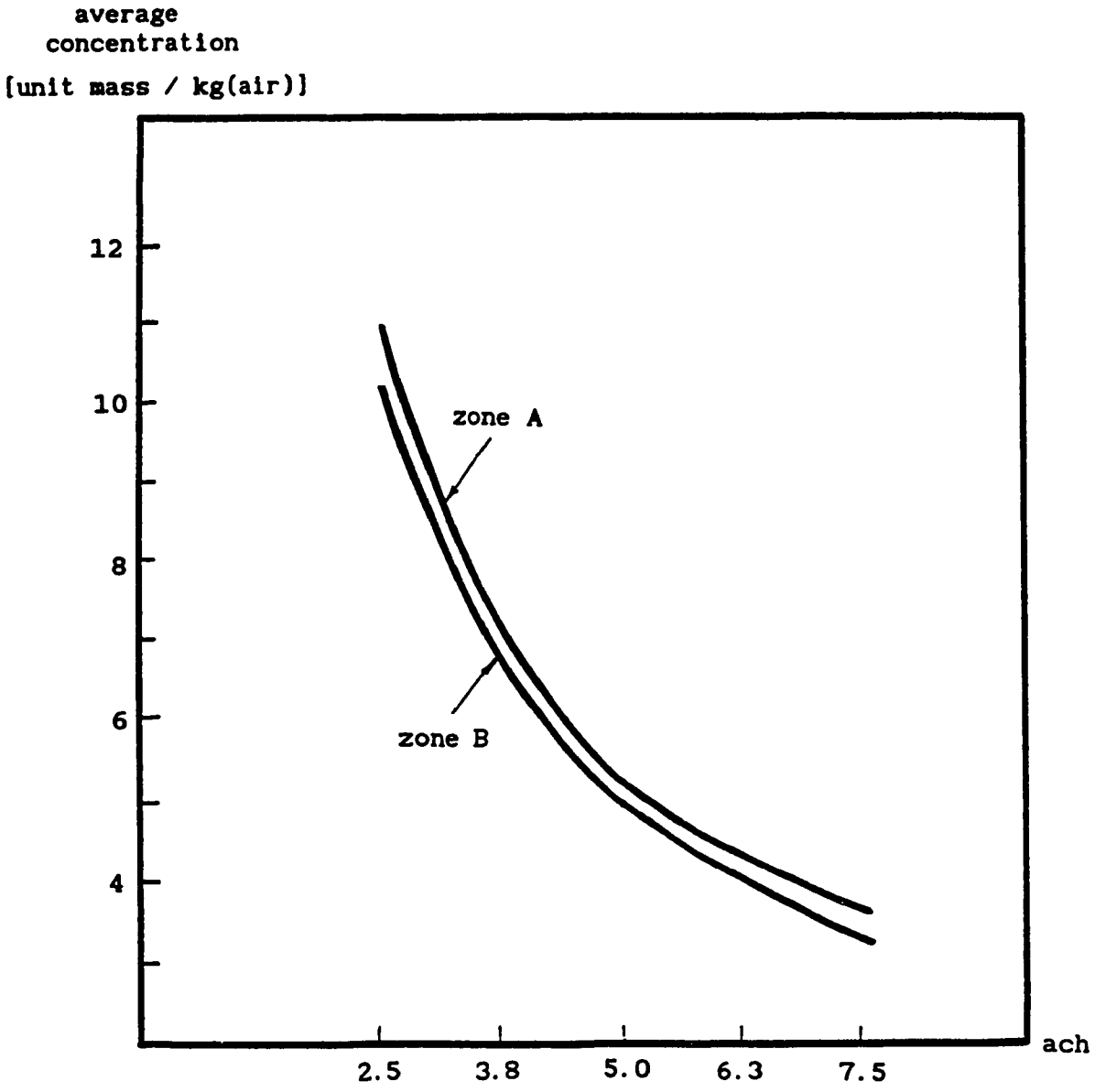

Figure 5.4.8 Variation of average concentration in each zone with ventilation rate

ventilation rate:	variable		
door location:	$x_D/L = 0.5$	$y_D/W = 0.5$	
supply location:	$x_I/L = 0.0$	$y_I/W = 0.46$	$z_I/H = 0.88$
exhaust location:	$x_E/L = 0.75$	$y_E/W = 0.88$	$z_E/H = 1.0$

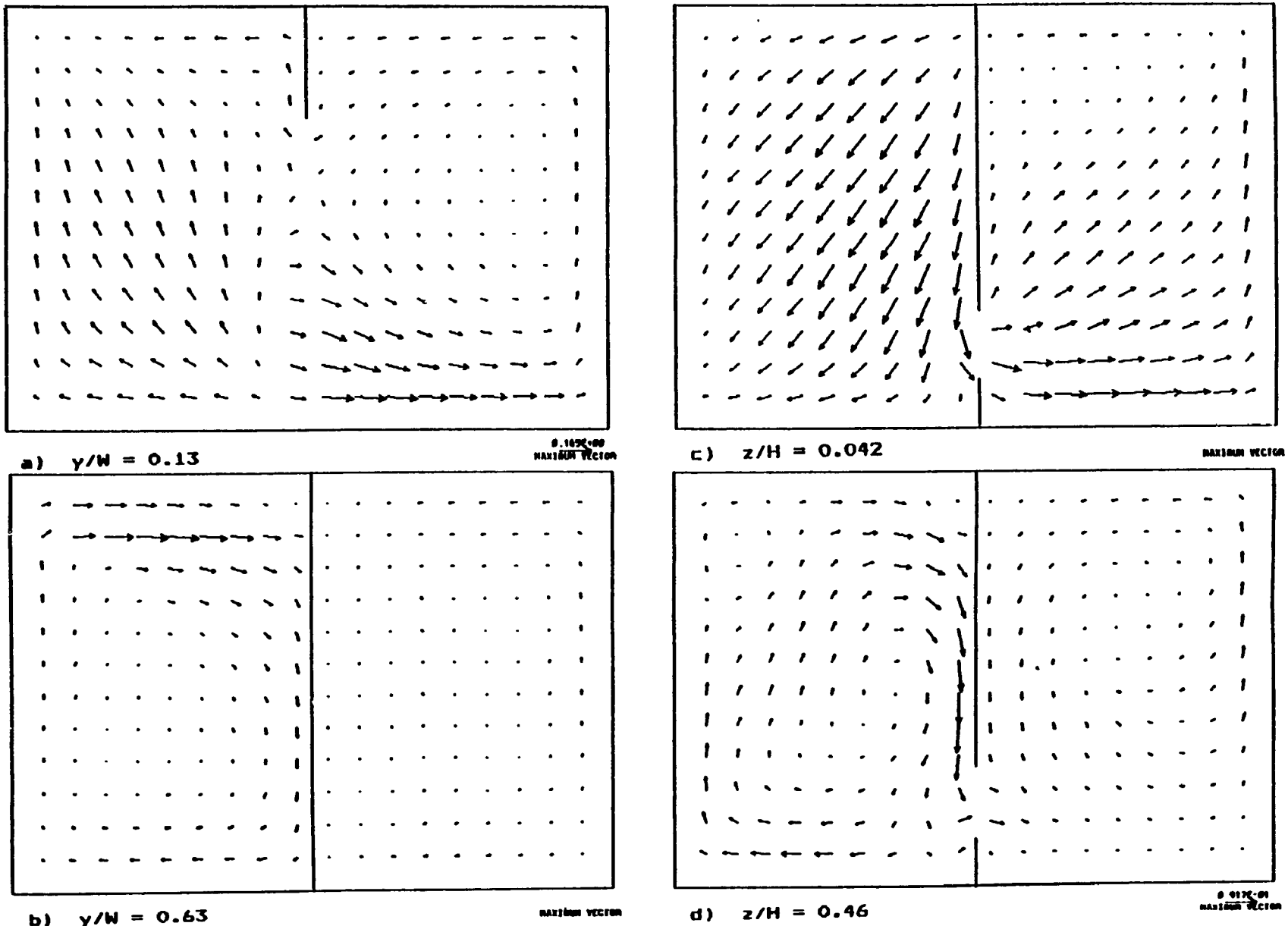

Figure 5.5.1 Flow patterns for the case with $y_D/W = 0.17$

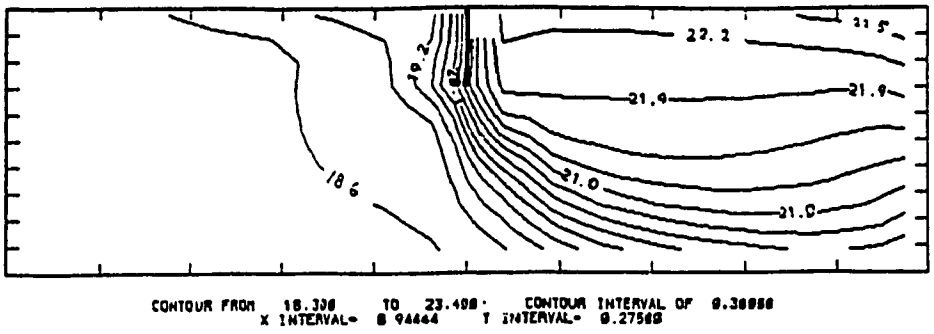

a) y/W = 0.13

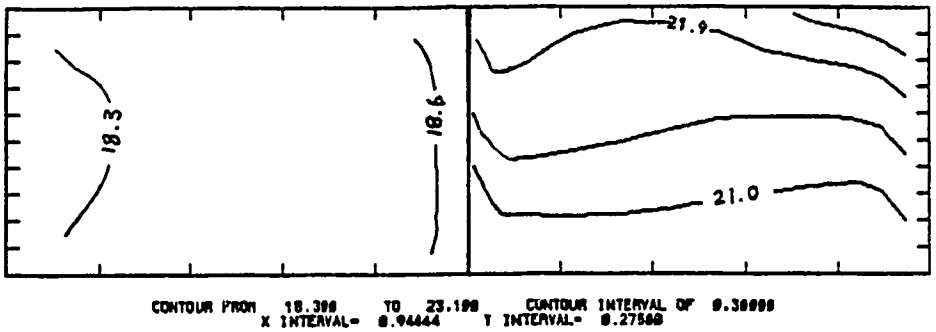

b) y/W = 0.79

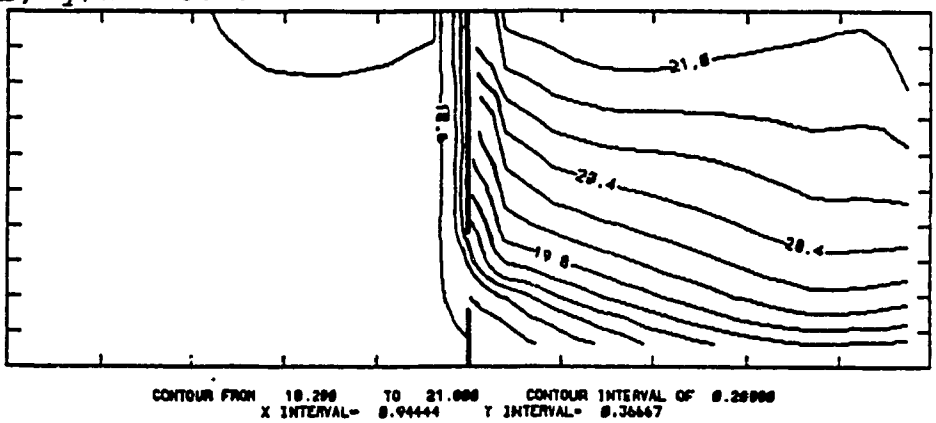

c) z/H = 0.042

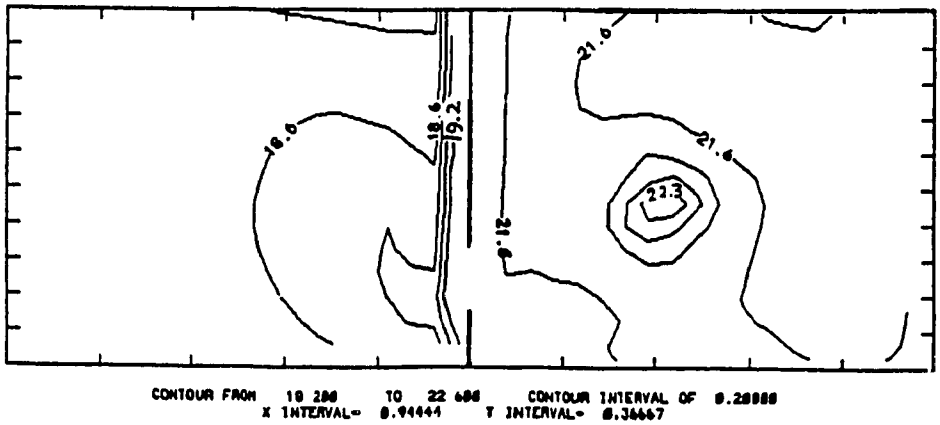

d) z/H = 0.46

Figure 5.5.2 Temperature distributions for the case with $y_D/W = 0.17$

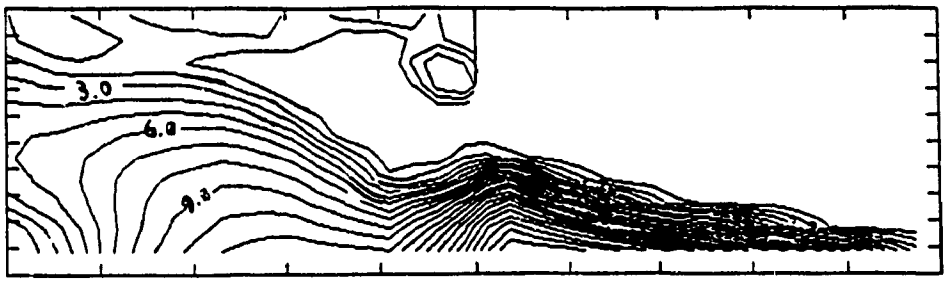

CONTOUR FROM 0.00000E+00 TO 24.000 CONTOUR INTERVAL OF 1.0000
X INTERVAL= 0.94444 Y INTERVAL= 0.27500

a) y/W = 0.13

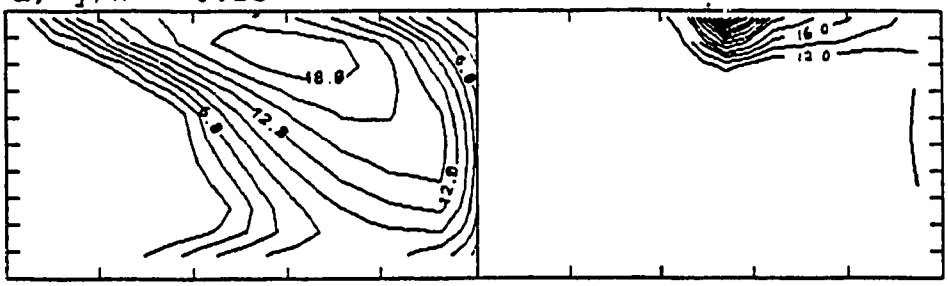

CONTOUR FROM 0.00000E+00 TO 32.000 CONTOUR INTERVAL OF 2.0000
X INTERVAL= 0.94444 Y INTERVAL= 0.27500

b) y/W = 0.88

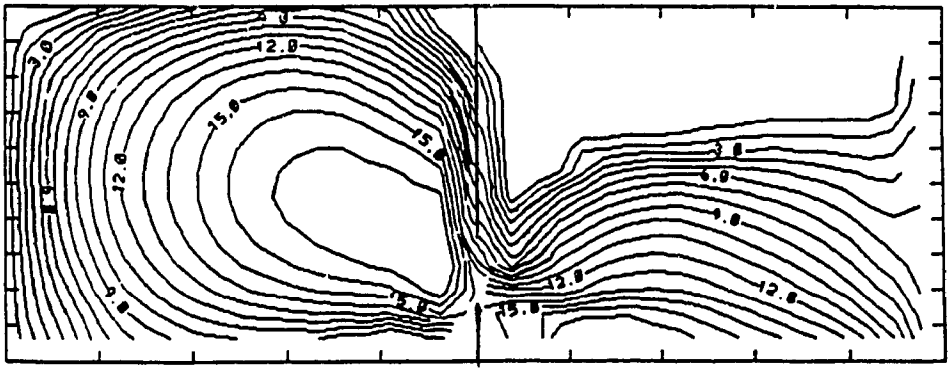

CONTOUR FROM 0.00000E+00 TO 28.000 CONTOUR INTERVAL OF 1.0000
X INTERVAL= 0.94444 Y INTERVAL= 0.36667

c) z/H = 0.042

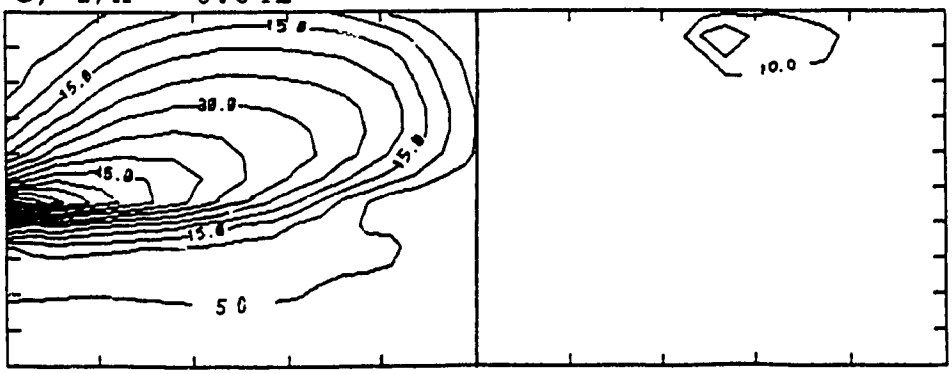

CONTOUR FROM 0.00000E+00 TO 60.000 CONTOUR INTERVAL OF 5.0000
X INTERVAL= 0.94444 Y INTERVAL= 0.36667

d) z/H = 0.88

Figure 5.5.3 PD distributions for the case with $y_D/W = 0.17$

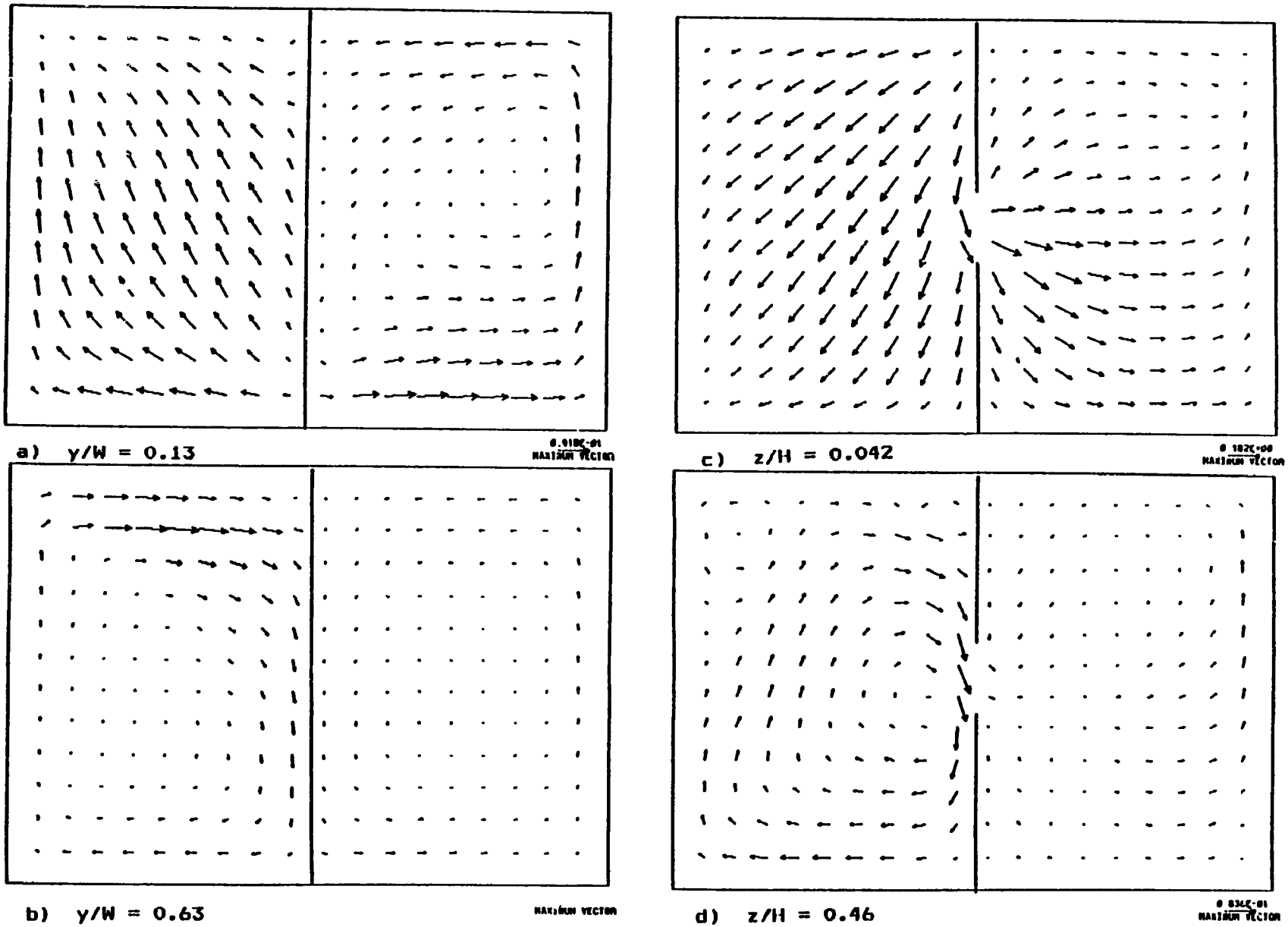

Figure 5.5.4 Flow patterns for the case with $y_D/W = 0.50$

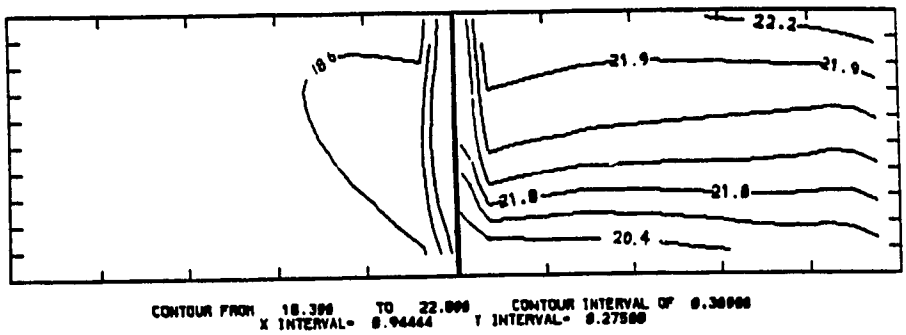

a) y/W = 0.13

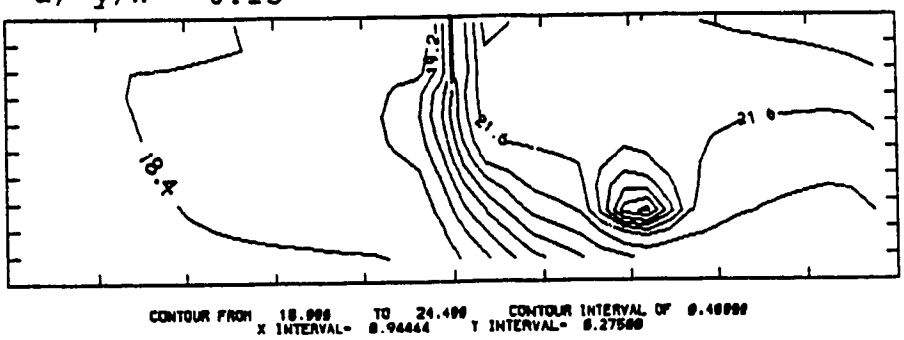

b) y/W = 0.46

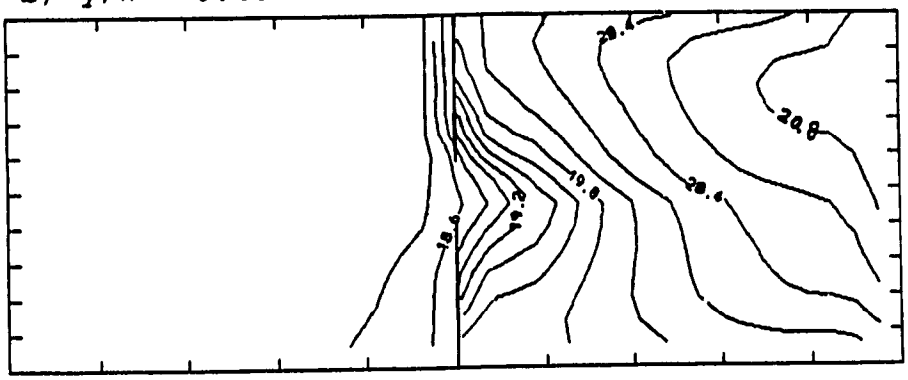

c) z/H = 0.042

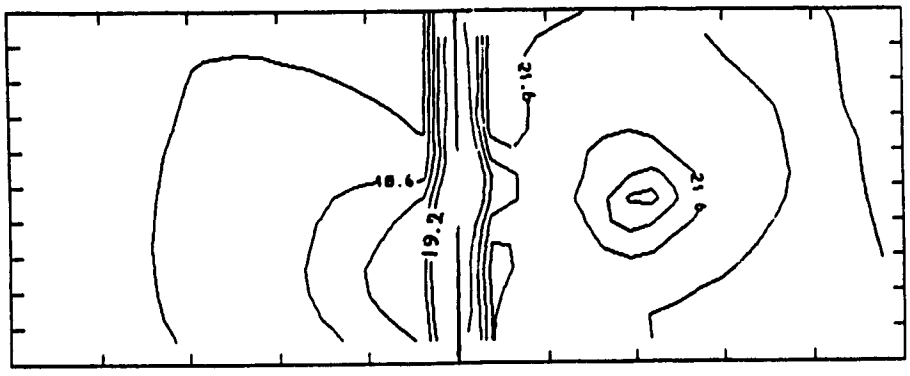

d) z/H = 0.46

Figure 5.5.5 Temperature distributions for the case with $y_D/W = 0.50$

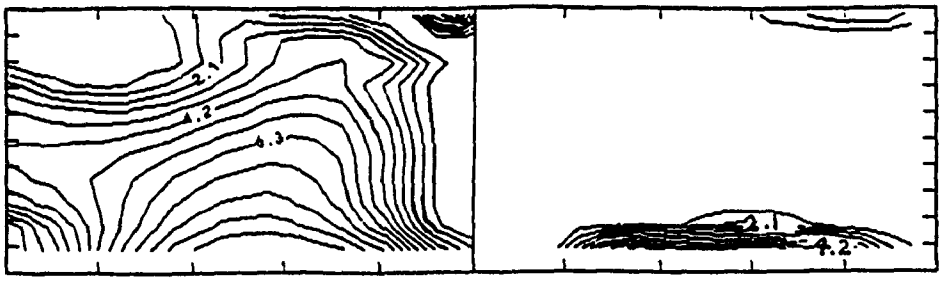

CONTOUR FROM 0.00000E+00 TO 19.598 CONTOUR INTERVAL OF 0.78938
X INTERVAL= 0.94444 Y INTERVAL= 0.27589

a) y/W = 0.13

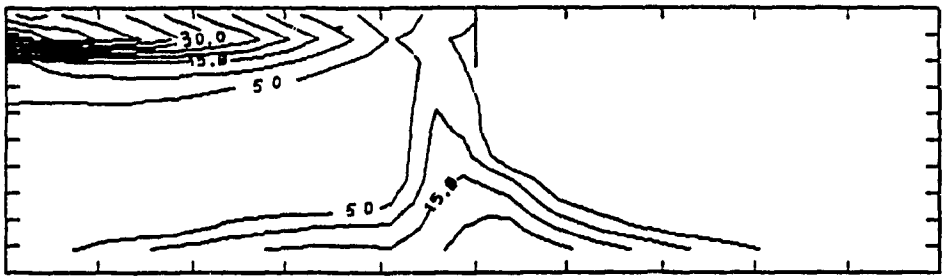

CONTOUR FROM 0.00000E+00 TO 60.000 CONTOUR INTERVAL OF 5.0000
X INTERVAL= 0.94444 Y INTERVAL= 0.27500

b) y/W = 0.46

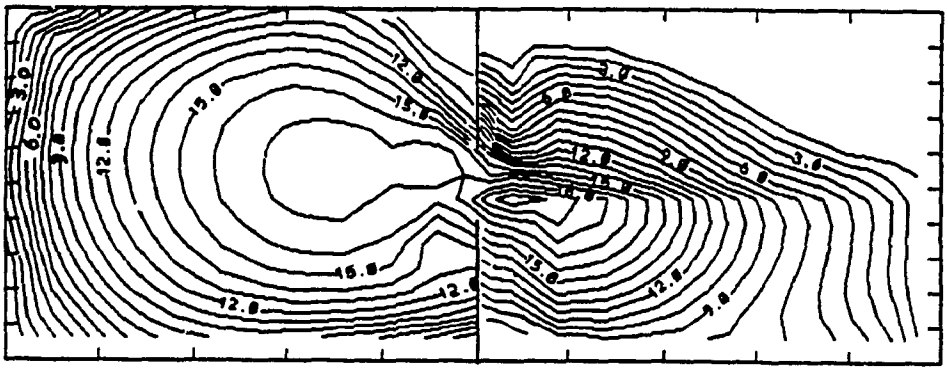

CONTOUR FROM 0.00000E+00 TO 22.000 CONTOUR INTERVAL OF 1.0000
X INTERVAL= 0.94444 Y INTERVAL= 0.36667

c) z/H = 0.042

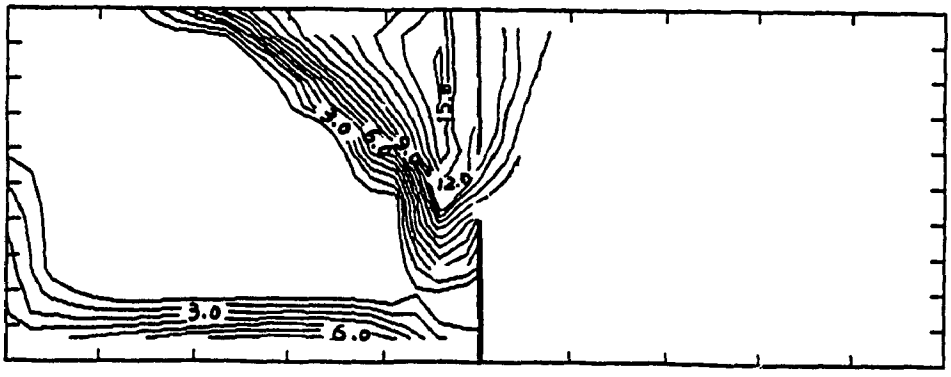

CONTOUR FROM 0.00000E+00 TO 17.000 CONTOUR INTERVAL OF 1.0000
X INTERVAL= 0.94444 Y INTERVAL= 0.36667

d) z/H = 0.46

Figure 5.5.6 PD distributions for the case with $y_D/W = 0.50$

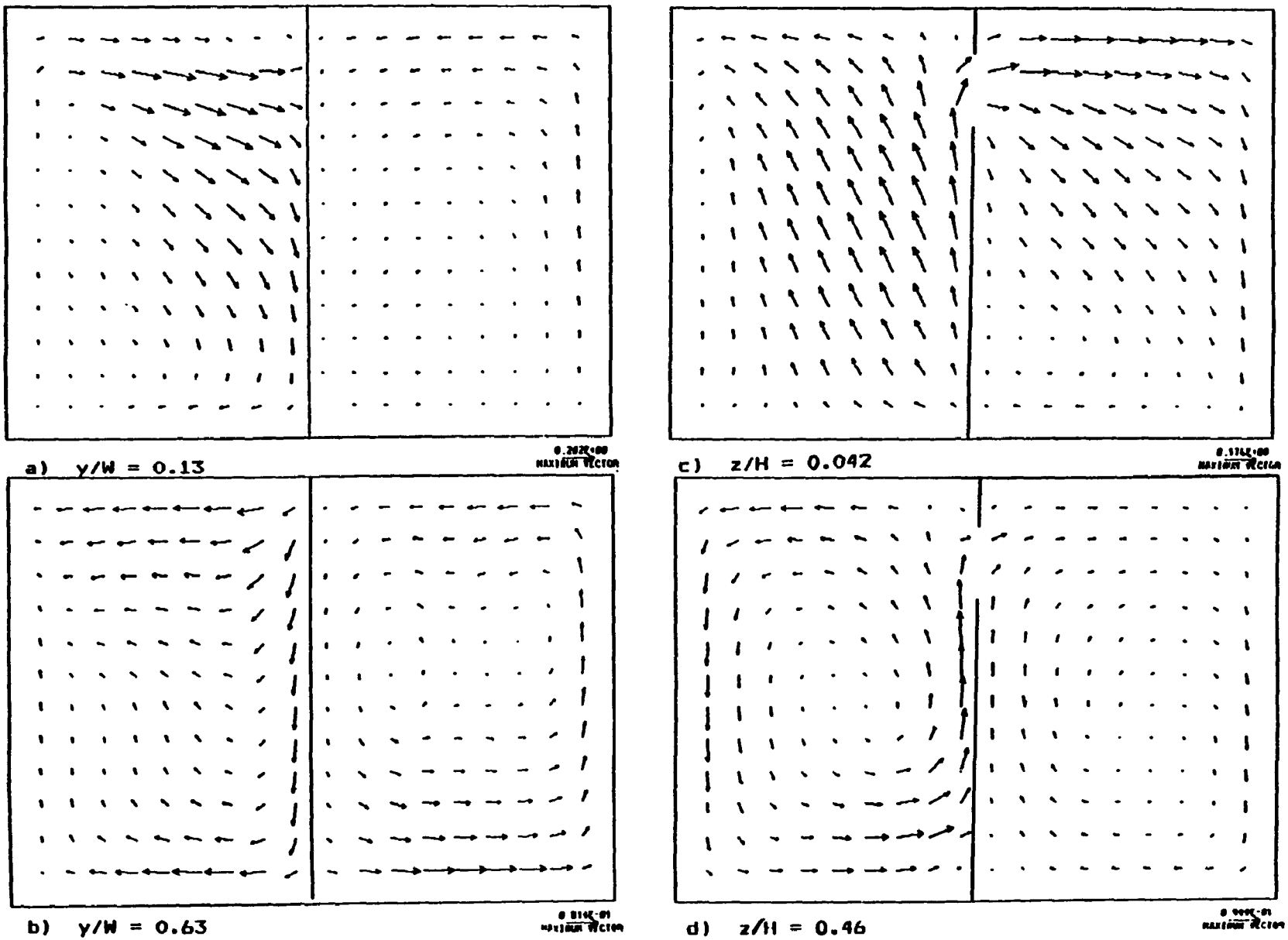

Figure 5.5.7 Flow patterns for the case with $y_D/W = 0.83$

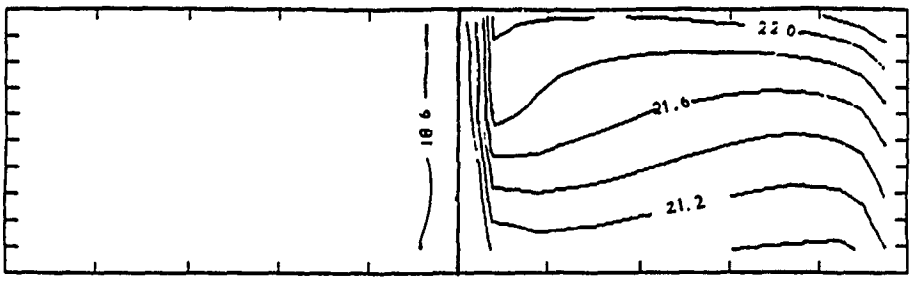

CONTOUR FROM 18.496 TO 22.896 CONTOUR INTERVAL OF 0.26936
X INTERVAL= 0.94444 Y INTERVAL= 0.27569

a) y/W = 0.13

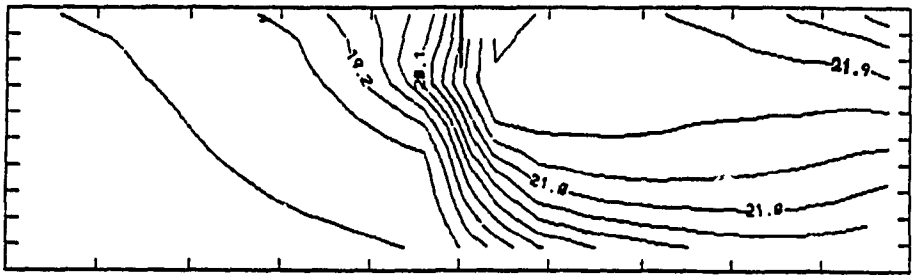

CONTOUR FROM 18.396 TO 23.196 CONTOUR INTERVAL OF 0.36889
X INTERVAL= 0.94444 Y INTERVAL= 0.27569

b) y/W = 0.79

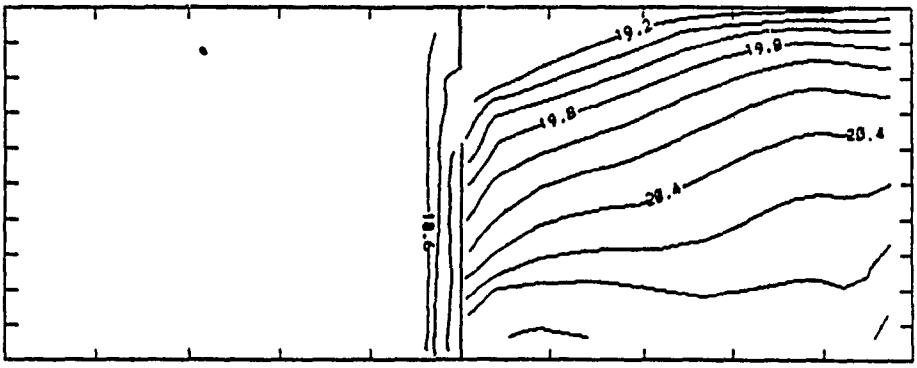

CONTOUR FROM 18.496 TO 21.696 CONTOUR INTERVAL OF 0.28908
X INTERVAL= 0.94444 Y INTERVAL= 0.36667

c) z/H = 0.042

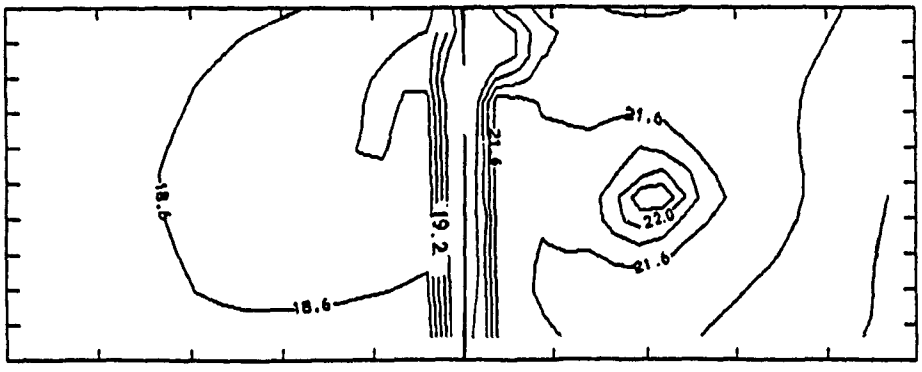

CONTOUR FROM 18.496 TO 22.696 CONTOUR INTERVAL OF 0.28896
X INTERVAL= 0.94444 Y INTERVAL= 0.36667

d) z/H = 0.46

Figure 5.5.8 Temperature distributions for the case with $y_D/W = 0.83$

PAGINATION ERROR.

TEXT COMPLETE.

ERREUR DE PAGINATION.

LE TEXTE EST COMPLET.

NATIONAL LIBRARY OF CANADA.

CANADIAN THESES SERVICE.

BIBLIOTHEQUE NATIONALE DU CANADA.

SERVICE DES THESES CANADIENNES.

TABLE 3.1.1

Source term for conservation equation

ϕ	Γ_ϕ	S_ϕ
1	0	0
u	μ_{eff}	$-\frac{\partial p}{\partial x}+\frac{\partial}{\partial x}\left(\mu_{eff}\frac{\partial u}{\partial x}\right)+\frac{\partial}{\partial y}\left(\mu_{eff}\frac{\partial v}{\partial x}\right)+\frac{\partial}{\partial z}\left(\mu_{eff}\frac{\partial w}{\partial x}\right)$
v	μ_{eff}	$-\frac{\partial p}{\partial y}+\frac{\partial}{\partial x}\left(\mu_{eff}\frac{\partial u}{\partial y}\right)+\frac{\partial}{\partial y}\left(\mu_{eff}\frac{\partial v}{\partial y}\right)+\frac{\partial}{\partial z}\left(\mu_{eff}\frac{\partial w}{\partial y}\right)$
w	μ_{eff}	$-\frac{\partial p}{\partial z}+\frac{\partial}{\partial x}\left(\mu_{eff}\frac{\partial u}{\partial z}\right)+\frac{\partial}{\partial y}\left(\mu_{eff}\frac{\partial v}{\partial z}\right)+\frac{\partial}{\partial z}\left(\mu_{eff}\frac{\partial w}{\partial z}\right)-\rho\beta g\theta$
h	$\frac{\mu_{eff}}{\sigma_h}$	0
k	$\frac{\mu_{eff}}{\sigma_k}$	$G_k-\rho\varepsilon+G_B$
ε	$\frac{\mu_{eff}}{\sigma_\varepsilon}$	$C_1\frac{\varepsilon}{k}\left(G_k+G_B\right)\left(1+C_3R_f\right)-C_2\frac{\rho\varepsilon^2}{k}$
c	$\frac{\mu_{eff}}{\sigma_c}$	0

TABLE 4.4.1

Under-relaxation factors

URF	u	v	w	h	pp	k	ε	c
Natural convection	0.3	0.3	0.3	0.25	0.5	0.8	0.8	1.0
Forced convection	0.3	0.3	0.3	-	0.2	0.8	0.8	1.0
Mixed convection	0.2	0.2	0.2	0.3	0.22	0.8	0.8	1.0

TABLE 5.2.1

Dimensions of openings

	door	supply	exhaust	source
w/W	0.17	0.083	0.083	-
h/H	0.75	0.083	-	-
l/L	-	-	0.056	-

TABLE 5.2.2

Arrangement of openings

first type: air infiltration through wall W	door location y_D/W	exhaust location x_E/L y_E/W
case 1B-1	0.17	
case 1B-2	0.50	0.75 0.71 (zone B)
case 1B-3	0.75	
case 1A-1	0.17	
case 1A-2	0.50	0.19 0.71 (zone A)
case 1A-3	0.75	
second type: supply opening on wall W at z_I/H=0.042, y_I/W=0.13	door location y_D/W	exhaust location x_E/L y_E/W
case 2B-1	0.17	
case 2B-2	0.50	0.75 0.88 (zone B)
case 2B-3	0.83	
case 2A-1	0.17	
case 2A-2	0.50	0.19 0.88 (zone A)
case 2A-3	0.83	

TABLE 5.3.1

Dimensions and locations of openings in infiltration study

	door	supply	exhaust	source
dimension				
w/W	0.17	0.083	0.083	-
h/H	0.75	0.083	-	-
l/L	-	-	0.056	-
location				
x/L	0.5	0.0	0.75	0.75
y/W	variable	0.125	0.875	0.875
z/H	-	0.042	1.0	0.125

TABLE 5.3.2

Average Concentration in Each Zone

in infiltration study

infiltration rate	-0.005	-0.01	-0.03
zone A	3.941	2.820	0.874
zone B	6.033	4.390	2.158

TABLE 5.4.1

Locations of openings for

basic model in ventilation effectiveness study

	door	supply	exhaust	source
x/L	0.5	0.0	0.75	0.25
y/W	0.5	0.46	0.875	0.46
z/H	-	0.875	1.0	0.46

TABLE 5.5.1

Dimensions and locations in mixed convection study

	door	supply	exhaust	sources
dimension w/W	0.17	0.083	0.083	
h/H	0.75	0.083		
l/L			0.056	
location y/W	variable	0.46	0.875	0.5
z/H		0.875	ceiling	0.29
x/L	0.5	$Wall_w$	0.75	0.69

TABLE 5.5.2

Average PD and contaminant concentration in each zone

in mixed convection study

	T_I = 18°C	T_I = 19°C	T_I = 20°C
y_D/W=0.17	PA=4.85 PB=0.80	PA=4.54 PB=0.73	PA=4.24 PB=0.68
	CA=5.52 CB=13.2	CA=5.50 CB=13.2	CA=5.48 CB=13.2
y_D/W=0.50	PA=4.66 PB=0.82	PA=4.37 PB=0.76	PA=4.07 PB=0.69
	CA=4.72 CB=12.3	CA=4.70 CB=12.3	CA=4.70 CB=12.3
y_D/W=0.83	PA=4.50 PB=0.91	PA=4.18 PB=0.84	PA=3.90 PB=0.77
	CA=6.96 CB=13.8	CA=6.91 CB=13.8	CA=6.88 CB=13.8

PA: average percentage dissatisfied people in zone A

PB: average percentage dissatisfied people in zone B

CA: average contaminant concentration in zone A

CB: average contaminant concentration in zone B

1. FLOW CHART FOR MAIN PROGRAM

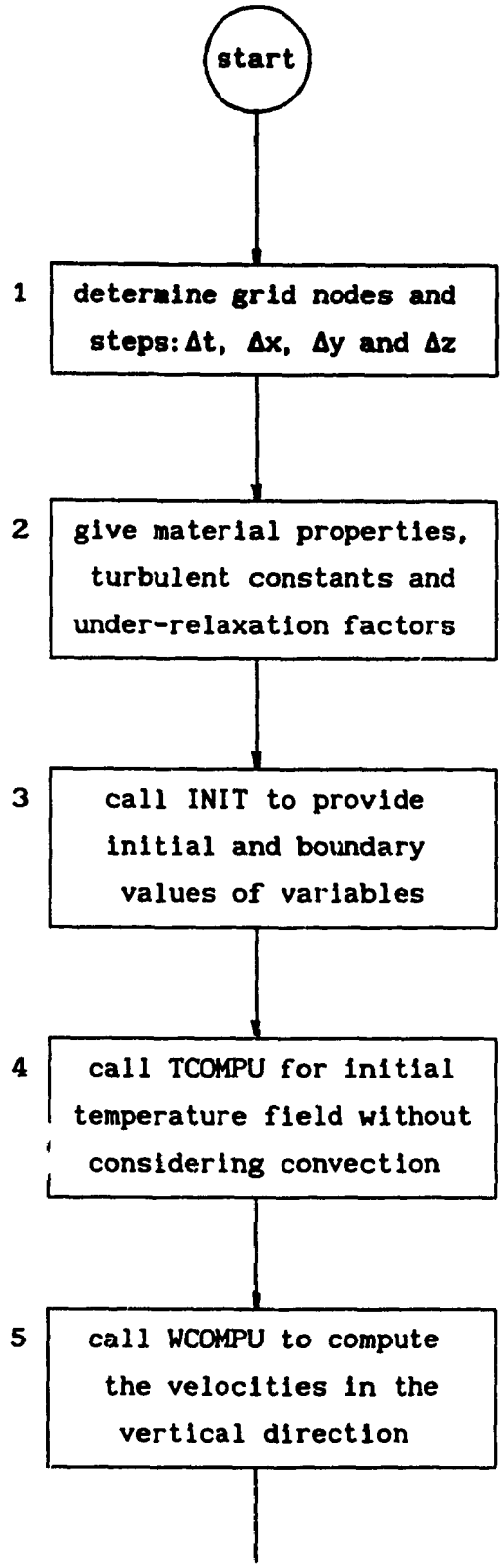

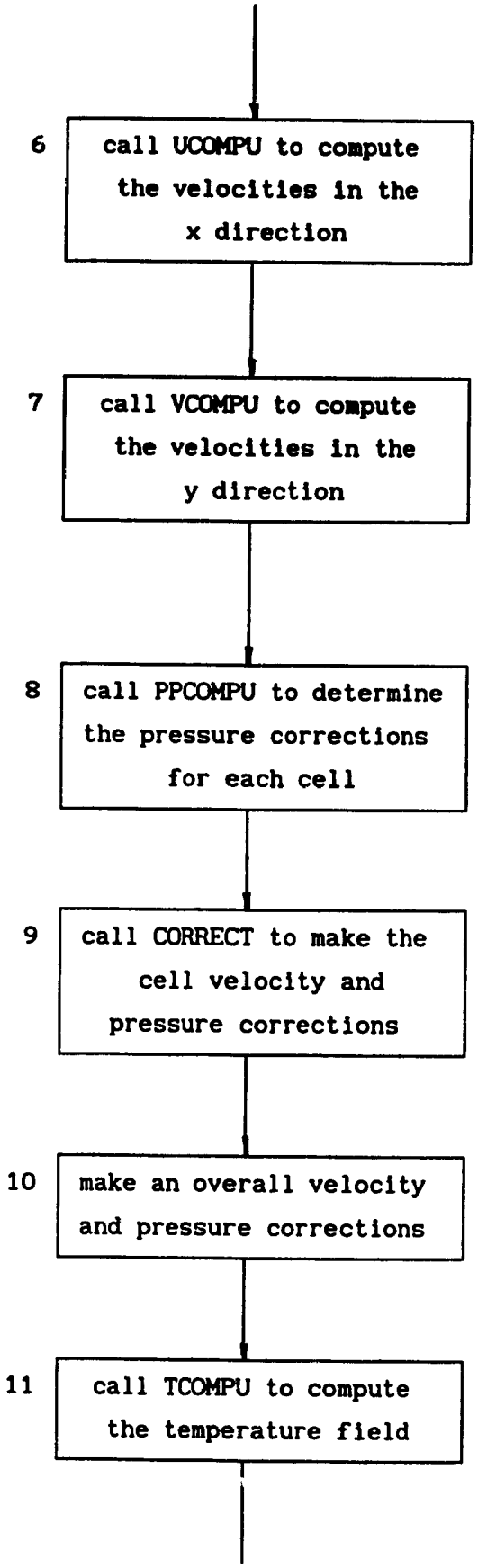
6
call UCOMPU to compute the velocities in the x direction
7
call VCOMPU to compute the velocities in the y direction
8
call PPCOMPU to determine the pressure corrections for each cell
9
call CORRECT to make the cell velocity and pressure corrections
10
make an overall velocity and pressure corrections
11
call TCOMPU to compute the temperature field

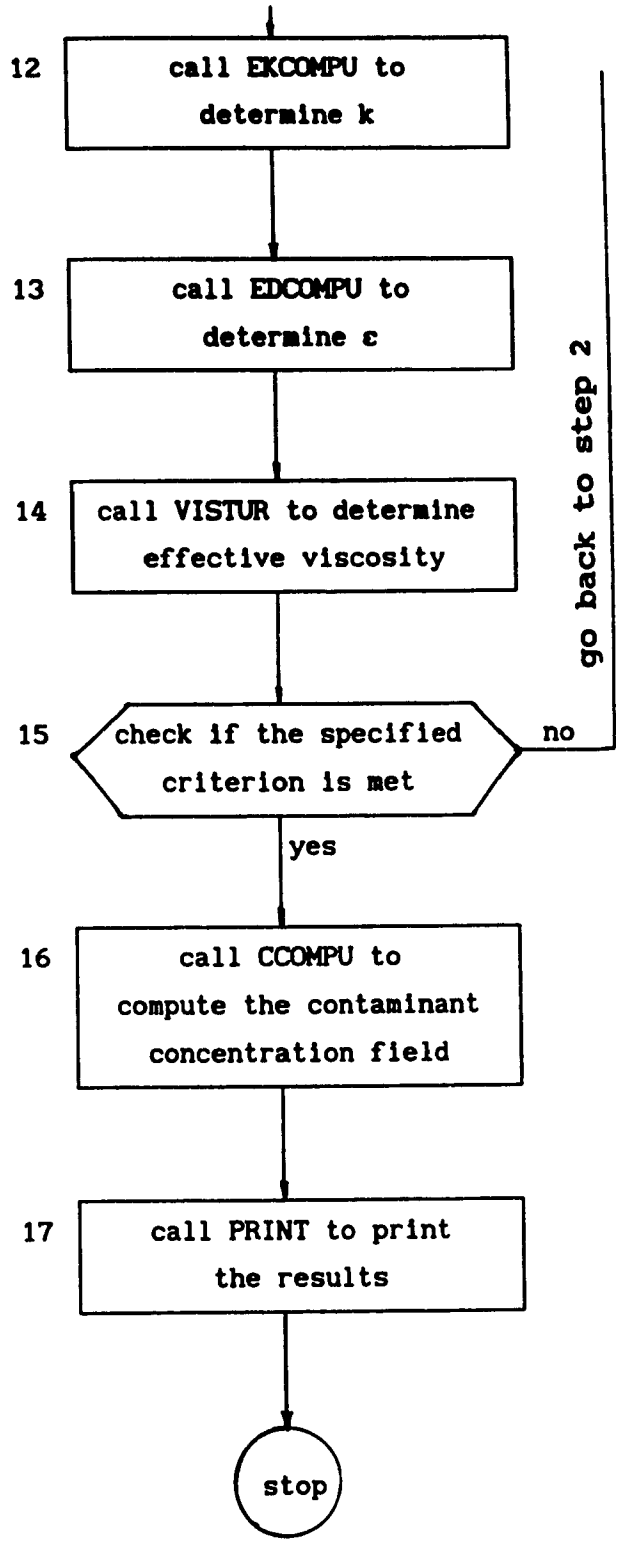
12
call EKCOMPU to determine k
13
call EDCOMPU to determine ε
14
call VISTUR to determine effective viscosity
15
check if the specified criterion is met
no
go back to step 2
yes
16
call CCOMPU to compute the contaminant concentration field
17
call PRINT to print the results
stop

2.FLOW CHART OF SUBROUTINE FOR COMPUTING VARIABLES

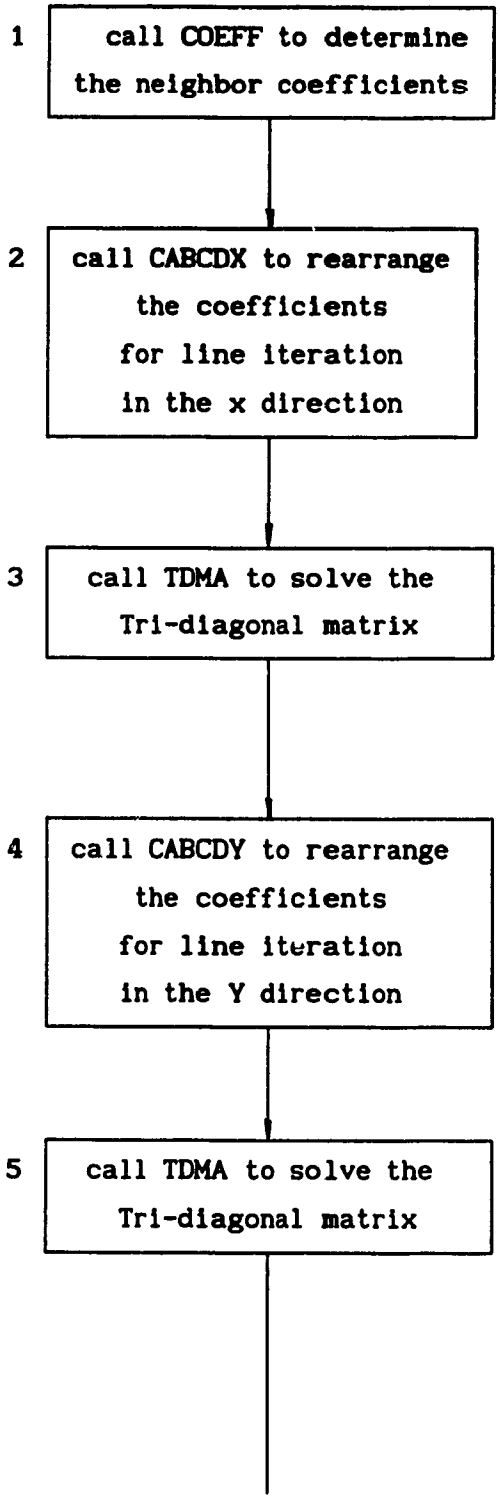

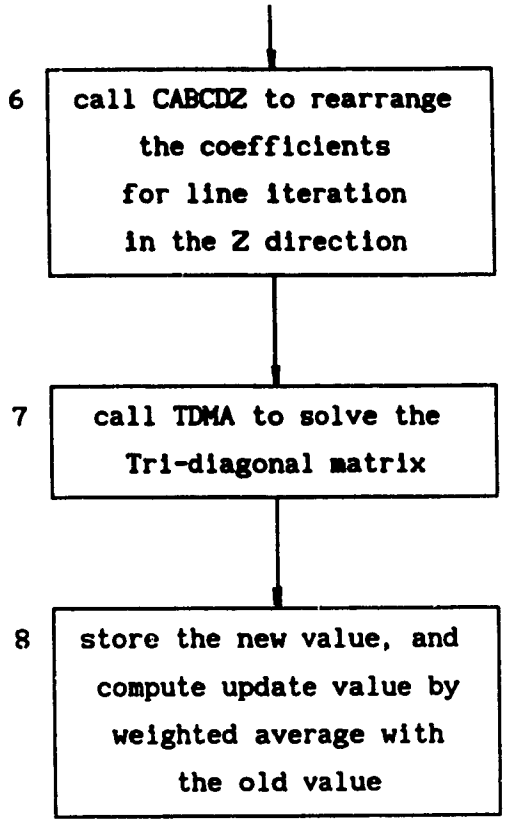
6
call CABCDZ to rearrange the coefficients for line iteration in the Z direction
7
call TDMA to solve the Tri-diagonal matrix
8
store the new value, and compute update value by weighted average with the old value

3. FLOW CHART FOR SUBROUTINE COEFF